Department of Electrical and Computer Engineering

Intelligent Control of PV Co-located Storage for Feeder Capacity Optimization

Manathum N. P. Jayasekara

This thesis is presented for the Degree of
Doctor of Philosophy
of
Curtin University

April 2015

DECLARATIONS

To the best of my knowledge and belief this thesis contains no material previously published by any other person except where due acknowledgment has been made. This thesis contains no material which has been accepted for the award of any other degree or diploma in any university.

Signature: M. N. P. Jayasekara **Date: 20/04/2015**

ABSTRACT

Battery energy storage is identified as a strong enabler and a core element of the next generation grid. However, at present the widespread deployment of storage is constrained by the concerns that surround the techno-economic viability. This thesis addresses this issue through optimal integration and management of battery storage to improve the quality, cost effectiveness and efficiency of the electricity grid. A holistic approach to optimal integration issue includes the development of effective methodologies for optimal siting, sizing and dispatch coordination of storage under the presence of high penetrations of distributed generation (DG).

The optimization of storage requires the determination of an optimal daily profile for the battery energy. All optimization processes rely upon repeated evaluation of a cost function for a proposed solution vector. The first goal of the thesis was to establish a superior method to represent the battery energy compactly utilizing a vector of Fourier coefficients. The compact representation reduces the dimensionality of problem, eliminates discontinuities in energy and inherently encapsulates constraints with respect to periodicity.

Secondly, an optimization algorithm and a simple rule-based approach for sizing and scheduling of community scale storage dispatch are developed for demand smoothing. The diurnal battery profile is updated as new information becomes available to respond to changing future predictions in load and generation. Thirdly, an optimization strategy that incorporates the costs of battery, peak support, energy losses and voltage regulation for optimal sizing and predictive management of storage is developed. This approach is then applied to carry out quantitative analysis on the performance of battery storage for single objective systems that target the control of voltage regulation, loss reduction or peak curtailment exclusively and multi-objective control. This method highlights the impact of the choice of installation site and application purpose on the dispatch management scheme and the size of the storage.

The thesis then develops a novel single analytical framework for the optimal placement, sizing and real-time charge/discharge management of single or multiple storage systems. The method is developed with the key objective of regulating the system voltages while improving the feeder capacity to absorb more DG. Secondary benefits include improved performance levels in terms of reduced losses, peak shaving and opportunity for smart coordination of available generation sources.

Considering the smart grid aspiration to decarbonize the electricity generation market, renewable DGs could be installed not only domestically but also at grid scales. To facilitate such DG integrations, last part of the thesis establishes an analytical approach for optimal sizing and siting of DG.

Solution for the optimal integration of storage and DGs for feeder optimization effectively reconcile feeder capacity and voltage limits violations that drive most infrastructure development projects. Further motivation is provided by the need to enhance the resilience of the energy market for the ultimate goal of transforming the existing grid to a decentralized intelligent power system.

ACKNOWLEDGEMENTS

The work presented in this thesis is a product of many hours of hard work and continuous support from several people. Firstly, I am immensely grateful for the expertise guidance, limitless motivation, support and enthusiasm that I received from my supervisor from Curtin University, Professor Mohammad A. S. Masoum through these years. His dedication and drive for knowledge is truly inspiring. His valuable inputs for the success of this thesis are greatly appreciated. I am thankful for the skills I have gained from him. It was an honour working with him.

I would also like to express my deepest gratitude to my associate supervisor Professor Peter J. Wolfs for making this journey an enriching and rewarding experience. His encouragements, efforts and expertise guidance were fundamental to the success of the research documented in this thesis. I am truly thankful for the opportunity to work with him, the knowledge he has shared and the skills I have gained from working with him. I am also thankful that he continued to supervise after his relocation to Central Queensland University.

Special thanks go to Australia Postgraduate Award (APA) made possible through Curtin University and the Curtin Research Scholarships (CRS) for the financial support. I would also like to thank the Department of Electrical and Computer Engineering for providing me the right environment to conduct this research work effectively. In addition, I acknowledge the reviewers and examiners of this thesis and related publications for their kind consideration, advice and time.

I would also like to acknowledge the support of Western Power in supplying network data, models and the data collected under the Perth Solar City Trial project, which is a part of the Australian Government's Solar Cities Program.

I would like to express my sincere gratitude and love to my parents, L. Banda Jayasekara and Wijitha Jayasekara. This work would not have been possible without their care, encouragements and unconditional support to keep moving forward in my professional life. Finally, I would like to thank my husband, sister and brother for their endless love and support during this journey. It is with great love that I dedicate this publication to you, my family.

Table of Contents

List of Figures

List of Tables

ABBREVIATIONS

Acronym	Abbreviation
AAC	All-aluminium conductors
ABC	Artificial bee colony
AMI	Advance metering infrastructures
APOM	Adaptive predictive optimization method
BCC	Battery capital cost
BESS	Battery energy storage system
BMS	BESS management system
BRC	Battery replacement cost
BWC	Battery wear cost
CA	Classical approach
CB	Circuit breaker
CF	Capacity factor
CSIRO	Commonwealth scientific and industrial research organization
DER	Distributed energy resources
DFT	Discrete Fourier transform
DFTM	Discrete Fourier transform based model
DG	Distributed generation
DMS	Data management system
DNO	Distribution network operator
DOD	Depth of discharge
DTFS	Discrete time Fourier series
EMS	Energy management system
FC	Fourier coefficients
GA	Genetic algorithms
HV	High voltage
IA	Improved analytical
IEA	International energy agency

IP	Interior-point
LDC	Load duration curve
LSF	Loss sensitivity factors
LV	Low voltage
MAE	Mean absolute error
MILP	Mixed-integer linear programming
MLA	Modified load flow approach
MV	Medium voltage
NN	Neural network
O&M	Operating and maintenance
OLTC	On-line tap changer
PCC	Point of common coupling
PEI	Power electronics interface
PF	Power factor
PI	Performance index
PS	Pattern search
PSO	Particle swarm optimization
PV	Photovoltaic
SCADA	Supervisory control and data acquisition
SoC	State of charge
T&D	Transmission and distribution
TCIM	Total current injection method
TS	Tabu search
VCZ	Voltage control zone
VSDG	Voltage support distributed generation
VSF	Voltage sensitivity factors
VUF	Voltage unbalance factor

Chapter 1. Introduction

1.1 Problem Statement

1.1.1 Transition of the Existing Grid

Over the past decades electricity has become one of the fundamental and indispensable resources for the people. At present, higher proportion of electricity is generated with fossil fired centralized large scale power plants. Hence, transmission and distribution (T&D) networks are designed considering centralized generation with unidirectional power flow from upstream to downstream consumers as schematically presented in Fig. 1-1. The direction of flow implies the electricity flow from highest voltage to the lowest voltage level.

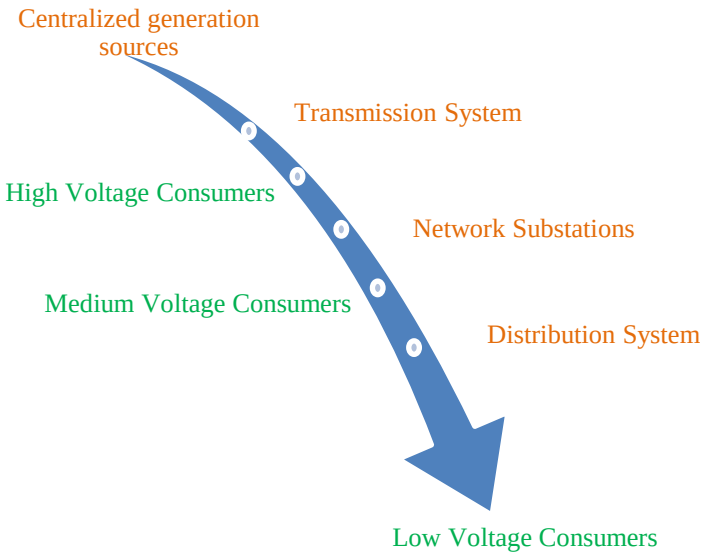

Fig. 1-1. The unidirectional existing grid hierarchy.

Despite the geographical differences, utility companies have adopted this basic topology and to date it remains unchanged. However, different levels of controls have materialized for troubleshooting, automation and performance monitoring of high voltage processes and upstream assets. The supervisory control and data acquisition (SCADA) is one of the extensively used systems.

Even though such systems offer certain level of control over upstream assets, distribution systems mostly operate with minimal or no automation controls. Therefore, generation dispatch control is typically centrally coordinated using forecasts of aggregated demand side requirements. Thus, the dispatch control has no real-time link between generation sources and end users. As a result, the power system is overdesigned to carry the maximum conceivable demand. As the peak is an infrequent incidence experienced by the grid, the system is economically inefficient [1]-[2]. In addition, due to the distance between the generators and consumers, power flow can be concentrated into a specific transmission line. This raises further issues like feeder congestion, high system losses and the supply to consumers being adversely affected if line failures occur.

Although, power system assets are utilized economically inefficiently, the rising peak demands that threaten the quality of supply and global climate targets intensely drive future long term network investments. According to IEA 2014 international reports, over the years 2014-2035, cumulative investment of $16.4 trillion will be required across the global power sector (generation capacities and T&D) [3]. These fundamental drivers for electricity network investments are influenced by the following three core factors:

1. **Decarbonisation -** Parallel to international trends, power sector is one of the leading sources of greenhouse gas emissions in Australia, accounting for 35% of the national emissions [4]. In the recent past, displacement of fossil based generation by renewable resources continued to rise in response to consumer demands and government subsidies [5]. In 2012-13, renewable generation in Australia represented 13% of the total generation. The increased adoption of renewable generation combined with the lowered electricity demand from centralized sources in 2012-13 resulted in 7% reduction of total emissions [4]. In the medium term, it is expected that the obligation to address the global climate targets will continue to drive investments in the necessary infrastructure needs and policy makings, to improve the grid compatibility to accommodate low carbon resources [6]-[7].

2. **Meeting customer expectations -** Power sector investment projects are typically planned and deployed in consultation with the community. Evaluating social aspects and impacts of investment projects from variety of perspectives that incorporate community attitudes, awareness, economic constraints, socio-political barriers, environmental constrictions and cultural believes as well as level of community acceptance (for new technologies such as photovoltaics) is an integral part of the decision making process [8]. Moreover, it is of paramount importance for utility providers to ensure that the services delivered to consumers meet essential performance requirements and standards for reliability, quality, availability of capacity and energy security [9]-[10]. This is an on-going commitment set by most utilities in their mission to fulfil rising consumer expectations cost effectively.

3. **Load growth -** Peak demands that result from new load connections and/or increased usage by existing consumers is the key driver for capacity and grid expansions [11]. Insufficient capability to meet the peak capacity can compromise the network performance due to low voltages, imbalances and disconnections from the network. Furthermore, under overload conditions when the peak demand exceeds the tolerance levels of the network equipment but yet stays connected, the stress on the assets could be significant. This increased pressure accelerates the degradation or cause premature failures resulting in high operating costs. Therefore, augmentation work to provide additional capacity should be planned effectively to avoid poor performance of existing network assets. This is in addition to the costs of replacing assets that are reaching their useful life or no longer comply within standards for quality and reliability [9].

Therefore, the integration of large quantities of renewable generation is critical when addressing the challenge of ensuring energy availability while minimizing the carbon footprint. In order to address these concerns, several policies and subsidies were established globally to support the deployment of non-hydro renewable distributed generation (DG), particularly wind and photovoltaic (PV). These measures and the technologies have attracted variety of investors in both private and government sectors transforming the typically monopolistic market [12]-[13]. As a result, a rapid

expansion of renewable generation has occurred in the recent years. These trends in the adoption of renewable DG and technology development arguably propose that traditional centralized paradigm might change in the years to come, converting the existing grid to a decentralized power system with bidirectional power flow [14]. Currently many studies are being carried out in the area of decentralizing the power system. However, the key focus at the moment is on modelling of distributed energy resources (DERs) considering their planning and operational impacts [15]-[16]. From power engineering perspective, these can be categorized into issues related to:

1. Integration of renewable DG and storage that allow local generation and reserve [17]-[21].

2. Control mechanisms that enable deliberate management of load and generation for improved energy efficiency [22]-[26].

1.1.2 Solar in the Generation Mix

Over the past decade, especially in developing countries power generation capacity investments have been driven mainly by this need to shift away from large scale centralized framework [3],[27]. Fig. 1-2 shows the global investment outlook from 2000 to 2012 by generation type. Based on Fig. 1-2, the global investments in generation capacity have tripled in 2012 relative to that spent in 2000. However, investments in 2012 declined by 5% compared to 2011.

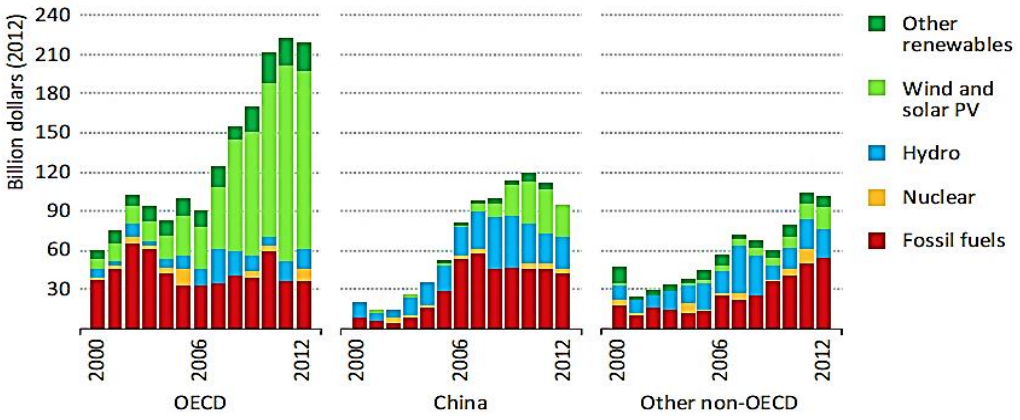

Fig. 1-2. Investments in generation: global outlook, 2000-2012 [3].

A similar trend was seen in Australian electricity market. Based on [10], 2012 forecast for capital investments in centralized generation required in the Australian National Electricity Market (excludes Western Australia and Northern Territory) over the next 25 years was $46 billion. However, a reassessment conducted in 2013 showed a drop to $27 billion. This reflects a change in the political environment and the willingness by governments to invest due to decreases in transmission assets utilization [10]. Furthermore, a decline of 2.5% in generation capacity from centralized sources occurred in 2012-2013 relative to the previous year [5]. Poor transmission assets utilization and the lowered consumptions reflect the adoption of energy efficiency measures encouraged by legislation on equipment such as light bulbs, changes in consumer equipment technology (for example LED televisions replacing plasma televisions), consumer response to rising electricity tariffs and largely the uptake of demand side generation sources like rooftop PV. From the previous year records, in 2012-13 PV generation rose by 58% to 2700GWh, contributing to 1.3% of the total electricity share [4].

The strong uptake of solar was also evident across the international market over the last decade. Solar generation rose by 50% each year, reaching almost 100TWh in 2012 [28]. In 2013, the worldwide installed capacity increased by more than 38GW [29]. The growth in every country was, however, principally driven by government incentive programs coupled with technological advancements. Several other factors also influence the short and long term PV market development [30]:

- Zero greenhouse gas emissions, thus successfully support the attempts to meet climate target obligations.

- PV can be installed at domestic, commercial, community or large scale levels, hence is a viable player in the renewable generation mix [31].

- Large availability of solar with significant access to the electricity grid. The annual irradiation on Australia is approximately 58 million PJ. This is more than 10 000 times Australia’s annual energy consumption [32]. Thus, it is projected to grow at a more rapid pace than wind over the coming years [6].

- Rural area electrification, where supplying electricity through centralized infrastructure is costly with reliability risks [33].

- Unlike gas, coal and hydro generators, PVs use power electronic interfaces exclusively. Compared to synchronous generators, these interfaces are programmable to obtain almost any technical feature required for the efficient operation of the electricity system [34].

- Rising electricity retail charges due to transmission network infrastructure expenditures [30].

- Declining capital costs of PV due to lowered manufacturing costs, improved efficiency as a result of maturity of the technology and competitive private sector market players [35]-[36]. Module cost is expected to fall below 50 cents per watt by 2017 [37].

- Requires zero to minimal maintenance, therefore, low operation and maintenance (O&M) costs.

Even though, PV generation costs have reached "socket parity" in most countries, over the next decade, the market growth is predicted to remain constrained by incentive schemes and policies [38]. Under new policy schemes, global electricity generation from PV is forecasted to rise up to 950TWh in 2035 [28]. With or without policy schemes, the decreasing costs of PV technologies, technical potentials and social opportunities make it possible to envision them as major source of electricity in the future grid [36].

However, deterministic and stochastic variability are major complications that need to be overcome before full potentials of PV can be realized. These effects, induced by the cloud movements, temperature fluctuations and sun incidence angle on a diurnal basis, pose significant challenges on the physical constraints of the power system and voltage profile. Thus, limit their widespread adoption. Some of the critical impacts include:

1. Voltage fluctuations due to stochastic variability - Voltage fluctuations are

strongly correlated to the intermittent output of PV system, typically due to passing of clouds. The variations could be sudden and large, therefore, they can adversely disturb the performance of protection and voltage regulation equipment leading to unstable grid operations, especially if the penetration levels are high or large scale systems are considered [39]-[40]. The magnitude and number of voltage fluctuations occur per unit time also referred to as flicker, has to comply within requirements specified in AS/NZS 61000.3.7. The short-term flicker severity (Pst), obtained for each 10 minutes period, should be less than 1 for low voltage connections and the long-term flicker severity (Plt), obtained for each 2 hour period, should be less than 0.65.In addition, when high penetrations of PV or large systems are connected, uncertainties due to intermittency also make it difficult to forecast PV generation. Therefore, generation dispatch planning and scheduling can become inefficient and uneconomic. As a result, minimizing the forecasting errors to improve the reliability of supply is rapidly becoming a mature field of study due to concerns over reserve energy requirements [34].

2. **Voltage rise due to deterministic variability -** Unlike conventional sources, outputs of PV systems are uncontrollable or non-dispatchable and only occur during sun hours. As the generation level increases mainly during low load conditions or as the power output of the PV system nears the total load, the voltage at the interconnection point will rise. Over voltages could disconnect the PV system from the grid. Typically PV inverters are designed to trip when the bus voltage vary ±10% from the nominal voltage. However, the threshold limits for inverter protection are typically higher than the voltage constraints for distribution networks. As a consequence, the feeder may experience over voltage while the inverter protection threshold limits are not breached [33]. With high capacities of PV generation, over voltages could potentially reverse the direction of power flow and increase system losses. The issue of reverse power flow can be significant in feeders with large scale integrations as well as in residential feeders with widely installed PVs where typical peak demand does not synchronize with peak generation. Furthermore, aggregations of such residential feeders could further impact the HV network voltages [41]. Fig. 1-3 shows the change in the aggregated HV load curve due to high penetrations of rooftop PV over four days in March

2010 and 2014 on the same feeder. From Fig. 1-3, the peak demands from the year 2010 to 2014 has not increased. This may be due to rising tariffs, load shifting to PV generation times and other energy efficiency measures by consumers. However, even with such measures PV generation is not utilized appropriately; a significant drop in the daytime demand is evident. The lowered daytime demands have caused a significant drop in the overall energy demand, but the peak demand remains unchanged due to poor distribution of available generation. Now the deviation of the peak demand is even higher relative to the average daily demand making system even more inefficient. Clearly, measures are needed to smooth the load curve for improving the system efficiency. In addition, high PV generation combined with imbalance of load on three phase systems can cause neutral voltage rises decreasing the hosting capacity of the grid.

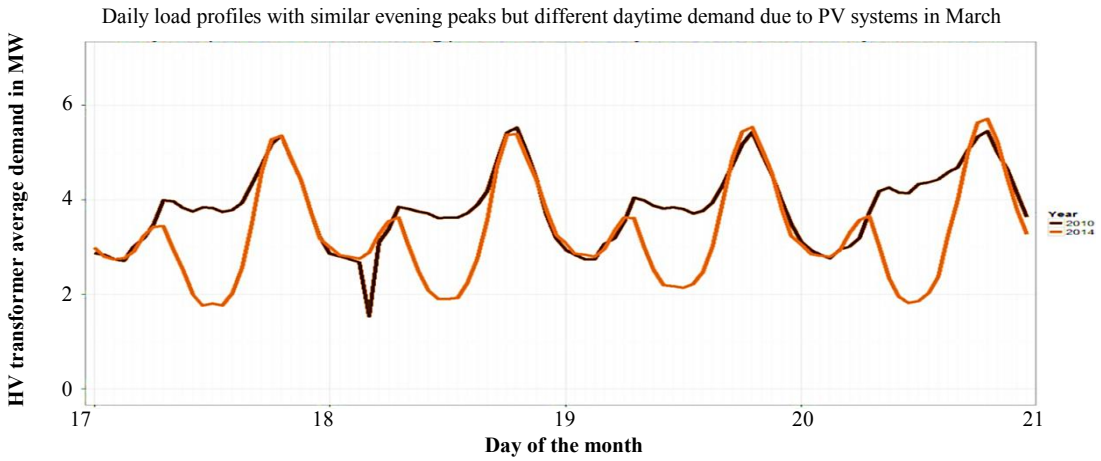

Fig. 1-3. Impact of high penetrations of residential PV on a HV feeder, Western Australia [41].

The intensity and the degree to which these voltage issues may arise depend not only on the capacity but also on the location of the PV system as well as network topology and load characteristics [33],[42]. Therefore, proper integration and management is essential to mitigate issues of variability while effectively facilitating techno-economic and environmental capabilities of DG [40].

1.2 Motivation

Summarizing from the previous sections, the development of decentralized network towards a liberalized electricity generation market has reached some impediments due to concerns over uncertainties associated with variability, location and coordination of available renewable capacities. The variability of PV output mainly affects the operation of generation sources in the mix while location and modularity impact the performance of the grid infrastructure [28].

Energy storage is increasingly becoming popular as a solution that facilitates seamless integration of DG [43]. The primary purpose of storage devices is to move energy through time, thus enable dispatchability. Although there are multiple types of storages, this thesis focuses on battery energy storage systems (BESSs). This is because batteries offer the flexibility in capacity, rapid response required to mitigate the challenges of PV intermittency and the advantage of being locatable in variety of configurations [44]-[45]. Currently, substantial research and demonstration investments are being made to study potentials of BESS [46]. Based on these studies, BESS has the potential to participate in the electricity market in a variety of ways, including [18], [47],[48];

- Energy arbitrage through shifting of excess generation from distributed PV to peak demand periods. Consequently, reduces the electricity capacity from centralized sources and high peak support costs.

- Provides flexible and continuous supply. Hence, improves the demand side supply reliability and energy security.

- Frequency regulation and response to reconcile momentary variations in demand and supply.

- Synchronized or non-synchronized spinning reserve for curtailing unforeseen unavailability of electricity supply.

- Voltage support during peak generation and load by absorbing generation and delivering energy respectively, to maintain voltage within regulatory

constraints.

- Inverter interfaced battery systems can be programmed to generate reactive power to offset reactance of HV lines for added voltage regulation.

- Able to "black start" after catastrophic system failures and can provide start-up power given its properly sited.

- Eliminates issues of inherent and stochastic variability of PV systems. Able to respond within a fraction of a second, far rapidly than plants with rotating machinery.

- Minimizes transmission line congestion due to reduced distance between generators and consumers. Thus, improves the cost efficiency through T&D system upgrade deferrals. The Australian Federal Government Energy White Paper establishes that 25% of retail electricity costs are derived from charges due to peak events that occur over a period of less than 40 hours per year [49]. Peak support by storage can improve the load and generation carrying capacity of power system assets.

- Offers consumers the flexibility to manage consumption and reduce peak demand charges for overall cost reductions.

- Supports electricity market deregulation and restructuring, therefore, is a strong sustainable enabler of the conceptual intelligent grid.

Historically, the integration of PV with battery energy storage systems (BESSs) has been an application that occurred primarily in the off or remote areas with minimal access to centralized generation due to high capital and O&M costs. Recent advancements in power inverters, control systems and battery chemistries such as Lithium-ion (Li-ion), advanced lead-acid (Pb-acid) and Zinc Bromine (ZnBr) along with competitive manufacturing in the electric vehicle market, have begun to steadily drop the cost of batteries [50]-[52]. Therefore, it is recognized that the potential storage market in grid applications (due to numerous benefits of combining PV with BESS) in the future will be much greater than the existing market [6].

However, the widespread deployment of storage is still restricted by the high capital costs. Reference [38] suggests that with current falling PV prices, "grid parity" against retail electricity prices could be achieved if battery storage prices drop to 20 cents per kWh. Business models and planning frameworks for the maximization of financial and technical benefits of battery storage in grid applications need to be established to be able to take full advantages. These tools could provide stakeholders a better understanding of potentials and role of BESS in the capacity mix and ultimately improve the cost competitiveness.

1.3 Objectives

Despite all the capabilities, current approach to network planning and management do not include energy storage modelling, meaning that aforementioned potentials cannot be realized effectively. This is primarily due to the complexity of the problem along with the lack of validations and familiarity with the battery storage technologies in power system applications. Complexity arises from variety of factors including the cost and the requirement for bi-directional power flow to function, as well as the fact that charging energy could be from range of sources and the ability to provide multiple services to the grid.

Therefore, this thesis aims to develop generalized methods which support research and development through quantification, qualification and validation of storage benefits in the context of decentralized intelligent grid. The approaches specifically deal with the issue of optimal integration that combine optimal dispatch control, siting and sizing of BESSs under various steady-state criteria for efficient integration to the grid. The key criteria analysed are voltage regulation and system loss reduction as well as the minimization of peak demand and energy from centralized sources for the optimal utilization of grid assets. Considering the cost sensitivity of the issue, BESS life time costs, both capital and operational costs, reduction is a mandatory inclusion in the proposed methods.

The proposed methods have the following characteristics,

- Capability to economically optimize the sizing and siting of BESSs while

allowing the coordination between the grid and storage assets for optimal operation.

- Modelling ability for large/grid scale or small storage devices considering network fundamental capacity and voltage restrictions in addition to battery constraints.

- Sound platform for comprehensive quantitative tradeoffs analysis and validations; thereby avoiding the need for resource intensive field testing.

- Ability to take into consideration various network topologies, load patterns and DG penetration levels.

- Flexibility to optimize for either exclusive or joint control of voltage regulation, peak demand reduction and loss minimization.

The optimal integration through the proposed frameworks alleviates the techno-economic challenges and maximizes the total value of storages allowing seamless integration of variable DG into the grid. Therefore, the method could be used to accomplish the following ultimate goals,

- Address the questions, what is the most efficient way to integrate storage to grid? How should it be controlled for best outcomes? What factors influence the above?

- Wide deployment of storage for improving the grid generation and load hosting ability; support the transformation to a decentralized system.

- Enable storage as a cost effective option for power quality and performance enhancement.

- Enable generation market competitiveness and optimal utilization of power system assets.

- Offer consumer the ultimate flexibility. No peak demand charges or forceful pricing schemes (designed to reduce peak) will be required.

1.4 Main Contributions

In today's liberalized market, no single entity has the total ownership or control over the infrastructures and power or information exchanges. As a result, this thesis assumes that there exists a centralized supervisory control centre which facilitates the coordination of resources through an intelligent communication infrastructure for optimal BESSs dispatch management.

Optimal dispatch control minimizes the cyclic operation of the battery by managing the battery external parameters; charge/discharge rates, depth of discharge (DOD) and daily cycling for the optimized service of the grid. Therefore, extend the life expectancy of the battery by avoiding wear and tear due to unnecessary cycling. Augmented cycle life can translates to lower ownership costs improving the overall performance and value. Dispatch management determines the extent to which source (grid or BESS) operates at any given time, amount of power exchange, direction of power flow and the mode of operation at the point of common coupling (PCC). In addition, the charge/discharge management strategies strongly depend on the location and the sizing. Therefore, optimal siting and sizing of BESSs are also addressed in this thesis.

The main thesis contributions are;

1. Fourier-series model that compactly represents battery daily energy profile in cost based optimization problems. Reduces the dimensionality of the optimization problem and a key optimization constraint that the solution is periodic, is inherently embedded allowing a number of optimization algorithms to be efficiently applied. Thus, improve the computational efficiency.

2. Adaptive scheduling strategy for dispatch management of community or grid scale storage. This is developed with the aim of load smoothing and optimizes the costs of peak support, energy and BESS. This method effectively adapt for forecasting errors.

3. A simple, low cost and adaptive rule-based dispatch management strategy.

This model is comparable to the optimization model in (2).

4. Strategy in (2) is improved to optimize for multiple grid services; voltage regulation, loss reduction, demand curtailment and peak reduction. This methodology provides the option to optimize storage for a particular service or multiple services to the grid.

5. Shows the potential of the optimization framework for conducting quantitative analyses on the techno-economic benefits of BESS installations against network technical performance constraints.

6. Highlights the impact of installation site and grid application on the dispatch management scheme and size of storage.

7. Develops a single analytical framework for the optimal placement, sizing and real-time charge/discharge management of single or multiple BESSs. The method is developed with the key objective of regulating the system voltages while improving the feeder capacity to absorb high penetrations of DG. Secondary benefits include improved performance levels in terms of reduced losses, peak shaving and smart coordination of available generation sources.

8. As an extension, thesis establishes an analytical approach for optimal allocation and sizing of DG for grid scale integrations with the primary aim of loss minimization. While storage is a key enabler of DG, optimal integration of large scale DG is imperative and further improves the system efficiency.

9. Develops an analytical approach for sizing and siting of voltage support DG (VSDG) for maximum voltage support.

10. Methods in 7, 8 and 9 minimize the costs of the units by finding the minimal ratings required.

The proposed BESS integration and management strategies can be used to assess and quantify benefits of BESS for systems with widely deployed PV sources or systems where BESS is co-located with PV. The methods are easily extensible for

distribution systems with other types of variable generation.

1.5 Thesis Outline

The work presented in this dissertation is organized into 9 chapters. The first chapter provides an introduction to the background, motivation, objectives and main contributions of this research work. The remaining chapters are organized as follows:

- **Chapter 2:** Provides a review on literature regarding the development of smart grid, battery technologies and previously established methods for BESS integration. In addition, deficiencies and short-comings of the existing models are outlined.

- **Chapter 3:** Introduces a Fourier series based model to represent battery energy effectively in cost based optimization problems. Method reduces the dimensionality of the optimization problem and improves the computational efficiency significantly.

- **Chapter 4:** This chapter studies the optimal dispatch management and sizing of BESS for distribution system peak shaving. Two novel predictive BESS management approaches that schedule optimal battery operation for twelve hours into the future are proposed. Chapter uses exponential smoothing to adjust and update the battery schedule to forecasting errors.

- **Chapter 5:** Provides a comprehensive approach for BESS sizing and dispatch management. The approach is able to consider, network characteristics, load/generation distributions, battery costs and ability of the BESS to provide several services to the grid; key services studied are voltage regulation, peak shaving and loss reduction. Furthermore, the effect of installation site is also investigated.

- **Chapter 6:** Method in Chapter 5 is improved for three-phase four wire residential distribution system with high penetrations of rooftop PV. This chapter considers residential scale BESS. Benefits of BESS and effect of installation site on the BESS dispatch strategy and size are explored.

- **Chapter 7:** A single analytical frame work that determine multiple or single battery placement, sizing and dispatch strategy is presented in Chapter 7. Economic gains are achieved by deriving the minimal sizing required to service the grid.

- **Chapter 8:** Develops two analytical approaches for sizing and siting of DG and VSDG. Methods facilitate large scale DG integrations and could be co-located BESS to improve dispatchability of renewable DG.

- **Chapter 9:** Concludes the thesis by proving a summary of main conclusions, contributions and recommendations for further improvements or future work.

1.6 List of Publications

The main contents of this thesis are supported by the following publications:

- **Journals:**

1. N. Jayasekara, P. Wolfs and M. A. S Masoum, "An optimal management strategy for distributed storages in distribution networks with high penetrations of PV," Electrical Power Systems Research, vol. 116, pp. 147—57, May 2014.

2. N. Jayasekara, M. A. S. Masoum and P. J. Wolfs, "Distributed Energy Storage for the Optimization of Distribution Network Load and Generation Hosting Capability", IEEE Transactions on Sustainable Energy, Under third review (TSTE-00336-2014).

3. N. Jayasekara, M. A. S. Masoum and P. J. Wolfs, "Analytical Solutions for Optimal Placement and Sizing of Multiple DG Units in Radial or Mesh Distribution Systems", IEEE Transactions on Smart Grid, To be submitted.

4. N. Jayasekara, P. J. Wolfs and M. A. S. Masoum, "Analytical Approach for Optimal Placement, Sizing and Management of Battery Storage for Voltage Regulation", IEEE Transactions on Power Systems, To be submitted.

- **Conferences:**

1. N. Jayasekara and P. J. Wolfs, “Optimal Power Management for LV Distribution Feeders with Finely Distributed PV and Co-located Storage”, IEEE Power and Energy Society General Meeting (PES), July 2013.

2. N. Jayasekara and P. J. Wolfs, “A Hybrid Approach Based on GA and Direct Search for Periodic Optimization of Finely Distributed Storage”, IEEE PES Innovative Smart Grid Technologies Asia, 2011.

3. P. J. Wolfs, N. Jayasekara and S. Subawickrama, “A Fourier Series based Approach to the Periodic Optimization of Finely Dispersed Battery Storage”, Australasia Universities Power Engineering Conference, Sept. 2011.

4. N. Jayasekara and P. J. Wolfs, “Analysis of power quality impact of high penetration PV in residential feeders”, Australasia Universities Power Engineering Conference, Dec. 2010.

Chapter 2. Literature Review

2.1 Introduction

This thesis addresses the issue of optimal integration of PV and storage for improving the quality and efficiency of electricity supply. A holistic approach to optimal integration issue includes the development of effective methodologies for optimal siting, sizing and management of these DERs. The main motivations for optimal integration and management of DER are: feeder congestion management, transmission and distribution loss reduction, voltage regulation, reductions in peak demand, improved power quality and energy efficiency while supporting the expansion of smart grid [53]-[54]. Improved technical aspects and energy efficiency essentially improve the life expectancy of power system assets and manage the cost of network upgrades or reinforcements [55].

At present, grid has a limited capability to accept larger penetrations of PV due to potential feeder voltage limit violation risks. This is especially true in the low voltage (LV) distribution networks where residential and smaller commercial arrays are connected. In addition, existing utility grid, as a result of increasing demand, experience issues such as low voltages, voltage sags and unbalances, challenging the capacity limit of feeders. Hence, solution approaches to optimal integration of DER for feeder optimization require the development of strategies that can effectively reconcile feeder capacity and voltage limits violations that drive most infrastructure development and reinforcement projects. Modelling techniques are further motivated by the preliminary need to enhance the resilience of the grid for the ultimate goal of transforming the existing grid to a decentralized intelligent system as envisioned by utility providers globally. Therefore, this literature review mainly concerns the key features of the intelligent grid. This chapter also provides an overview of developments in the battery energy storage along with their economic and technical capabilities. Lastly, existing state of the art feeder optimization models as well as their deficiencies and short-comings are discussed.

2.2 The Intelligent Grid or "Smart Grid"

The speed of the transition to decentralization depends on the network's ability to adopt innovation that include development of new strategies and technologies that allow better utilization of power system assets, thus deliver best techno-economical efficiencies [1]. Despite the restrictions, most utilities agree that widespread deployment of DER (DG and storage) is essential to effectively meet the challenges of the future grid expansions [1],[2],[56].

Main advantages of decentralized systems with large propagations of DERs include:

- Improved ability to encourage energy efficiency from both technical and economical viewpoints [54],[57].
- Improved economic benefits through low cost infrastructure needs from being close to the end users and reduced demand from fossil based generation [58]-[60].
- Energy security as zero fuel cost renewable DERs are insulated from variations in fossil fuel prices. Costs of these DERs are mainly limited to operational costs and show steady decline in the average capital costs over the past years [6],[61].
- Consumers will have access to diversified range of supply sources, thereby offers further improved energy security [62].
- In contrast to exhaustible fossil fuel based centralized generation, renewable DG are well distributed and do not diminish with use, thus increase the market competition [14]-[15].
- Reduced greenhouse gas emissions by the increased fuel efficiencies due to integration of more renewable or low carbon DER [63]-[64].
- Allows the connection of environmental friendly technologies like plug-in electric vehicles [65]-[66].
- Increased amounts of DER can impact the development of fossil fuel based electricity supply infrastructures [15],[67].

- The expansion of DER technologies is elevating the necessity to amend standards and policies established for their connections to the grid [1],[55] [68],[69].
- DER can reduce the impacts of feeder congestion to a greater extent; that otherwise occur due to limited resources [70].
- Availability of DER can delay investments in new power plants, new T&D lines and network reinforcements [2],[71].
- Improved power supply quality and reliability [7],[59],[67].

The successful implementation of a dynamic decentralized network will require advance metering infrastructures (AMI) for the convergence of technology and bi-directional communication links with power engineering [72]-[73]. Through AMI, it is possible to not only monitor the supply and demand but also to control assets in real-time for efficient performance of the grid, thus transforming the existing grid into an intelligent grid. This fully integrated decentralized system, where all grid functionalities are met through exchange of data and intelligent management of assets, is commonly referred to as a "smart grid" [72],[74]. Existence of the AMI enable a self-healing ability to efficiently recover from system failures [7],[75].

The transition towards "smart grid" is expected to begin at distribution level, the demand side of the supply chain. Fig. 2-1 shows a number of connected feeders that illustrate the likely future developmental path for smart distribution systems. A zone substation with an on-line tap changer (OLTC) equipped transformer supplies multiple high voltage (HV) feeders through circuit breakers (CBs). Traditionally, a residential feeder could supply from a few hundred to as many as 5,000 homes distributed over a feeder length, tens of kilometres. A zone substation will typically supply up to a dozen feeders.

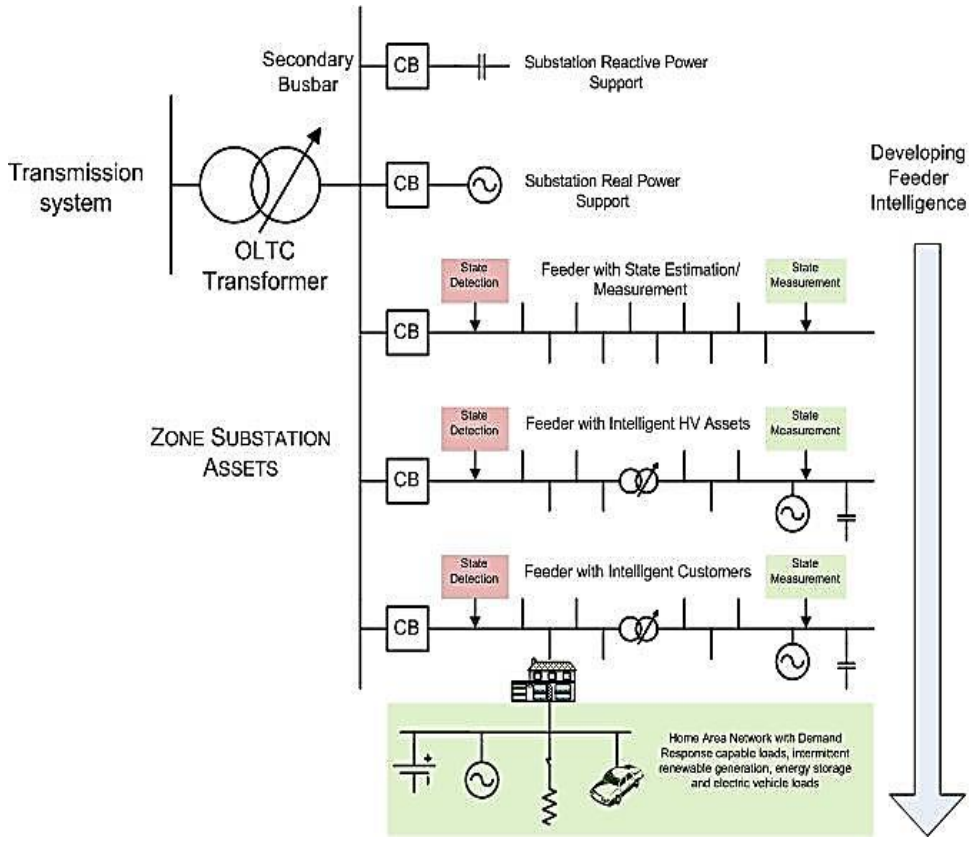

Fig. 2-1. The evolution of intelligent feeders.

In Fig. 2-1, the first feeder includes a combination of state estimation and direct state measurement. Estimated voltages can be used to optimize the operation of the OLTC. The next evolutionary stage, seen in the second feeder, is the deployment of intelligent devices such as voltage regulators and HV capacitor banks in the HV distribution network. The final evolutionary phase incorporates active and intelligent devices at distribution level and/or consumer level for coordinated control of the grid components. These could include smart appliances, renewable DG and storage from finely distributed battery systems and/or electric vehicles with vehicle to grid regeneration capability [2],[67],[76].

Thus, it is predicted that renewable DERs will be an integral part of the future intelligent grid gradually phasing out fossil based generation. However, large penetrations of DG have the potential to challenge the voltage quality of the grid. Enabling voltage and demand control mechanisms through the use of BESS could mitigate challenges of DG on the power system infrastructure and improve the

quality of supply [77]. In conclusion, the next generation grid will, therefore, materialize through strategic integration of DG, BESS and mechanisms that facilitate demand & supply management and energy efficiency.

2.3 Battery Energy Storage Technologies

Battery energy storage can fundamentally revolutionize the way we generate, deliver and consume electricity. They have the ability to entirely or partially alleviate the challenges of both stochastic and deterministic variability associated with renewable generation, hence is recognized as a strong enabler of decentralized power systems [43]. Conventionally, grid connected BESS comprises of the battery bank, control system, power electronic interface and transformer to convert the voltage, depending on the interconnection voltage level. Power electronic interface is typically bi-directional with the capability for four-quadrant operation. In other words, it can be modified to deliver or absorb real and reactive power [18]. Therefore, BESS can provide reactive support for added voltage regulation even during off renewable DG generation hours, like PV sources that are generally disconnected from the grid during off sun hours.

Based on the technology BESS can be categorized into two types; solid state batteries and flow batteries [78]. Commonly known solid state batteries are Li-ion, Nickle-Cadmium (NiCd), Pb-acid and Sodium-Sulphur (NaS) while Redox, Iron-Chromium (ICB), Vanadium-Redox (VRB) and ZnBr are widely used flow batteries. These technologies are currently in various stages of development, ranging from mature and tested (Li-ion, NaS & Pb-acid) to research and development (advanced Pb-acid & ZnBr) batteries [79]. As identified in [47], their power and energy relationship is characterized by the integration level to the grid and the purpose. General depiction is graphically presented in Fig. 2-2, however, most of these technologies have multiple uses, wider durations and power ratings than illustrated [47].

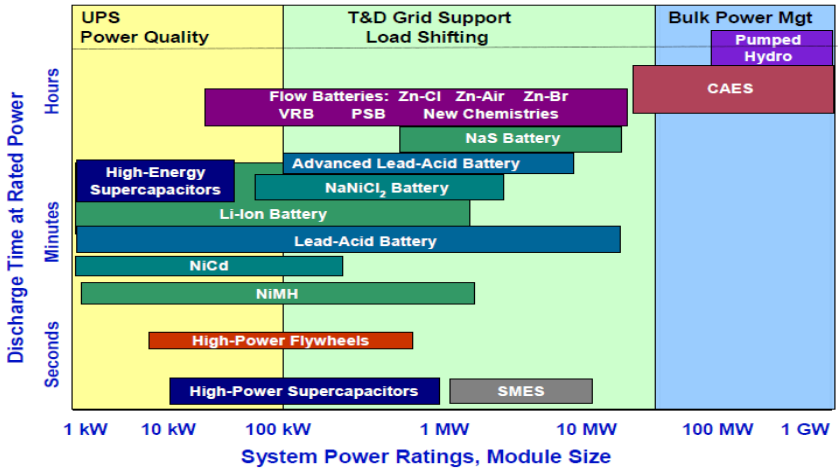

Fig. 2-2. Energy storage positioning [47].

For the purpose of discussion, advanced Pb-acid, ZnBr, and Li-ion batteries which are widely demonstrated at large scale are chosen [46].

Valve regulated Pb-acid (VRLA) batteries extends from Pb-acid batteries one of the earliest type of rechargeable storage technologies. The Commonwealth Scientific and Industrial Research Organization (CSIRO, Australia) have recently developed a unique design (namely UltraBattery) that combines Pb-acid batteries with super-capacitors [81]. The conventional Pb-acid chemistry is modified by incorporating solid electrolyte electrode or capacitors to improve their shortcomings. Therefore, advanced Pb-acid batteries offer high energy density and fast response like flywheels [47],[80]. The Fig. 2-3 demonstrates the hybrid design. The superior model is economical (no additional controls or maintenance required) and lighter, with super-fast charge/discharge rates and long cycle life. According to CSIRO, the UltraBattery has been commercialized since 2005 through various vendors in the United States, Mexico, Japan, Canada, Thailand and China.

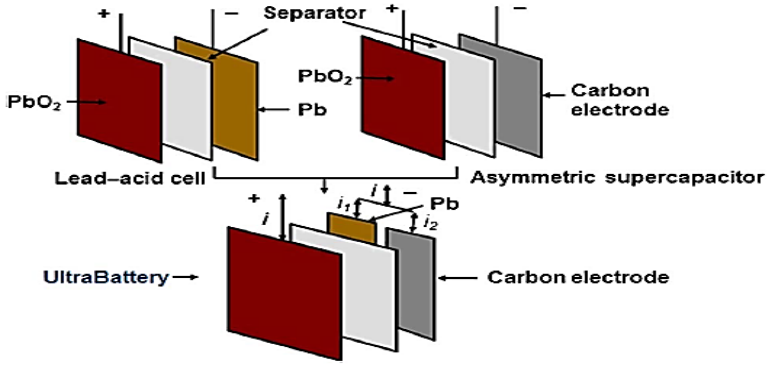

Fig. 2-3. Ultra-Battery [81].

ZnBr is a flow battery in which each cell contains two electrolyte flow streams as depicted in Fig. 2-4. Bromine is dissolved in the electrolyte, when charged or discharged; the bromine solutions get pumped through a stack of reactors and circulate back in to the reservoirs. The Anolyte tank stores the positive electrode reactions while the other is for negative reactions. The drawbacks of ZnBr batteries arise from two factors; corrosive nature of bromine electrolyte and low energy density due to the pumping mechanics and chemistry. However, these shortcomings have no implications for grid installations. The significance of this type of battery is that it can be fully discharged with no damage as the active materials do not degrade [47]. Therefore, ZnBr is still a competitive option for grid applications offering high DOD rates and long cycle life [80].

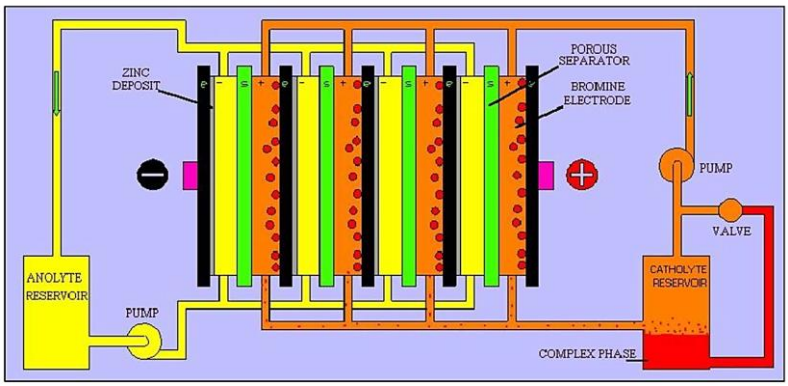

Fig. 2-4. ZnBr battery [47].

Li-ion battery technology is relatively new and was first commercialized in 1991 [78]. However, it is emerging as one of the robust and fastest growing technologies

with applications in consumer electronics, electric vehicles and currently making its transition into electricity market applications [46]. Due to its maturing position in the plug-in hybrid and all electric vehicles markets, it is predicted that Li-ion battery cost currently scaling at $274/kWh would fall to $150 by 2030 [50]-[51]. In addition, upon completion of Tesla's Gigafacory, the costs of their batteries are expected to fall by 30% to $100/kWh [50]. Batteries will be removed from vehicle once their capacity degrades to a point where the vehicle range is unacceptably reduced. These batteries may have 80% of their original amp-hour charge capacity remaining. Therefore, once removed from a vehicle, battery has a scrap value for recycling and a second-use value if it can be sold into an alternative market place [82]. Retired electric vehicle batteries provide a lower-cost storage opportunity for grid support [44].

From the performance perspective, Li-ion batteries show high energy density, high cycle life and low self-discharge rate with no hydrogen gassing [79]. The most common types of Li-ion characterized by the cell chemistry are cobalt, manganese and phosphate [80]. The Nanophosphate Li-ion technology is currently being positioned as the leading technology. Compared with other Li-ion batteries, Nanophosphate Li-ion deliver high power, improved energy density and further extended cycle life. Moreover, it is abuse tolerant with minimal internal power losses and show excellent ability to maintain power consistently over a wide range of state of charge (SoC) [83].

Fig. 2-5(a) demonstrates the capacity and impedance as a function of cycling for a 12V A123 ALM 12V7 Lithium-ion (Li-ion) battery rated at 4.6Ah/10A [83]. From Fig. 2-5(a), at the 1C/1C rate and 100% depth of discharge (DOD) the battery deliver more than 7,000 cycles with excellent energy preservation capability. Fig. 2-5(a) shows that the internal cell impedance is a function of battery cycle life. The terminal voltage characteristics against the discharging capacity at various discharge rates are illustrated in Fig. 2-5(b). Battery voltage is almost flat in the region between 0% and 90% discharge capacity and rapidly drops over 90% discharge capacity. Thus, it is advisable to operate batteries within this region.

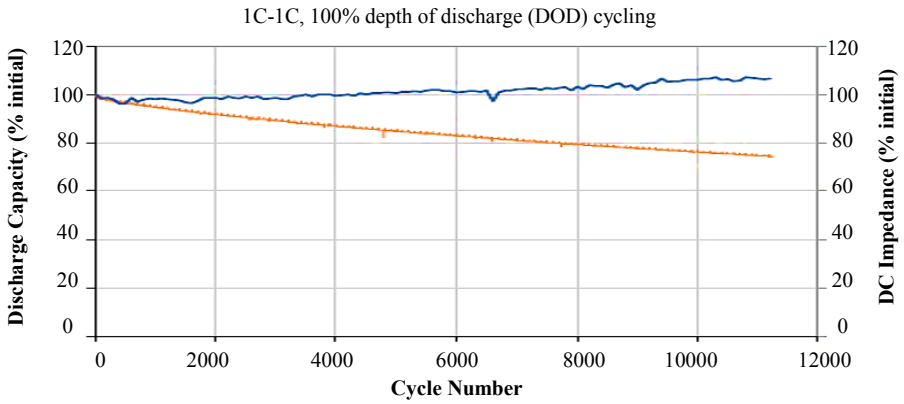

(a)

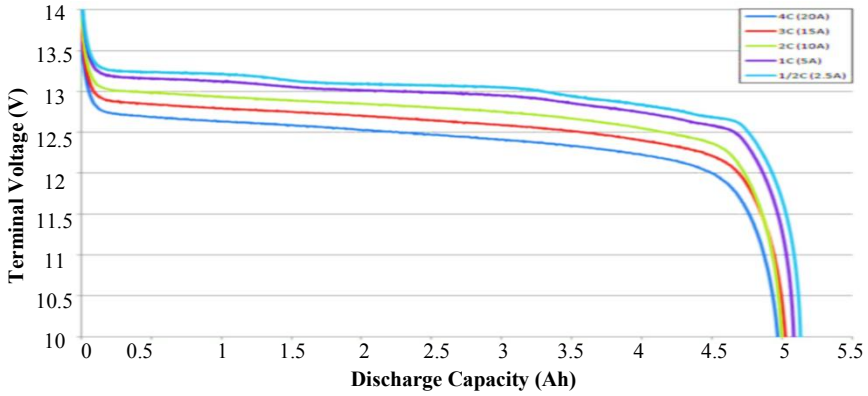

(b)

Fig. 2-5. (a) Capacity & impedance as a function of cycling at room temperature (b) Terminal voltage against discharge capacity at various discharging rates and 40^{o}C [83]-[84].

Summary of cost, technical performance and market assumptions for the selected battery technologies are presented in Table 2-1. The performance characteristics cycle life and round trip efficiency are addressed while the unit power and energy cost estimates represent average values based on information from variety of vendors according to [44].

TABLE 2-1: COST (AUD), TECHNICAL PERFORMANCE AND AVAILABILITY OF THE SELECTED BATTERY TECHNOLOGIES [44].

Parameter	**Advanced Pb-acid**	**ZnBr**	**Retired vehicle Li-ion**
Survey year	2012	2012	2012
Energy related cost ($/kWh)	682	400	291 in 2020
Power related cost ($/kW)	400	400	309 in 2020

O&M cost ($/kW/year)	43	28	28 (10 $/kWh to switch cells)
Cycle life	4,500	10,000	1,800
Round-trip efficiency	90%	70%	90%
Useable charge range	65%	80%	70%
Availability in 2030	Unconstrained	Unconstrained	933 MWh
Availability in 2050	Unconstrained	Unconstrained	22,383 MWh

2.4 Current Methods for the Optimal Integration of BESS and DG

2.4.1 Optimal Allocation and Sizing of DER

The topic of optimal integration of DER (DG and distributed storage) into the distribution system for the maximum utilization began in the 1980's [85]. Distributed generation integration techniques have been extensively studied for wind generation. Solar generation and BESSs are currently the focus of growing considerations. Due to high costs associated with them, storage systems in particular, the deployment and the research and development in the area has been slow. Over the past decade, owing to the technological progress and climate concerns, the storage has become an active field of research once again. Optimal siting and sizing of DER can ensure high penetration levels with minimal impact to the grid. The techniques proposed in literature for determining the optimal parameters fall into three main categories, (1) analytic, (2) numerical & exhaustive search and (3) meta-heuristic approaches.

Analytical approaches are structured closed-loop formulations that minimize or maximize certain objectives (i.e losses, energy). An approximate analytical approach for DG integration known as the "2/3 rule" is proposed in [86] for radial feeders with uniformly distributed loads for minimizing losses and voltage deviations. This rule suggests a DG of 2/3 of the demand requirement to be placed at 2/3 of the length of the feeder. The approach is simple and widely accepted for capacitor allocations,

which are a reactive power source, but cannot be effectively applied to feeder with non-uniformly distributed loads or meshed systems and cannot model multiple DGs. Two analytical approaches for optimal placement of a single DG unit in radial and meshed systems is presented in [87]; however, optimal sizing is not considered as the size of DG operating at unity power factor (PF) is assumed to be known. In [88], loss sensitivity factors are derived using the equivalent current injection formulations for radial systems to determine the optimal size of the required DG. The total loss sensitivity factor is minimized at each bus to obtain this optimal size. The optimal location for the DG in [88] is then determined as the bus at which lowest losses are achieved, using an exhaustive search approach.

The publications [89] and [90] propose analytical methods based on exact loss formula for optimal placement and sizing of single/multiple DGs for loss reduction. These methods adopt an approximate DG sizing formula to resolve the optimal siting issue and the optimal size is determined by incrementally increasing the DG size while observing the change in the system losses. Reference [91] presents a simple analytical approach based on algebraic equations for quick approximation of DG parameters in radial distribution feeders with uniformly distributed loads for improving voltage profile. However, distribution networks are not always radial and loads are typically non-uniformly distributed.

Typical numerical methods include exhaustive search, dynamic programming, gradient search, sequential quadratic programming, interior-point (IP) method and linear/nonlinear programming [92]. The problem of optimal DG sizing and siting to minimize financial investments in radial microgrid is solved in [93] by means of mixed-integer linear programming (MILP). Paper [93] optimizes capital and maintenance costs of DG as well as emissions costs of fossil fuel based generation in a microgrid. An exhaustive search is applied in [94] for optimal DG placement in distribution systems with variable loads to minimize system losses or main substation loading. Although the method in [94] is computationally expensive, it identifies the importance of considering voltage dependency of loads when planning DG integrations. DER allocations based on constant power loads are not technically feasible in real distribution systems. An exhaustive search approach using a c-

language tool to optimize the size and location of DG in radial systems is presented in [95]. Optimal solutions for DG site and size are determined by analysing all possible combinations of sites and sizes using the c-language tool that minimize losses and voltage drops.

Publication [96] proposes a method for allocating a storage system in distribution systems with high penetrations of wind DG. This method determines the size of storage system based on the need to reduce spillage of wind energy and the site is determined by minimizing the annual electricity cost. However, the approach in [96] cannot optimize for multiple storages and does not fully exploit storage capabilities such as peak shaving and voltage regulation. In [97], IP method based optimization problem is established to optimally allocate and size storage to provide several ancillary services to the grid. The multi-objective optimization problem in [97] minimizes storage and grid operational costs. However, this method considers radial distribution networks only and dispatch management of storage is not addressed. A MILP based method that analyses economic benefits of storage is developed in [98] for optimal sizing and management of BESS in the context of a microgrid. A unit commitment problem is formulated for dispatch scheduling and the size is derived considering peak shaving, however method cannot identify optimal BESS location and does not consider network characteristics.

Meta-heuristic optimizations minimize or maximize problems using meta-heuristic algorithms such as Genetic Algorithms (GA), Tabu Search (TS), Particle Swarm Optimization (PSO), Direct Search and Artificial Bee Colony (ABC) [92]. Characteristically, these algorithms generate a diverse range of solutions to explore in a search space and then the convergence is achieved through intensification within the search space. In [99], an ABC has been utilized for DG allocation and sizing in distribution systems to minimize system losses under constraints for feeder capacity. Costs that incorporate upgrade investments, losses and interruptions are minimized in [100] by optimally allocating and sizing non-dispatchable wind or solar DG. The method was implemented using GA for radial feeders.

GAs are extensively used in literature for optimal allocation of DER. The optimal

size of a NaS BESS is evaluated by means of GA in [101], considering cost tradeoffs between storage size, wind power and load curtailment and reliability requirements for isolated or rural grids. Paper in [102] employs a GA combined with dynamic programming to site and size distributed storage in medium voltage systems for minimizing capital and operational costs of the distribution system. The authors in [103] propose a methodology for optimal sizing and day ahead economic dispatch of storage in a microgrid with high penetrations of PV. The optimization problem in [103] minimizes capital and operation costs of storage as well as fuel and start-up costs of fuel based DGs while maximizing earnings from selling power to grid. Approach takes into account dynamic models of storages (Li-ion and VRB) and is evaluated using GA.

A TS method is presented in [104] for deriving the optimal size of storage that is integrated with thermal plants. Method minimizes storage system life cycle costs to ensure low overall production costs. A storage optimization strategy for sizing, siting and operation is developed in [105] using fuzzy PSO. Siting and sizing method in [105] maximizes the profits from energy trades, system planning, and operation cost savings in feeders with large quantities of DG. However, the rule-based operation strategy is implemented considering the need to balance demand gaps. Therefore, due to the inconsistency in the rule-based operation strategy and optimal sizing/siting objectives, the storage dispatch does not achieve the best possible outcomes and the purposes in [105].

Meta-heuristic methods like GAs show a superior performance in terms of solution errors. However, the main drawback of most meta-heuristic approaches is the low computational efficiency, thus require additional measures such as fuzzy rules or combination with numerical algorithms [106].

2.4.2 Optimal Dispatch Management

The DER dispatch management schemes are modelled for variety of purposes, ranging from economic dispatch, ancillary services and unit commitment for efficient participation in grid environments.

Publication [101] presents an optimal sizing and dispatch control strategy for a NaS battery in isolated grids where generation is primarily from wind generation. Method minimizes the cost of battery and wind generation while curtailing the load to determine the optimal size. BESS control strategy compensates power imbalances and provide frequency and voltage control if required.

In [22], a method is proposed for household energy management using energy storage to facilitate demand response management. The dynamic charge/discharge dispatch management strategy in [22] is either driven by the daily pricing signal, SoC of the storage system or the peak demand. This paper conducts a benefit quantification in terms of energy cost and investment deferral but does not consider the network characteristics or storage system life cycle costs.

Rule based control techniques for storage dispatch control are proposed in [107] for BESS installed with PV/wind systems to mitigate issues of intermittency while effectively supporting the load. This method uses hourly forecasted PV and wind generation information to determine the power level at PCC. The rule based BESS dispatch strategy in [107] ensures the desired power level is maintained while ensuring battery constraints are satisfied. Reference [108] proposes a rule based BESS dispatch management strategy to alleviate high frequency variations in rooftop PV generation while capturing surplus PV energy effectively. This approach actively monitors the PCC voltage and BESS operates when the change in the voltage exceeds a predetermined threshold limit given that the battery constraints are not violated.

The paper in [109] also proposes a rule-based operation method for commercial battery systems with PV for distribution networks with high penetrations of PV. This method assumes the cooperative participation from both network operator and consumer for voltage management. Network operator controls the dispatch of BESS in response to voltage limit violations during periods of peak demands using AMI. However, BESS is not managed during peak PV generation. Consumers who owned the PV and BESS system will in turn receive a subsidy for their participation to manage feeder voltage. Economic assessment is conducted from both consumer and

network operator's perspectives considering costs of voltage violations, peak and required equipment.

A control strategy and optimal sizing of BESS for small isolated grids with diesel, wind and PV generation are proposed in [110]. The BESS operating technique relies on a short-term forecast (hourly) unit commitment decision. The system is assumed to contain 20% spinning reserve to accommodate forecasting errors. Optimal sizing of system components in [110] are determined by minimizing levelized energy cost using GA. The levelized energy cost includes the costs of BESS, greenhouse gas emissions, O&M and fuel for diesel DG as well as fixed costs of power station.

An optimal predictive scheduling algorithm for peak load shaving for a system with PV and storage is presented in [23]. Charge/discharge control in [23] is achieved through day-ahead power management strategy that optimizes battery daily degradation and peak demand. Constraints for both battery and PCC are included in the optimization. A day-ahead scheduling strategy with real-time monitoring scheme is employed in [111] to improve renewable penetration level. A centrally coordinated day-ahead optimization method for management of demand side DG and storage systems is proposed in [112]. Method in [112] is aimed to reduce consumer momentary energy cost through demand side management but it is unable to consider grid characteristics and limitations. An hourly dispatch control and optimal sizing method is presented in [113] for a hybrid system of generators and large scale storage. The day-ahead economic dispatch and optimal sizing in [113] are determined by minimizing a cost function of annual capital and operating costs of the hybrid system. However, the issue of optimal location is not addressed.

2.5 Conclusions

So far the adoption of storage has been limited by its costs. Thanks to technology enhancements largely driven in the automotive sector, the costs of storages are declining steadily. Energy storage installation and coordination can integrate large volumes of renewable generation with the grid and support smart grid objectives. The literature review from the previous sections has shown that energy storage will

become an integral and fundamental resource altering the electricity landscape in the near future.

Many publications address the issue of dispatchable/non-dispatchable DG siting and sizing. Reference [92] contains a thorough analysis on the state of the art analytical, heuristic and numerical optimization models applied to the optimal DG placement problem, as well as future research and trends. However, minimal research studies have investigated the issue of optimal integration and management of BESS. Out of the existing storage research, most studies have been carried out in the context of microgrid, isolated grids or radial distribution systems with DGs. Typically, these methods do not take network characteristics, limitations or multiple storage installations into consideration.

In much of the literature, the DER siting and sizing optimization problem is framed as a cost function that minimizes peak demand, energy, power imbalance, energy losses, instantaneous power loss and/or financial investments in generators and storage systems. The problem is either formulated as a multi-objective or single objective function with or without constraints. Common constraints are power flow and DG/battery power/energy limitations.

Storage dispatch management is either achieved through day-ahead optimization strategies or rule-based approaches. Day-ahead schemes are formulated with the objective of minimizing a cost function similar to the siting/sizing problem. However, they do not consider the daily cycling of the storage unit and are typically unable to adjust for forecasting errors. Rule-based methods typically operate in response to pricing signals, demand gaps, voltage or power tolerance limits. Battery cycling cost is, therefore, not integrated into the methods.

In addition, two key common drawbacks of the above approaches were found:

1. The inability to assess the complete problem of siting, sizing and management of DER of the target decentralized grid. This is a critical issue as the benefits of BESS and dispatch management strategies strictly depend on the location and sizing:

2. The lack of consideration of the storage's capability to provide ancillary services to the electricity network particularly voltage control.

Practical distribution systems are often heavily loaded, geographically extensive and feed non-uniform loads. Therefore, consumers' power quality is impacted by low voltages and network operator incurs energy losses. Furthermore, the over voltage problem during peak PV generation places a limit on the amount of PV that can be connected to the grid without the need for system upgrades or reinforcements. Poor voltage profiles can cause several issues including overheating, equipment failures, nuisance tripping and decelerate the useful life of power system assets. Therefore, the problems of DER optimal siting, sizing and dispatch management needs to be assessed considering voltage violations in combination with peak shaving to ensure voltages supplied to the consumers are not affected and within permissible limits for the safe operation of the grid.

Chapter 3. A Fourier-Series Representation of Battery Energy Profile

The numerical or heuristic BESS dispatch optimization problems rely on the repeated evaluation of a solution vector of battery power or energy. The length of the vector depends on the sampling interval and the amount of batteries involved. This vector should be subject to a daily energy balance constraint to avoid over-charging or over-discharging. The dimensionality of the solution vector including the constraints add significant burden on the optimization time and the efficiency. The optimization of distributed storages in distribution systems could become even more computationally expensive due to the need to evaluate dispatch of multiple storages while satisfying various additional network constraints and topologies.

Therefore, this chapter develops a method to represent the battery energy profile compactly using a vector of Fourier coefficients in battery storage optimization problems. A key optimization constraint, that the solution is periodic for energy balance, is inherently embedded allowing a number of optimization algorithms to be efficiently applied. A compact representation can reduce the dimensionality of the optimization problem and consequently improve the speed of the optimization.

To illustrate the effectiveness of the Fourier-series based model, an optimization problem that minimizes energy costs and peak demand charges through optimal sizing and management of BESS is framed for a residential grid connected PV system with storage. Simulations were carried out using forecasted generation and demand information for day-ahead power flow management.

3.1 Compact Model of the Battery Cyclic Energy Profile

The energy of a residential battery storage system (E_B), operating with uniform daily patterns of energy demand and generation, will follow a uniform periodic cycle. A stable periodic solution requires that the remaining energy at the end of each day is constant. Any discrepancy in charge would accumulate over time leading to over-charging or over-discharging.

Fig. 3-1 shows a highly simplified battery power and energy variations. The battery storage operates over a cycle period T which is often a single day or a single week. The battery discharges at relatively high power ${P_B}^{discharge}$, during a period of peak energy demand or high tariff. The battery is recharged over the remainder of the cycle at a power of ${P_B}^{charge}$. The battery energy is the integral of power and varies between minimum (${E_B}^{min}$) and maximum (${E_B}^{max}$) limits. This is shown is equations (3-1) and (3-2). The battery energy is a continuous state variable while both power and energy are periodic functions.

$$E_B(t) = E_B(t+T) \tag{3-1}$$

$$E_B(t) = E_B(0) + \int_0^t P_B(t)\, dt \tag{3-2}$$

Where, E_B, t, T, $E_B(0)$ and P_B are battery energy, time, period, initial battery energy and battery power respectively.

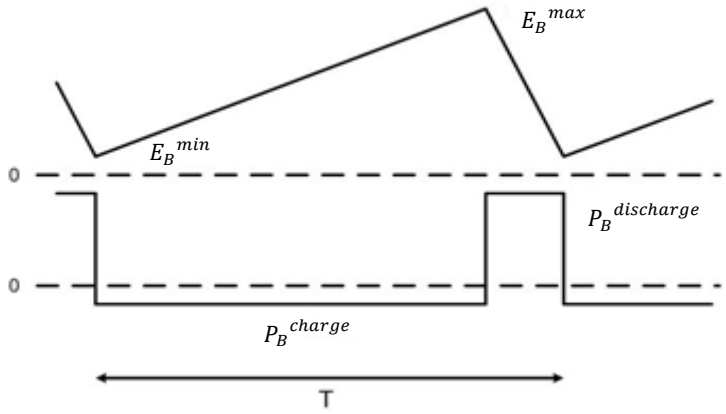

Fig. 3-1. A simplified state of charge cycle.

The optimization of a residential battery storage system will require the determination of an optimal daily profile for the battery energy. Energy cost is often a key component of the cost function to be optimized. This optimized battery energy profile determines the following parameters;

- The instantaneous battery power,

- The net instantaneous demand from/to the network, and
- Ultimately, the consumer energy supply cost.

If the daily battery energy is known, the instantaneous charging power is determined and ultimately the consumer energy cost can be determined.

The solution could be a sequential list of the energy values (C_{iT}) during the day as shown in (3-3). A vector of length (N) 24, 48 or 96 could list the E_B at one hour, 30 minute or 15 minute intervals.

$$C_{iT} = \begin{bmatrix} E_B(1) \\ \vdots \\ E_B(N) \end{bmatrix} \tag{3-3}$$

Numerical optimization processes rely upon the repeated evaluation of a cost function for a proposed solution vector. The proposed solution vectors are generated with knowledge of problem-specific constraints. In addition,

- Only limited differences can exist between any two adjacent charge states. Any limitation or constraint on the battery power places as limitation on the rate change of the E_B. A charging power limitation imposes an absolute value constraint on the difference between each adjacent E_B value within the solution vector or N constraints, where N is the same order of (3-3). This introduces a computational burden that will slow the optimization algorithm.
- The final charge state must be close to the initial charge state for the following day. This avoids over charging or discharging at the end of a cycle and correctly set the battery for flexible operation on the following day.
- A charging power constraint might be more easily applied by framing the solution vector as a list of average charging powers over each time interval. This has another disadvantage. Power can be a discontinuous function and the daily charging power frequency spectrum has increased higher frequency components relative to the energy spectrum. As such a power vector is

resistant to efforts to compactly represent a solution. A compact representation can reduce the dimensionality of the optimization problem.

A superior approach (implemented in this thesis) is to represent the periodic battery energy solution utilizing a vector of Fourier coefficients (C_{iF}) such that:

$$C_{iF} = \begin{bmatrix} a_1, b_1 \\ \vdots \\ a_n, b_n \end{bmatrix} \tag{3-4}$$

$$E_B(t) = a_0 + a_1\, cos\left(\frac{2\pi t}{T}\right) + b_1\, sin\left(\frac{2\pi t}{T}\right) + \dots\dots + a_n\, cos\left(\frac{2\pi nt}{T}\right) + b_n\, sin\left(\frac{2\pi nt}{T}\right) \tag{3-5}$$

Where, a_0, a_n, b_n, and n are the constant Fourier coefficient, Fourier cosine coefficients, Fourier sine coefficients and amount of Fourier coefficients respectively

The vector C_{iF} represents the battery energy which is, by definition of equation (3-5), periodic and continuous. Fig. 3-2 shows the battery energy profile over two periods assuming the network is stationary and operates in a truly periodic manner. Fig. 3-2 shows that the battery energy at any point in the day is the same as the energy state 24 hours before or hence. In Fig. 3-3 the battery optimization algorithm is re-applied at the end of the first cycle to allow the battery energy profiles to be progressively updated as new information and trends emerge in the operating distribution network. It must be noted that repeated and frequent re-evaluation is crucial to ensure that changing operating circumstances are smoothly integrated into the battery profiles.

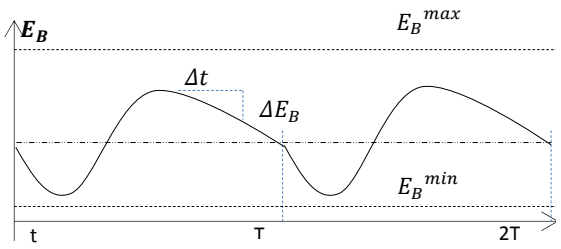

Fig. 3-2. Periodic battery energy curve over two periods.

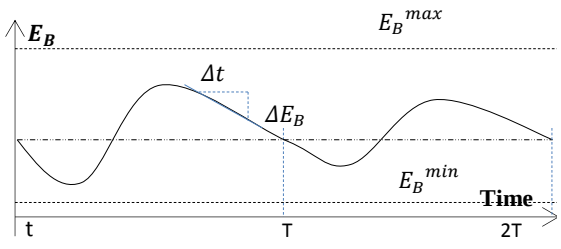

Fig. 3-3. Quasi-periodic battery energy curve over two periods.

The following points should be noted:

- As E_B is a continuous function the solution vectors will be shown, in the following sections, to be relatively short. Case studies show E_B is often an approximately triangular function and the Fourier coefficients reduce proportionally to $1/n^2$.

- A solution based on battery power, the first derivative of energy, would show a $1/n$ dependence and require a larger set of Fourier coefficients;

- The coefficient a_0 does not need to be included in the solution vector. The presence of a constant does not affect the battery charge or discharge power and has no impact on the daily energy cost. The coefficient can be set after the optimization process to ensure that ${E_B}^{min}$ is not negative or higher than an operationally required value.

Charging power does not explicitly appear in the solution vector. The peak charging powers are limited as the E_B solutions are continuous and are represented by a relative short Fourier series with rapidly diminishing high order coefficients. It will be shown that higher charging powers can be effectively discouraged by the inclusion of a peak capacity charge in the optimization cost function.

As depicted in Fig. 3-2, battery power or the rate change of E_B, can be calculated using the difference between two consecutive states of battery energy as shown in (3-7) and (3-8). Charging power of the battery is assumed to be positive and discharging power to be negative.

$$\Delta E_B = E_B(t) - E_B(t-1) \tag{3-6}$$

$$P_B(t) = \Delta E_B/(\Delta t \times \eta_c) \quad if\ P_B(t) > 0 \tag{3-7}$$

$$P_B(t) = \Delta E_B \times \eta_d/\Delta t \quad if\ \ P_B(t) < 0 \tag{3-8}$$

Where, $\eta_c = \eta_d = \sqrt{\eta_{bat}}$, η_c, η_d, η_{bat}, and Δt are battery charging efficiency, discharging efficiency, battery round trip efficiency and sampling interval respectively.

Inclusion of the battery cycling efficiency in the battery model promotes further reductions in the daily SoC swing optimizing the cycle life. Size of the BESS (3-9) is found as the difference between the maximum and minimum battery energy (found from optimization for different seasons) divided by the maximum DOD (DOD_{max}).

$$BatterySize(kWh) = \frac{|{E_B}^{max} - {E_B}^{min}|}{DOD_{max}} \tag{3-9}$$

Where, ${E_B}^{max}$ and ${E_B}^{min}$ are the maximum and minimum battery energy respectively.

Battery real life depends on number of charge/discharge cycles (3-10). The real life, q (in years), of the battery can be calculated as the ratio between rated cycle life and real cycle life (3-11).

$$Cycles = \frac{1}{2}\frac{\sum_{t=1}^{T}|E_B(t) - E_B(t-1)|}{DOD.\ BatterySize} \tag{3-10}$$

$$q\ (years) = CycleLife/(Cycles.D) \tag{3-11}$$

Where, $Cycles$, D, $CycleLife$ and q are the number of daily battery cycles, number of operating days, nominal cycle life of BESS and the battery's real life in years respectively.

3.2 Battery Cost Modelling

A comprehensive battery model that considers the cycling wear cost will be incorporated in the cost function to be minimized. The cycling component eliminates unnecessary cycling to avoid wear. Hence the model economically captures charging

and discharging cycles, thus improves the battery performance and reduces the linear SoC swing. Total battery cost ($C_{battery}$) in (3-12) considers a battery wear cost (BWC), capital cost (BCC) and replacement cost (BRC).

$$C_{battery} = \sum(BWC + BCC + BRC) \tag{3-12}$$

In this thesis, it is assumed that battery operates within the name plate ranges for temperature and charge/discharge rates. Given that battery operates within the nominal temperature range, the cycling primarily contributes to the capacity degradation affecting the performance [114]. Therefore, with decreased charge/discharge cycles, cycle age of the battery increases.

3.2.1 BWC Derivation

The relation between the DOD and cycle life is logarithmic for most cell type batteries [115]. Therefore, practical cycle life of a battery reduces significantly with higher DOD. Inclusion of a wear cost factor (3-13) captures the true cost of the battery degradation with use.

$$BWC = \frac{Cycles}{CycleLife} * BatteryCost \tag{3-13}$$

Where, $BatteryCost(\$) = BUC(\$/kWh) * BatterySize\ (kWh)$ and BUC is the battery unit cost ($/kWh). BUC is set to include an operational and maintenance cost factor.

3.2.2 BCC Derivation

Battery capital cost can be presented as a stream of equal annual payments over a specific period considering a predefined interest rate and the real life of the battery. The annual payment can be further divided by the number of operating days to determine the daily cost;

$$BCC = BatteryCost.CRF/D \tag{3-14}$$

Where, CRF is the capital recovery factor with an interest rate of i_r and $CRF = (i_r(1+i_r)^q)/((1+i_r)^q - 1)$.

3.2.3 BRC Derivation

When batteries are used as the storage elements co-located with PV, they may have to be replaced one or more times during the life span of the PV system. Generally PV systems have a life span of about 20-25 years.

Number of times battery needs to be replaced can be calculated as (3-15),

$$y = PVlife/q \tag{3-15}$$

Hence battery replacement cost calculated daily assuming $i_{d=}i_r$,

$$BRC = BCC.\sum_{y=1}^{Y}(1+i_d)^{-qy} \tag{3-16}$$

Table 3-1 shows the summary of battery parameters used in the battery cost modelling.

TABLE 3-1: BATTERY PARAMETERS.

BUC	$CycleLife$	DOD_{max}	D	i_r	$PVlife$	η_{bat}
300 $/kWh	3000 Cycles	80%	285 Days	4%	20 Years	90%

3.3 PCC Operation of PV, Battery Model

Battery storage units are co-located with domestic PV installations to enable power flow management. Fig. 3-4 demonstrates the PCC operation and model of a residential PV system integrated with a battery device.

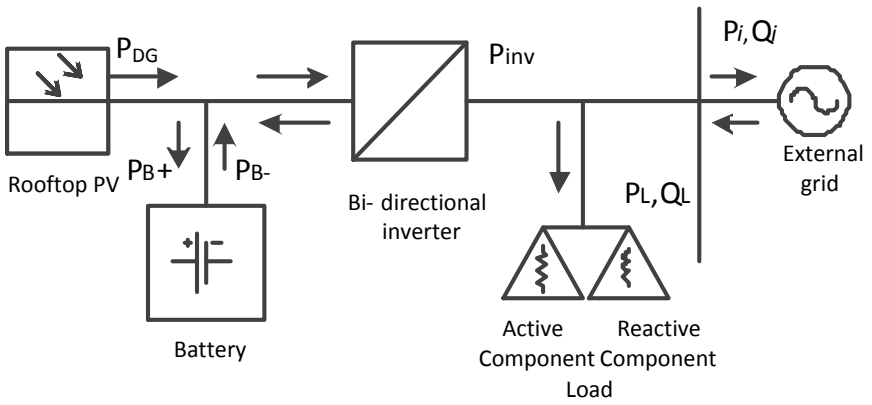

Fig. 3-4. PV and battery grid connected system.

Equation (3-17) evaluates the inverter power at unity PF. Equation (3-17.1) defines the inverter export power (positive) when the solar generation is greater than the battery charging power or when the battery is discharging with or without solar generation. The second equation (3-17.2) defines the inverter import power if the battery is charging from the grid and/or solar. If there is no solar generation battery charging will be purely from the grid.

$$S_{inv}(t) = P_{inv}(t) = \begin{cases} [P_{DG}(t) - P_B(t)] \cdot \eta_{inv} if\ P_{inv}(t) > 0 \\ [P_{DG}(t) - P_B(t)]/\eta_{inv}\ if\ P_{inv}(t) < 0 \end{cases} \quad (3\text{-}17)$$

Where, P_{inv}, P_{DG}, S_{inv} and η_{inv} are inverter power, DG output power, inverter apparent power and inverter efficiency respectively.

PV inverters are typically designed to operate in both active and reactive power modes. As specified in AS4777.2 the PF of the inverter, unless exempted by the network operator, shall be in the range of 0.95 leading to 0.95 lagging for all outputs from 20% to 100% of rated output. However, reactive power capability is not activated by default. The current practice is to operate the inverter at unity, hence do not inject or absorb any reactive power [39]. Nonetheless, there is a growing awareness to make use of the reactive power capability of large scale PV plants for voltage regulation [116]. Due to low X/R ratios reactive power is less effective in regulating the voltage magnitudes in LV distribution feeders than in HV grids. Thus, voltage support in distribution systems requires more real power management. Hence

the PF will generally be restricted to a limited range around unity PF. However, at high penetration levels reactive power from PV can reduce the investment needs for voltage regulators but this could lead to higher current and losses thus lower the system performance efficiency.

Equation (3-18) calculates the reactive power supply if the inverter is set to operate in both active and reactive power generation mode. Equation (3-19) evaluates the corresponding active power output at non-unity PF.

$$Q_{inv}(t) = S_{inv}(t).sin\theta \tag{3-18}$$

$$P_{inv}(t) = S_{inv}(t).cos\theta \tag{3-19}$$

Where, θ is the PF angle.

If the system in Fig. 3-4 is connected to distribution system at bus i, the active (P_i) and reactive (Q_i) power balance at the load bus i can be expressed as shown in Equations (3-20) and (3-21). P_i and Q_i will be positive when power is being exported, otherwise negative.

$$P_i(t) = P_{inv-i}(t) - P_{L-i}(t) \tag{3-20}$$

$$Q_i(t) = Q_{inv-i}(t) - Q_{L-i}(t) \tag{3-21}$$

Where, i is the bus number $i = j = 1,2,..,nbus$, P_i, Q_i P_{L-i}, Q_{L-i} and P_{inv-i} are bus i active power, bus i reactive power, active load power at bus i, reactive load power at bus i and grid connected inverter power at bus i respectively.

3.4 The Optimization Problem

3.4.1 With the Fourier Representation – Case 1

The optimization problem target is to optimize the battery dispatch to minimize the daily energy cost and peak demand charges while ensuring economic performance of the battery. Optimal size of the BESS (3-9) can be found as the difference between the maximum and minimum battery energy (found from optimization for different seasons).

The objective function is formulated as:

$$min\ f(C_{iF}) = C_{energy} + C_p + C_{battery} \tag{3-22}$$

Where, C_{energy}, C_p, $C_{battery}$ are cost of energy, peak demand support and battery.

- The daily energy cost is determined by the tariff rate $Rate(t)$ and the $P_i(t)$. C_{energy} ensures that the total load is not increased.

$$C_{energy} = \sum_{t=1}^{T} \begin{pmatrix} |P_i(t)|.Rate(t).\Delta t & if\ P_i \le 0 \\ -P_i(t).S_{Rate}.\Delta t & if\ P_i > 0\ and\ |P_{DG-i}| \ge |P_i \\ -(P_{DG-i}(t).S_{Rate} + |P_i(t) + P_{DG-i}(t)|.S_{NRate}).\Delta t & if\ P_i > 0\ and\ |P_{DG-i}| \le |P_i \end{pmatrix} \tag{3-23}$$

Where,P_{DG-i}, $Rate, S_{Rate} = 40c/kWh$ and $S_{NRate} = 7c/kWh$ are DG power at bus i, energy sale tariffs (Peak 7am–11am and 5pm-9pm, 40.14c/kWh; Shoulder 11am-5pm, 20.42c/kWh and Off-peak all other times 10.78c/kWh), renewable energy buyback rate and non-renewable energy buyback rate respectively.

- C_p is the peak supporting cost as expressed using a peak demand charge r_{pk} and the peak power (P_{max}) as seen at battery PCC.

$$C_p = P_{max}.\Delta t.r_{pk} \tag{3-24}$$

Where, P_{max} and $r_{pk} = \$200/\text{kVA/yr}$ are magnitude of the peak power (export or import) and peak demand charge respectively.

The consumer energy bill is usually determined by the C_{energy}. A negative C_{energy} would indicate that the consumer is making a profit; otherwise it is payment to the utility operator. In many instances a societal benefit can be realized by controlling the peak demand. Residential battery storages are technically able to limit the peak demand placed on the distribution infrastructure but an appropriate price signal is required. This can either be a cost, in the form of a peak demand charge, or a benefit, in terms of a reduced head-works charge prior to connection. Therefore, the cost component C_p is adopted in the optimization algorithm to minimize peak. The peak demand charging was applied equally to the import and export of power.

The cost component $C_{battery}$ effectively minimizes daily cycling through optimal charge/discharge and DOD management. Therefore, extend the life expectancy of the battery by avoiding wear and tear due to unnecessary cycling. Augmented cycle life will translates to lower ownership costs improving the overall performance and value.

A direct search optimization algorithm named Pattern Search (PS) by Matlab optimization toolbox is used to carry out the simulations of the unconstrained problem in (3-22). The meta-heuristic tool ensures that the solution reaches a global minimum and is suitable to demonstrate the effectiveness of the Fourier-series representation of battery.

3.4.2 Without Fourier Representation – Case 2

The optimization problem without the Fourier representation is a function of C_{iT} and can be expressed as;

$$min\ f(C_{iT}) = C_{energy} + C_p + C_{battery} \tag{3-25}$$

The objection function is now subject to an energy balance constraint (3-26) to set the BESS correctly for the following day operation.

$$|E_B(t-1) - |E_B(t)| < \Delta {E_B}^{max} \tag{3-26}$$

Where, $\Delta {E_B}^{max} = 1kWh$ and $\Delta {E_B}^{max}$ is the maximum change in the two consecutive charge states. This was chosen based on Case 1 results which had a maximum change of 0.7kWh.

3.5 Test System Data

The Fig. 3-5 shows the 24 hour (sampled at 15 minute interval) domestic load and PV generation profiles for a synthetic residential customer with a solar array and battery storage system. The daily energy consumption is 25.1kWh. While this example is artificial the daily load pattern and energy consumption are broadly representative of domestic winter loads. The solar generation data are taken from an existing 6kW array, [117]. The winter day solar generation is 17.7kWh.

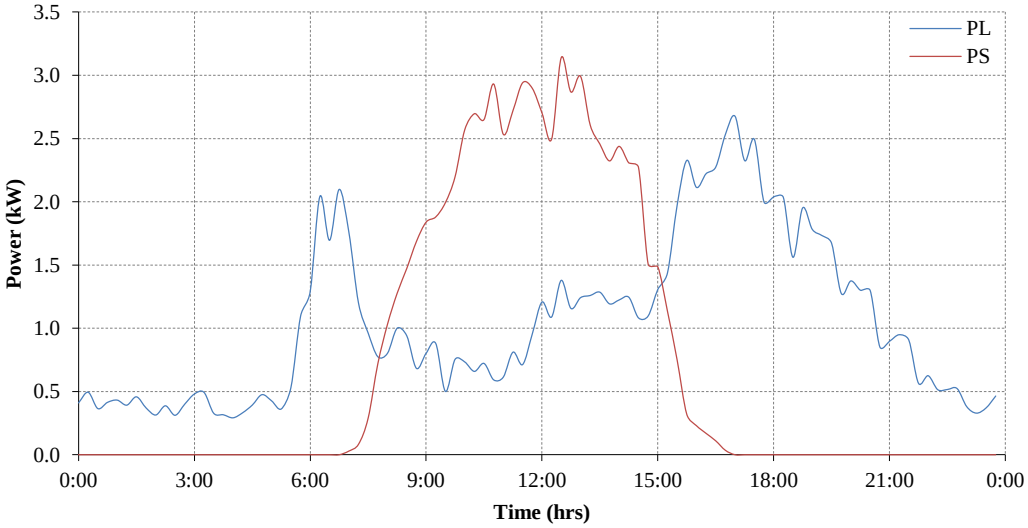

Fig. 3-5. Daily load and PV generation profiles.

3.6 Discussion

The optimization results are summarized in Table 3-2 for three different optimization scenarios. In the Table 3-2, Base, Case 1 and Case 2 indicate the scenarios without optimization, optimization with Fourier coefficients (FC) and optimization without FC respectively. The optimization results included in Table 3-2 are the optimized battery storage capacity, daily energy cost and the simulation time.

The issue of the solution vector length is considered in Case 1. The length of the Fourier series coefficient vector (n) has been varied from 1 to 16. The following points can be made in relation to the FC vector length;

- The major features of the solution are captured with vectors of length four or higher.
- With 16 coefficients the solution time is over a minute; this is about 10 times that of with 8 coefficients.
- With 16 FCs the improvement in the daily energy cost is no more than \$0.05 compared to the profit from the previous case with 8 FCs.
- Although, Case 2 results show bit more improvement in the cost figures, the computational time is significantly high due to the vector length as well as the constraints. Optimization takes more than 8 minutes to reach the solution; 65 times larger than Case 1 with 8 FCs.
- Therefore, for the balance of this thesis a vector length of 8 (n =8) is recommended for the numerical optimizations of storage integration problem in the following chapters.

Rapid fluctuations in load power cannot be compensated given the bandwidth restrictions of a short solution vector. For a solution vector of 8 (8 sine and 8 cosine), the highest frequency components have a three hour period. Load fluctuations, however, can occur in 15 minutes intervals. The Table 3-3 presents the Case 1 FC values. From the case studies, the Fourier coefficients reduce proportionally to $1/n^2$

and battery energy curves are often approximately triangular functions (Fig. 3-6).

TABLE 3-2: SUMMARY OF RESULTS.

Case		**Battery Size (kWh)**	**Daily Energy Cost ($)**	**Time (s)**
Base		NA	1.21	0.05
Case 1	No. of FC (n)			
	1	15.58	-1.08	0.11
	2	20.73	-2.29	0.56
	4	22.19	-2.65	2.69
	8	23.72	-2.88	7.92
	16	23.45	-2.94	79.89
Case 2		22.05	-2.98	515.92

TABLE 3-3: CASE 1 SOLUTION FOURIER COEFFICIENTS.

No. of FC (n)		**1**	**2**	**3**	**4**	**5**	**6**	**7**	**8**
1	Sine	4.702							
	Cosine	-4.090							
2	Sine	6.202	1.127						
	Cosine	-4.948	-0.952						
4	Sine	6.342	1.013	0.171	0.022				
	Cosine	-4.525	-1.069	0.375	0.519				
8	Sine	6.565	1.227	0.006	0.029	0.077	-0.082	-0.079	0.010
	Cosine	-5.127	-0.943	0.432	0.466	-0.060	0.020	0.015	-0.044
16	Sine	6.531	1.329	0.116	-0.097	0.047	-0.064	-0.162	0.010
	Cosine	-4.020	-1.112	0.381	0.581	-0.075	-0.009	0.013	-0.034
		9	**10**	**11**	**12**	**13**	**14**	**15**	**16**
	Sine	0.039	-0.004	0.010	0.042	0.014	-0.052	-0.027	0.013
	Cosine	-0.072	0.002	0.054	-0.003	-0.026	0.040	0.004	-0.024

The Fig. 3-6 shows the battery energy profiles for each simulation scenario. It must be noted that coefficient a_0 or the minimum SoC is not included in the curves as it has no effect on the battery power or rate of change in battery energy. The optimal

size of the battery with 8 FCs was found to be 23.72kWh. This is slightly lower than the daily energy demand of 25.1kWh.

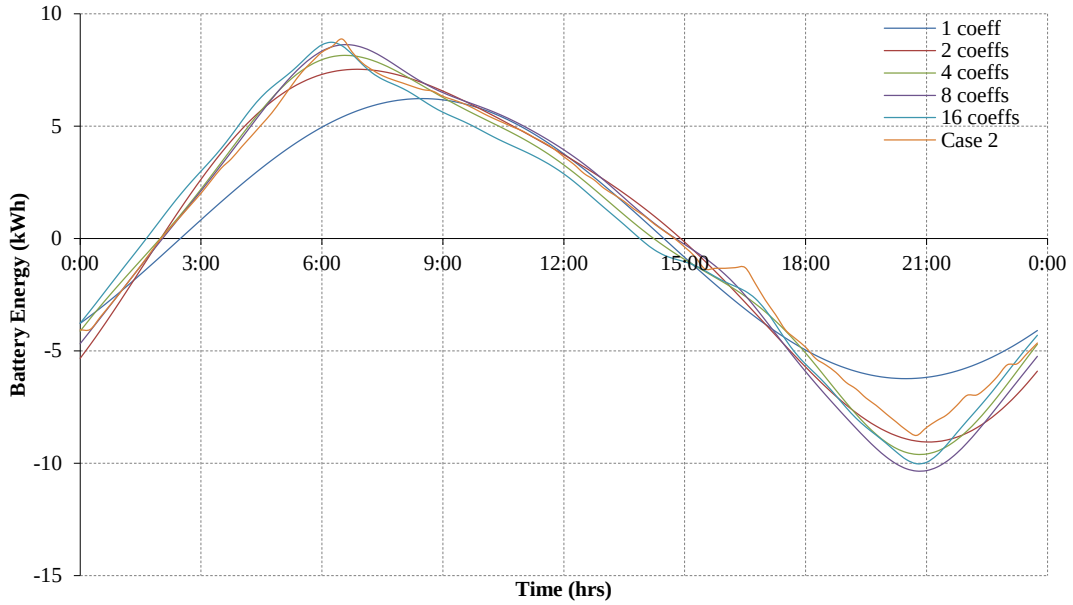

Fig. 3-6. Battery energy profiles.

Fig. 3-7 and Fig. 3-8 show the resulting battery and grid power curves respectively for all simulation cases. The results with 8 FCs show the following features:

- The battery discharge is controlled during the day to maximize the export of solar power between 7.30AM and 3.30PM, the peak export is 3.01kW;
- The discharge is controlled to force the grid power to near zero between 4.00PM and 5.00PM (shoulder) and 5.00PM and 9.00PM (peak);
- Energy is purchased between 9.00PM and 7.00AM (off-peak), the peak import power is 3.01kW;
- There is a short period 7.00AM to 7.15AM where some energy is purchased on the peak. This is a common feature across all simulation scenarios. The algorithm has had difficulty in dealing with a rapid change in consumer load at that time.

The results of optimizing the cost function with the peak charge has restricted the peak import to 3.01kW and this closely matches the solar export, remains effectively

unchanged at 3.01kW. An equal use of the system capacity represents the best economic use of the available capacity if export and import are equally weighted. It is notable that the grid demand is held close to the peak value from 11.00PM until 5.00AM.

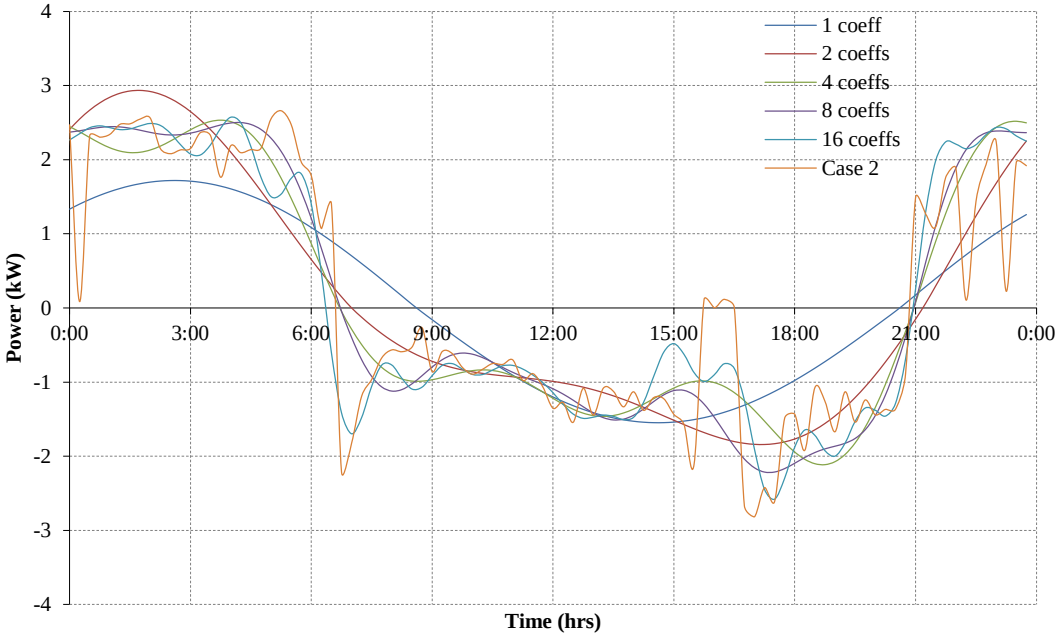

Fig. 3-7. Battery power curves.

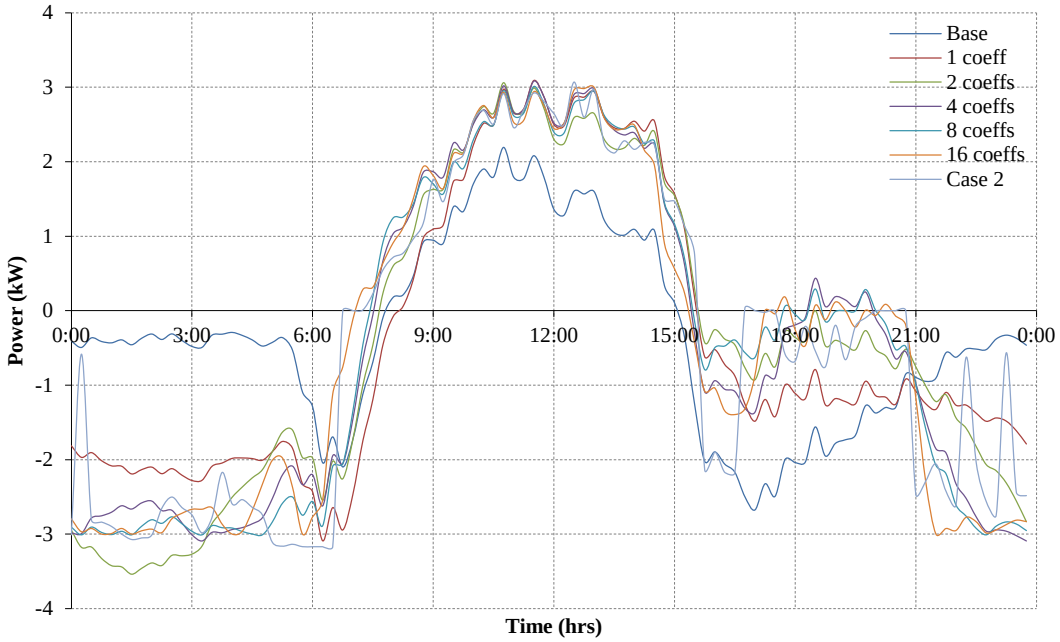

Fig. 3-8. PCC power.

3.7 Conclusions

The control of dispersed generation will require new tools for the optimization of large numbers of storages. The daily energy of a battery storage system can be compactly represented by means of a Fourier series coefficient vector. The Fourier representation of stored energy has advantages when used to frame optimization problems. Energy is a continuous variable. A short vector representation that inherently encapsulates constraints with respect to periodicity and continuity will help reduce the dimensionality of any optimization problem. This chapter has shown the performance of the compact Fourier representation in terms of convergence speed, accuracy, continuity and periodicity. The absence of discontinuities places some inherent restrictions on battery power. A Fourier vector length of 8 was proven to show superior performances; achieves great balance between simulation speed and optimized energy cost.

The generic optimization tool, Matlab PS, was easily able to optimize the operation of the domestic battery storage with a time-of-use tariff and solar energy buy-back incentive using the Fourier representation. The inclusion of the peak demand cost was effective in balancing the battery and grid peak power.

Distributed storage provides a degree of freedom for customers to control their consumption patterns, source of generation and, in turn manage time of use energy costs and peak demand charges. Improved flexibility on consumer side would facilitate active consumer participation in the electricity market. Providing the flexibility especially in feeders with high penetrations of small scale generation like rooftop PV, ensure that the community's demand for electricity is met by the lowest cost combination of demand and supply side options.

Chapter 4. Adaptive Management of Community Scale BESS for Peak Shaving

4.1 Introduction

Optimal connection of distributed storage either at grid or community scales can improve the utilization of existing network assets and support the uptakes of DG. This chapter aims to examine the integration of community scale battery storage into low voltage distribution networks with high penetrations of DG for load levelling and peak curtailment. The BESS could be owned and operated by various entities. Distribution system operators may co-locate storages with distribution transformers to provide local support in LV networks with capacity or voltage regulation constraints. Local collectives such as gated or housing communities may operate storage to reduce energy costs. In either case, the dispatch of BESS must be optimized with respect to the timing of energy imports or exports.

This chapter presents two algorithms for optimizing the size and diurnal operation of large scale grid tied BESS. The battery diurnal energy profile is represented using a vector of Fourier coefficient as proposed in Chapter 3.

Two novel predictive BESS management approaches that schedule optimal battery operation for twelve hours into the future are proposed. Method uses forecasted load and generation data; data could be measured at a desired sampling interval.

- The first model proposes a cost based adaptive predictive optimization method (APOM). Financial benefits of BESS are analysed against its ability for demand management.
- The rule-based second approach uses a Fourier series approximation of forecasted aggregated load to determine the BESS operation schedule.

Battery evaluation is updated six hourly as new information become available, to respond to changing future predictions in load and PV generation. The proposed strategies can readily be applied to storage systems co-located with distributed renewable energy sources. The methods are tested using data gathered from a Western Australian distribution feeder studied under the Solar City PV Saturation Trial.

4.2 Proposed System

4.2.1 Representation of the System

Deployment of storage can be done either at a fine scale and spread across the customers of the distribution network or centrally located at the distribution substations or a selected bus. Higher degree of flexibility and load levelling can be achieved with finely distributed BESS. However, cost for development of communication infrastructures for the management of these storage units will be relatively high. Capital costs of equipment, infrastructure and installation as well as operational, administration and maintenance costs increase with the dimensionality of the communication framework [118]-[119].

Hence, the first stage storage integrations in the evolution of the electricity grid are likely to emerge at the distribution side mostly co-located with distribution transformers; and it will be a core ingredient in smart grid. These centralized systems would be more appealing as a result of reduced dimensionality of the required advanced communication infrastructures thereby offering improved accessibility for performance monitoring and data transmission, with low overhead requirements.

The construction of an efficient communication layout for the next generation grid still needs extensive studies. Papers [73] and [120] give a comprehensive review on standards, technologies and design & implementation requirements for communication protocols.

In this chapter, joint operation of the distribution network and BESS is considered with the opportunity for centralized co-ordination of battery energy storage at the distribution level. The objective is to develop an optimal management strategy that

enables the operation of BESS in parallel with the grid and/or loads. The conceptual design of the system is demonstrated in Fig. 4-1.

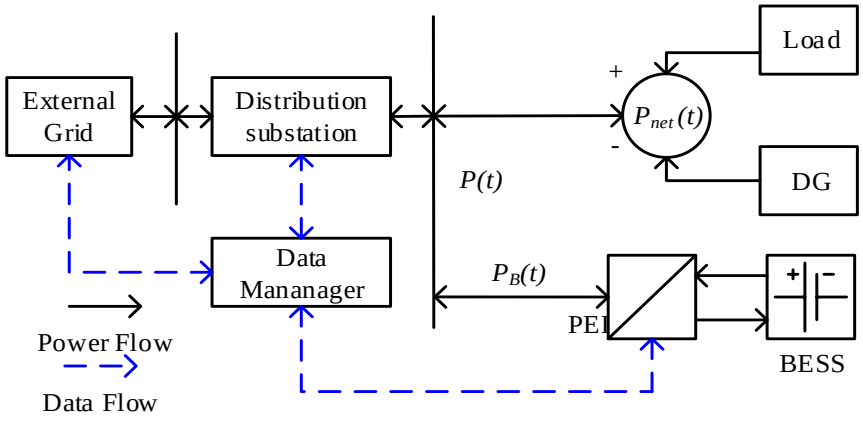

Fig. 4-1. Conceptual system design.

The grid scale battery unit is connected to the grid through a bi-directional power electronics interface (PEI). A PEI typically contains an inverter/charger, bi-directional switches, protective equipment and communication devices. Each respective component in PEI will typically be integrated with distinct control systems in smart grid.

Chapter assumes the operation of the bi-directional inverter/charger in the active power mode (in the unity PF mode). Therefore, does not inject or absorb reactive power. However a four-quadrant power electronic converter for the BESS can inject reactive power to the network providing improved voltage regulation and reduced reactive power losses. The X/R ratios of distribution lines are typically low. Reactive power injections or absorption does not strongly affect voltage at distribution level but certainly can impact upon losses.

The instantaneous power at the PCC in Fig. 4-1 can be expressed as,

$$P_i(t) = P_B(t) + P_{net}(t) \tag{4-1}$$

Where, P_{net} is the net load and generation power at battery bus.

The net power (P_{net}) is the aggregated sum of loads and DER generations. On

occasions of reverse power flow total P_{net} can become negative.

Fig. 4-2(a) illustrates the issue of peak demand and peak generation during low load conditions. The Fig. 4-2(b) is an example of anticipated ideal smoothed load curve with the optimal management strategy in place.

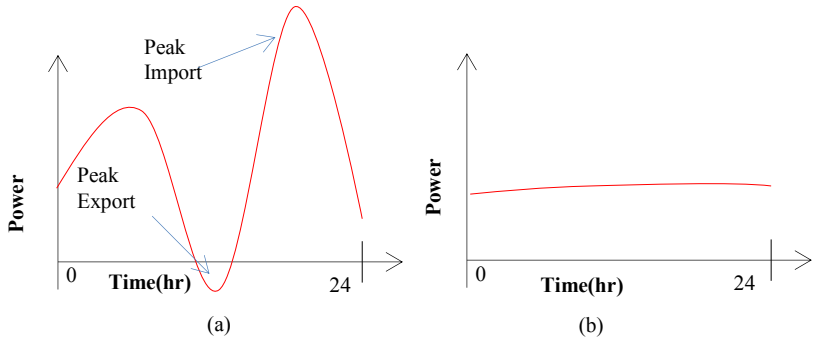

Fig. 4-2. Load distribution at distribution substation (a) Exemplary load distribution with no control (b) Smoothed load distribution with control.

4.2.2 Hierarchical Approach

This chapter proposes a receding horizon hierarchical control approach for BESS management. The structure of the system is presented in Fig. 4-3.

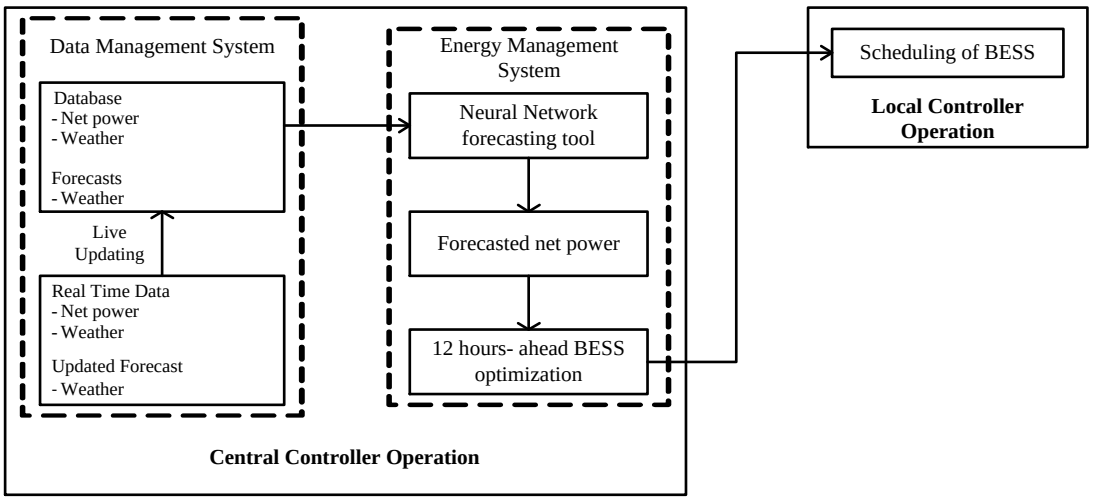

Fig. 4-3. Proposed system architecture.

Central controller performs the proposed predictive optimization to identify the optimal charge profile of the BESS. It is composed of two systems, data management system (DMS) and an energy management system (EMS). DMS establishes a bi-

directional communication link with the network for online data acquisition. DMS monitors net power flow P_{net} as well as climate information including temperature, solar radiation and humidity at a predefined sampling interval. Typical sampling intervals (Δt) are 10, 15, 30 minutes or one hour.

By centralizing the information and controls the DMS is able to consistently monitor the performance and provide safety oversights. As new information become available the DMS archives them in the historical database and process them along with future forecasts of weather. Collected data are then fed to EMS. EMS first carries out the forecasting of the P_{net} 12 hours into the future using the neural network (NN) forecasting tool. BESS management system (BMS) uses the forecasted load data to solve the battery management problem. BMS determines the optimized dispatch schedule of the BESS in terms of charging/discharging response and charge state.

The EMS then sends the optimized battery set-points for 12 hour ahead scheduling of the BESS to the local controller in PEI. Battery set points can be transferred as the charge/discharge rates or battery energy.

Operation of the proposed system is conducted for twelve hours into the future at a twelve hour receding horizon prediction scale and a six hour update time scale. Six-hourly updating scheme is aimed at adaptive minimization of prediction errors while maximizing the value of the overall system. The daily energy consumption and peak demand is a strong function of exogenous variables especially temperature, relative humidity. Adaptive management technique captures and updates real time data and any discrepancies in the forecasted parameters improving the accuracy and efficiency of the proposed system.

4.3 Adaptive Predictive Optimization Model (APOM)

4.3.1 Optimization Problem

Performance of BESS depends on several internal and external parameters. Internal parameters like production technology, design and material are usually uncontrollable and set by manufacturer. However external parameters charge/discharge rates and DOD are easily manageable and have large impact on the

battery cycle life. By managing the battery rates a tradeoff between battery cost and system performance can be achieved with extended cycle life.

The optimization problem defined in (4-2) aims to minimize the daily operational cost by optimizing the use of battery for power flow management. Daily operating cost is obtainable in terms of costs incurred due to peak support (C_p), daily energy ($C_{energy-new}$) and battery ($C_{battery}$). The terms C_p and $C_{battery}$ are as derived in Chapter 3.

Cost function is repeated below,

$$min\ f(C_{iF}) = C_p + C_{energy-new} + C_{battery} \tag{4-2}$$

As P_{net} is the aggregated load and generation, in this study, cost of energy ($C_{energy-new}$) is expressed below,

$$C_{energy-new} = \sum_{t=1}^{T} P_i(t).Rate(t) \tag{4-3}$$

4.3.2 Battery Constraints

Below battery constraints are implemented for the battery power and energy to ensure safe operation and protect the battery from over charging or over discharging.

$$P_B{}^{min} < P_B(t) < P_B{}^{max} \tag{4-4}$$

$$E_{Bat}{}^{min} < E_B(t) < E_{Bat}{}^{max} \tag{4-5}$$

Where, $P_B{}^{min}$ and $P_B{}^{max}$ are lower and upper limits of P_B respectively and $E_{Bat}{}^{min}$ and $E_{Bat}{}^{max}$ are lower and upper limits of E_B respectively.

However, the battery constraints were not imposed in the optimization as the sizing of the BESS is part of the problem at hand. Nonetheless, as discussed in Chapter 3,

the absence of discontinuities due to Fourier method poses some inherent restrictions on battery power.

4.3.3 Optimization Algorithm

The constrained non-linear problem is solved using a hybrid GA and PS algorithm in MATLAB [121]. Utilization of the hybrid approach improves the convergence efficiency of the optimization. The convergence speed of the direct search tool PS is improved by providing GA solution as an initial solution.

4.3.4 Adaptive Optimization

This section provides a description on the methodology followed, also summarized in Fig. 4-4. The optimization was applied at a 6 hour time step to predict the next 12 hour BESS schedule. Key steps are,

Step 1. The NN tool forecast the future net load values at hourly intervals for the next 12 hours. $P_{net}(t+m); m \in (0,12/\Delta t]$.

Step 2. The forecasted values are then supplemented with previous true values of $P_{net}(t-m); m \in [0,12/\Delta t - 1]$;extending eleven hours into the past to produce a 24 hour net load profile.

$$P_{net}(t+m); m \in [-12/\Delta t - 1,12/\Delta t] \tag{4-6}$$

Step 3. Optimization is carried out for the 24 hour P_{net} to determine the optimal daily battery energy profile that minimizes the cost function.

Step 4. Obtain the optimized BESS energy profile and send to local controller.

Step 5. Repeat Steps 1-4 in six hours.

Step 6. The new predicted battery charge profile $E_{B-new}(\phi)$ is then used to update the previously optimized energy profile $E_{B-old}(\phi)$ for the current updating time step ϕ (includes the overlapping time gap). Updating is performed using an exponential smoothing technique;

$$E_{B-updated}(\phi) = \alpha . E_{B-new}(\phi) + (1-\alpha) E_{B-old}(\phi) \quad (4\text{-}7)$$

Where, α is the smoothing factor; $0 < \alpha < 1$.

Step 7. Repeat the process every six hours (the updating time step).

Exponential smoothing is applied recursively at each updating time step. Each updated smooth battery forecast is computed as the weighted average of the new forecast and the previous smoothed battery forecast for a given ϕ. Balance between the new and old forecasts are controlled by the smoothing factor α.

A largest value to the α is given to allow the recent values of battery profile forecast to have a greater influence on $E_{B-updated}(\phi)$, less weight to the immediately preceding forecast and even less weight to the forecast from before that and so on. The weighting decay exponentially with the distant to past forecast for the current time step.

Algorithm 1: Adaptive Predictive Optimization

1. **Inputs**: $P_{net}(t+m); m \in [-12/\Delta t - 1, 12/\Delta t]$ as defined in Step 1 and Step 2, battery constraints ${P_B}^{min}$, ${P_B}^{max}$, ${E_B}^{min}$, ${E_B}^{max}$ and R_B.
2. Initialize inputs and generate initial C_F.
3. **while** $|\Delta f| > tol.f$ **and** $constraints > tol.cons$ **do**
   3.1. Evaluate cost function f in (3-22).
   3.2. Evaluate constraints.
4. **end do**
5. **Output**: Optimized f and C_{iF}.
6. Evaluate E_B(3-5) and charge/discharge rates as in (3-7)-((3-8).
7. Repeat 1-6 in six hours (updating time step).
8. Update E_B for time step ϕ using (4-7).

9. Repeat 1-8 6 hourly using updated P_{net}.

Battery size could be found from (3-9).

Fig. 4-4. Pseudo code for APOM to determine optimal battery energy and charge/discharge rates. Δf is the change in f, $tol.f$ and $tol.cons$ are tolerance level for Δf and constraints.

4.4 Rule-Based Discrete Fourier Transform Model (DFTM)

Discrete Fourier Transform (DFT) based model is developed based on a Fourier series approximation of the net demand (P_{net}). DFT coefficients of the P_{net} are evaluated using,

$$A_0 = \frac{1}{N}\sum_{m=1}^{N} P_{net}(m) \tag{4-8}$$

$$A_k = \frac{2}{N}\sum_{m=1}^{N} P_{net}(m).cos(k\frac{2\pi}{N}m) \tag{4-9}$$

$$B_k = \frac{2}{N}\sum_{m=1}^{N} P_{net}(m).sin(k\frac{2\pi}{N}m) \tag{4-10}$$

Where, k is the frequency index. P_{net} is sampled at Δt and has a vector length of N.

Discrete Time Fourier Series (DTFS) or the inverse DFT of P_{net} can be numerically derived as expressed in (4-11). $x(m)$ is the low frequency estimation of P_{net}.

$$x(m) = A_0 + \sum_{k=1}^{k_{max}}[A_k\, cos(k\frac{2\pi}{N}m) + B_k\, sin(k\frac{2\pi}{N}m)] \tag{4-11}$$

Where, k_{max} is the highest value of k.

Fig. 4-5 shows the 24 hour exemplary P_{net} and its DTFS with p set to one, four and eight. As theoretically expected the accuracy of $x(m)$ increases with more coefficients. A strong consistent low frequency estimation of P_{net} is achievable with eight coefficients. Aggregated load curve appear to be greatly dominated by the low frequency components implying that capturing of the key turning points of the load is

conceivable with the low frequency representation.

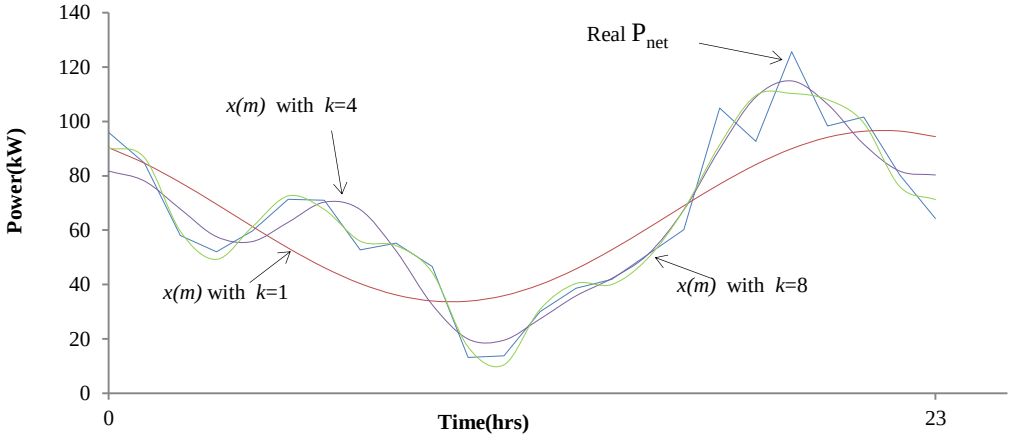

Fig. 4-5. A real load curve and its Fourier series with varying number of coefficients.

The proposed rule-based strategy can be explained as below.

Step 1. Obtain true P_{net} for a period of 24 hours from true values extending 11 hours into the past and 12 hours into the future; same as (4-6).

Step 2. Derive the Fourier series $x(m)$ and DFT coefficients $[A_0\ A_k\ B_k]$ of P_{net}. The value of k is set to eight.

Step 3. The value of A_0 will be set as the desired smoothed load as shown in Fig. 4-6.

Step 4. Strategic approach is to identify the key turning points to define periods of BESS charge/discharge and battery rates. The charge (t_{ch1}) and discharge periods (t_{dch1} and t_{dch2}) are estimated as demonstrated in Fig. 4-6. Identification of charging periods and discharging period allows the effective evaluation of charge/discharge rates.

Step 5. Fig. 4-7 illustrates the technique to evaluate the discharging rates. h_m is the discharging rate at time m. This is the difference between the $A_0(m)$ and $x(m)$ and it can be defined as $h_m = A_{0(m)} - x(m)$. Battery rate after period p would be h_{m+p}. Amount of energy discharged would be A as shown in Fig. 4-7.

Step 6. Adjusting h_m at each consecutive time can affect the cyclic performance and cost of the BESS. Hence the strategy can be applied using the mean discharge rate over a period p given that change in x duing this period is within a tolerance level ε. This can be written as $\varepsilon > |x_m - x_{m+p}|$.

The discharge rate for this period will still be required to attain the area A, the energy loss in the BESS due to discharge (4-12). Hence the discharge rate (DCH) for the period p can be calculated as in (4-13).The sign of A or the $DCH_{m\to m+p}$ will be negative since the value of A_0 is lower than value of x during this interval.

$$A = \int_m^{m+p} h_m = \int_m^{m+p} (A_{0(m)} - x(m)) \tag{4-12}$$

$$DCH_{m\to m+p} = A/p \tag{4-13}$$

A similar approach can be followed to derive the charge rate (CH). However, the direction would be reversed. It will hold the sign of A in (4-14).

$$CH_{m\to m+p} = A/p;\ \ {P_B}^{max} \geq CH_{m\to m+p} \tag{4-14}$$

Step 7. Once the BESS reaches its maximum charge state, it can be set to an idle mode until discharging begins. In an event where calculated battery rate violate its boundary limits, $DCH\ or\ CH$ can be adjusted to its boundary limit. However, the loss or gain in charge due to this action has to be attained during the next period (ϑ). If the battery energy loss or gain is $B_{m\to m+p}$,

$${A^{updated}}_{m+p\to m+p+\vartheta} = B_{m\to m+p} + A_{m+p\to m+p+\vartheta} \tag{4-15}$$

By updating the subsequent A as expressed in (4-15), new battery rate can be calculated by substituting to (4-13) or (4-14). This ensures battery charge reaches the expected value at the end of $m + p + \vartheta$.

Step 8. Battery energy E_B is derived mathematically by substituting optimal charge/discharge rates to equations (4-16), (4-17) and (4-18).

$$\Delta E_B(m) = CH * (\Delta t \times \eta_c) \quad if\ charging \tag{4-16}$$

$$\Delta E_B(m) = DCH * \Delta t/\eta_d \quad if\ discharging \tag{4-17}$$

$$E_B(m) = \Delta E_B(m) + E_B(m-1) \tag{4-18}$$

Step 9. The process will be repeated at the desired time step of 6 hours. Exponential smoothing can be utilized again to update A_0 recursively; and then the battery parameters can be updated accordingly. Approach is summarized in Fig. 4-8.

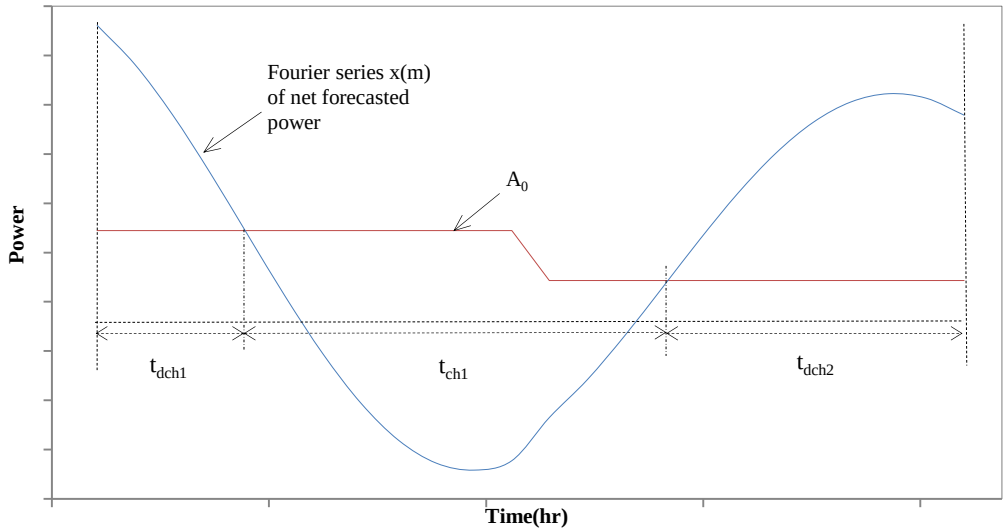

Fig. 4-6. Definition of charging and discharging periods.

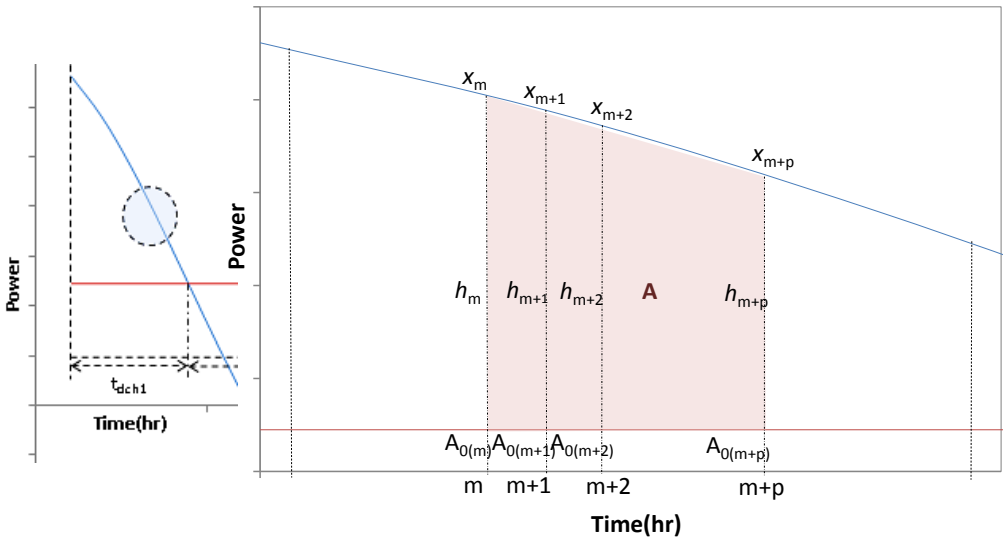

Fig. 4-7. Discharge rate evaluation approach.

Algorithm 2: Adaptive predictive discrete Fourier series model

1. **Inputs**: $P_{net}(t+m); m \in [-12/\Delta t - 1, 12/\Delta t]$ as in (4-6) battery constraints ${P_B}^{min}$, ${P_B}^{max}$, ${E_B}^{min}$, ${E_B}^{max}$ and R_B.
2. Evaluate DFT coefficients $[A_0\ A_k\ B_k]$ and x.
3. Determine charging periods t_{ch} and discharging periods t_{dch} using tolerance ε.
4. Evaluate respective charge/discharge rates $CH_{m\to m+p}$ and $DCH_{m\to m+p}$ using (4-13) and (4-14).
5. Check **if** $constraints \leq tol.cons$ **then**
   5.1. Set battery rates to that found in 4.
   5.2. **else if**
   5.3. Set battery rates to its boundary limit.
   5.4. Adjust battery rate in the consecutive period based on (4-15).
   5.5. **end if**
6. **Output**: Optimal DCH and CH. Derive E_B using (4-18).

Repeat 1-6 6 hourly using updated P_{net}, Update A_0 using exponential smoothing.

Battery size could be found from (3-9).

Fig. 4-8. Pseudo code for DFTM to determine optimal battery energy and rates.

4.5 Short Term Charge/Discharge Mode

Local controller first applies the charge/discharge rates schedule as predicted using APOM or DFTM. However during battery operation, the forecasted P_{net} may drop or increase substantially due to variations in the projected system and climatic conditions. These variations are generally classified as high frequency perturbations. This can be monitored through on-line supervision of power balance at PCC. In situations where these high frequency perturbation exceed a threshold limit ($\varepsilon_{perturb}$), the BESS can be set to operate in a short term charge/discharge mode while making sure that other battery constraints are within permissible limits. The loss or the gain due to this will need to be captured to ensure the efficient power flow coordination. Hence the consecutive battery rate needs to be adjusted. This can be achieved as follow,

1. APOM: If $(t-1)$ is the time at perturbation occurred, $\Delta E_B(t)$ in (3-6) can be modified with the new $E_B(t-1)$. Charge/discharge rates during the consecutive time instant can be recalculated from (3-7) - (3-8).

2. DFTM: Equation (4-15) can be used to determine the $A^{updated}$. Charge/discharge rates can be adjusted accordingly using (4-13) and (4-14).

Short term mode is more advantageous when the proposed predictive battery system is co-located with PV systems to account for high fluctuations in the generation.

4.6 Neural Network Application

Load forecasting is an essential component of the proposed approaches. Accuracies of the models are highly dependent on the data handling capacity of the forecasting tool. In the recent years, NN are persistently used for power system forecasting applications such as load forecasting, power electronic controllers, harmonic forecasting, stability analysis and fault protection [122]-[123]. Popularity of NN is as a result of its ability to recognize pattern through continuous training and mapping of historical data.

This chapter applies the basic NN implementation using the default MatLAB

toolbox. Feed-forward training was adopted using the Levenberg–Marquardt algorithm with the standard back-propagation learning algorithm. The data from input layer are propagated through to a hidden layer before reaching the output layer.

Training process attempts to minimize the performance metric, Mean Absolute Error (MAE), iteratively. The introduction of the hidden layer makes it possible for NN to identify nonlinear relationships. The size of the hidden layer typically depends on the complexity of the problem and number of input and output layers. Determination of the number of neurons for the hidden layer is a very challenging issue. In the literature, genetic algorithm based approaches are established to dynamically adjust optimal number of neurons and structure of the problem [124]. However, these approaches are highly problem specific. As a rule of thumb, number of neurons in the hidden layer is decided as a value (a) between the size of input and output layer, (b) 2/3 of the size of the input layer (c) less than twice the size of the input layer [125].

Number of neurons in the input layer is equivalent to number of input features. The input features to the network are,

- Relative humidity;
- Dry bulb temperature;
- Solar radiation;
- Hour of the day;
- An integer representing the day of the week;
- An integer flag indicating if the day is a working day or holiday;
- Load 24 hours previously;
- Load 168 hours previously;
- Average load in the past 24 hours.

The network comprises of an output layer of one neuron representing the total net load and a hidden layer of 6 neurons.

A test model was developed from the data collected at a 200kVA 400/230V distribution transformer supplying a low voltage three phase four wire LV feeder

within the Perth Solar City PV Saturation Trial. This feeder feeds 77 residential houses where 29 residences have roof top PV systems. The total PV generation is 54kW. Power flow reversals are observed at the distribution transformer at times of low load and high PV generation which often occurred at noon on week days.

A training data set was created using hourly data records from 17th October 2011 to 22nd February 2012. The training set included the annual peak load day and broader range of climatic conditions. Test set data were assembled using hourly data collected between 23rd February 2012 and 26th February 2012.

Fig. 4-9 provides a comparison between the actual load and forecasted load. Results are derived from two operating time scales; twelve and 6 hour receding horizon prediction time scale. NN was trained and validated several times. At each validation, the returned MAE performance metric ranged from 10kW to 8kW at 12 hour update scale and 4kW to 6kW at 6 hour update scale. The resultant individual errors or fluctuations are either positive or negative. From the comparative results, it is evident that MAE performance improves with the reduced update duration and the convergence performance of the NN tool.

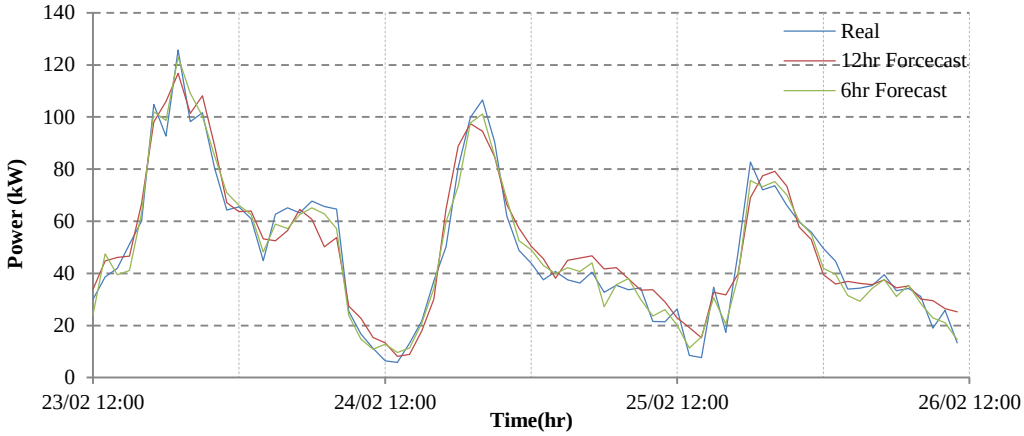

Fig. 4-9. NN forecasted net load.

Even though forecasted values fluctuate slightly from the actual value, the curve fitting ability of NN is able to identify the periods of peak and off peak effectively. Convergence level of the forecasting tool is satisfactory for the application of deriving the proposed battery control strategies. However, further improvement can be achieved with larger historical databases.

4.7 Results and Discussion

Battery dispatch management approaches were developed using the test model used for building the NN training tool. Real time testing was executed for the period from 23rd February 2012 to 26th February 2012. Efficiencies of the proposed battery management strategies are discussed in terms of its ability of the systems to improve the dispatchability and economic performance. Realized economic improvements are attributed to reduced peak demand charges, energy costs and increased battery cycle life under the optimized scheduling.

4.7.1 Ideal Smooth Response

This section demonstrates the true desired smooth demand curve during the test period. In the next subsection, the results obtained with the battery management strategies are compared against the ones established here.

Fig. 4-10(a) shows the actual power flow in the distribution network and the ideal smoothed load with a BESS. Ideal load curve is derived as the 24 hour (11 hours into the past and 12 hours into the future) mean load. Mean load is re-evaluated adaptively every 6 hours. Battery power in Fig. 4-10(b) is derived from the difference between the actual load and the required smooth load.

During the investigation period the peak value of the actual load curve and the smoothed load are 126kW and 63kW respectively. The system peak is reduced by 50% with the battery. However, achieving this ideal smoothing will require the knowledge of future load with a high degree of certainty.

The corresponding battery power and energy profiles are shown in Fig. 4-10(b) and Fig. 4-10(c) respectively. Minimum of the energy profile is added to the initial value to ensure battery energy profile is not negative. The size of the BESS required is 360kWh. The cyclic performance is 3.1cycles over the 72 hours.

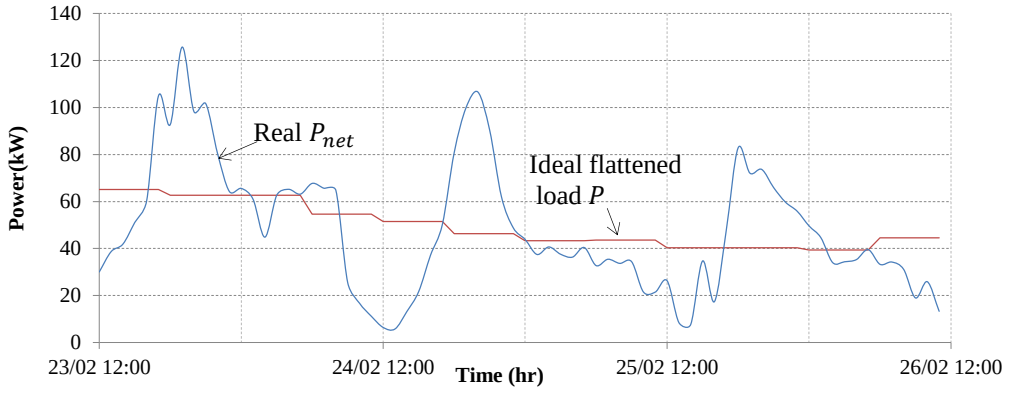

(a)

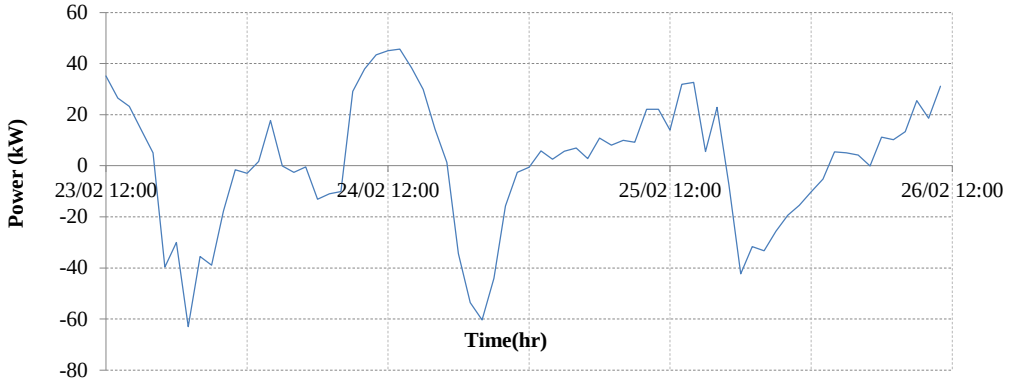

(b)

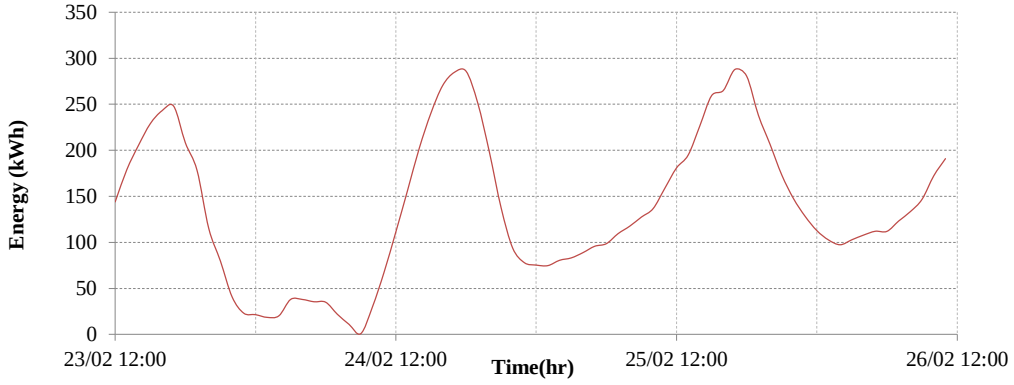

(c)

Fig. 4-10. (a)Instantaneous real and ideal levelled net load, (b) Required battery power to achieve the ideal net load, (c) Battery energy profile or the SoC swing.

4.7.2 Real Time Application

BMS models first predict the battery states and rates for the next 12 hour period using forecasted data. Then this is applied in the real conditions. The instantaneous battery power schedule facilitates the battery online dispatch. Power balance equation (4-1) evaluates the grid power at PCC for real power coordination.

There are no high frequency perturbations that varied significantly from the forecasted load. Low frequency components are effectively balanced at the PCC. Fig. 4-11 and Fig. 4-12 provide detailed comparisons of the load responses with APOM and DFTM controls respectively. The curves "Forecasted *P* with BMS" are the forecasted load with the battery control. The traces "Real *P* with BMS" show the actual instantaneous reflection of power exchanged with battery operation.

The peak reduction achieved with DFTM management strategy was estimated to be approximately 40% and 38% with APOM. Peak arbitrage is proportionate to the percentage peak reduction. APOM achieves slightly less reduction. Reason behind this behaviour lies in the approach used. Main and only focus of DFTM is peak shaving and load levelling whereas APOM balance the cost of battery against the amount of energy cost reduction. The difference in peak reduction by APOM in comparison to DFTM is less than 2%. Approaches minimize the peak effectively and ensure the instantaneous PCC demand at any given instance is near the daily average load. Amount of reduction is also function of the renewable energy capacity in the network.

The discrepancy between the forecasted optimized load and the real reflection is a result of the NN tool forecasting error. The MAE of the optimized load with the DFTM approach is approximately 5kW and with the APOM is 4.1kW. MAE performances are comparable to the NN tool MAE performance measure.

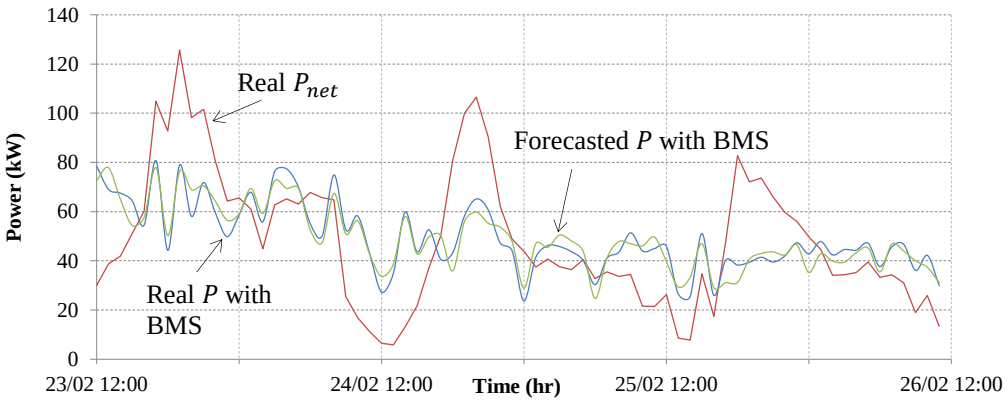

Fig. 4-11. $P(t)$ with and without the application of BESS with APOM.

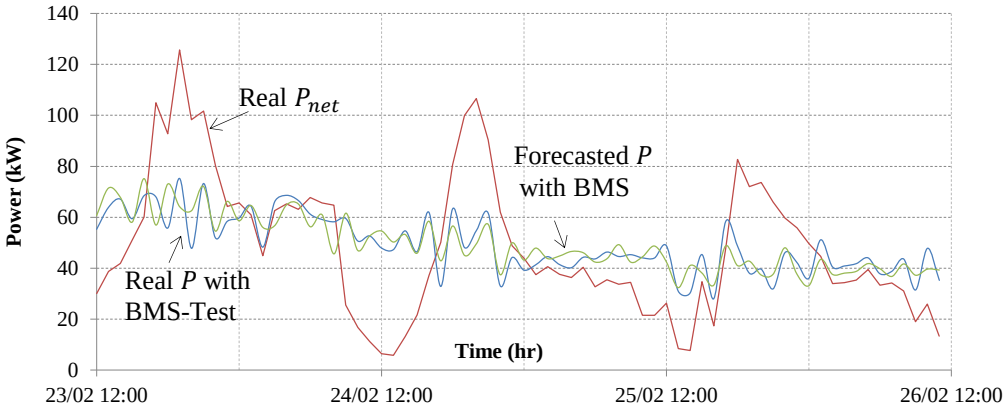

Fig. 4-12. $P(t)$ with and without the application of BESS with DFTM.

Fig. 4-13 and Fig. 4-14 give the battery power and energy profiles respectively by both techniques. DFTM battery distribution matches very closely with the APOM result. In both cases, battery charge state and power vary along the 72 hours allowing variations in the consumption and generation. Minimum size of the battery required with APOM and DFTM are 310kWh and 330kWh.

The size of the BESS with APOM is lower compared to that of with DFTM as a result of its ability to optimize the total energy cost and battery cyclic cost. APOM manages the cyclic performance through the minimization of the cost function defined in (4-2). DFTM achieves improved cyclic performance through its ability to monitor low frequency components effectively with fewer adjustments in the battery power. Cyclic performance of BESS with APOM and DFTM were estimated to be 2.5 cycles and 2.7 cycles respectively over the 72 hours. Assuming a typical cycle life of 3000 cycles and 285 days of operation, a battery system managed with APOM would have a life expectancy of 12.76 years. Note: the number of cycles with no controls was 3.1 cycles over the 72 hours.

Capability of APOM methodology to rigorously optimize the cost effectiveness of storage makes it a better tool for the determination of optimal sizing and rates. However, typically DFTM will require much less overhead to develop and implement since it does not require mathematical optimization techniques like with the APOM. Transformer loadings are usually an aggregated load response with dominant low frequency components, thus DFTM approach is able to produce similar results as with the APOM.

Regardless of the approach utilized, BESS can be designed to operate on an idle mode if the value of coefficient A_0 and the forecasted peak power is below a predetermined threshold level. This further extends the life expectancy of the BESS. APOM would be highly applicable where a high tradeoff between the battery cost and the energy cost is essential. Especially when several BESS units are installed in the network and management of them aims at achieving load levelling as well as high levels of voltage regulation.

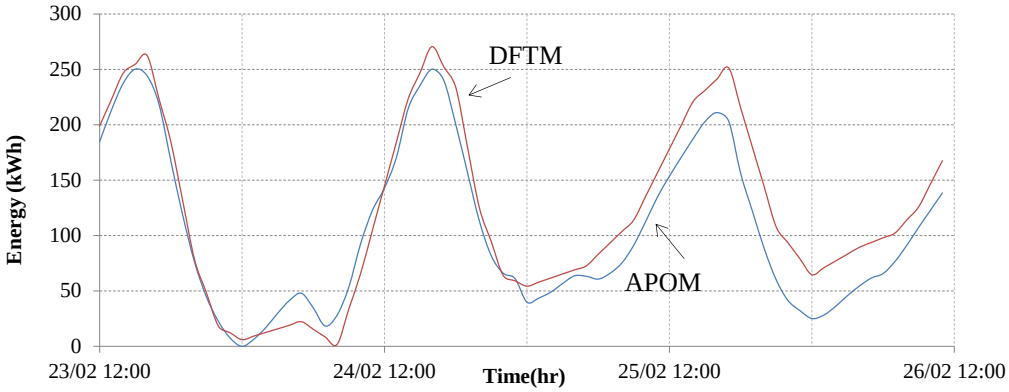

Fig. 4-13. BESS energy profiles.

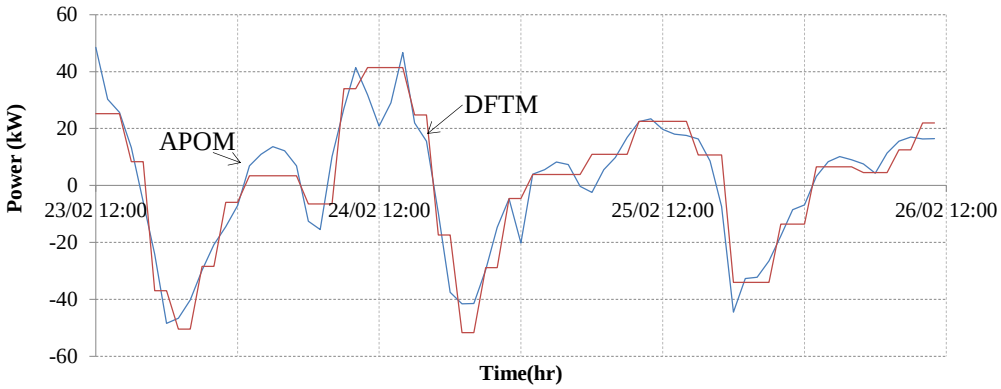

Fig. 4-14. Battery power profiles.

4.7.3 Storage as the Main Source of Supply

Integration of high penetrations of distributed renewable generation to the electricity distribution network is one of the key aspects of smart grid. The vision of smart grid is to add energy storage and manage the power dispatch through remotely controlled systems. CSIRO in Australia has recently produced a report on the types and role of energy storage for a 100% renewable supply study project [44]. The project is an

initiative by the Australian federal government undertaken by Australian Energy Market Operator. Findings show significant potential for storage. With higher levels of DG the possibility exists for storage to become the main source of supply in the future grid with backup supply from the grid.

Fig. 4-15, Fig. 4-16 and Fig. 4-17 show a representative case considering battery storage as the main supply and grid as the secondary supply. The power exchanged with the grid ($P_i(t)$) is fixed at the forecasted A_0 (updated adaptively) while any variations in the forecasted values are supplemented by BESS. The corresponding battery power and energy profiles are illustrated in Fig. 4-16 and Fig. 4-17 respectively.

The method has the potential to enable flexible supply options in networks with high penetrations of DG. With optimal management strategy, battery storage could have a key role to play in the next generation grid. However, development of energy storage market will further require continued engagement from various business parties; utilities, regulators and manufactures.

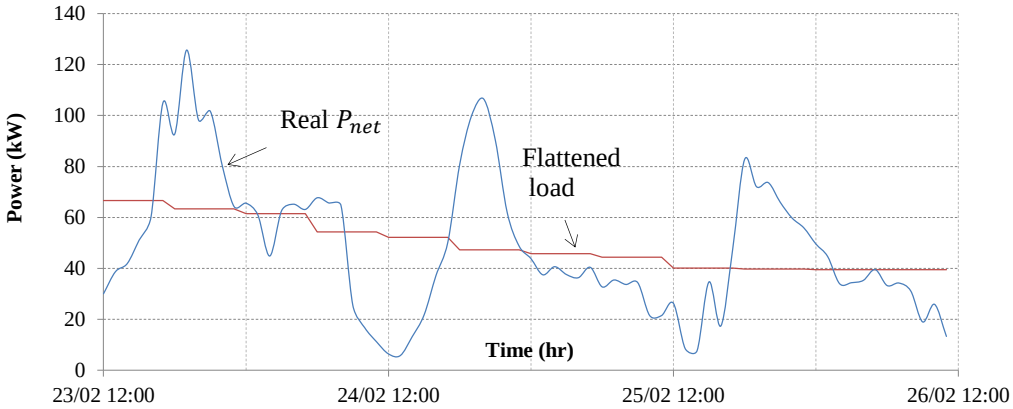

Fig. 4-15. Flattened load at grid with energy storage as main supply.

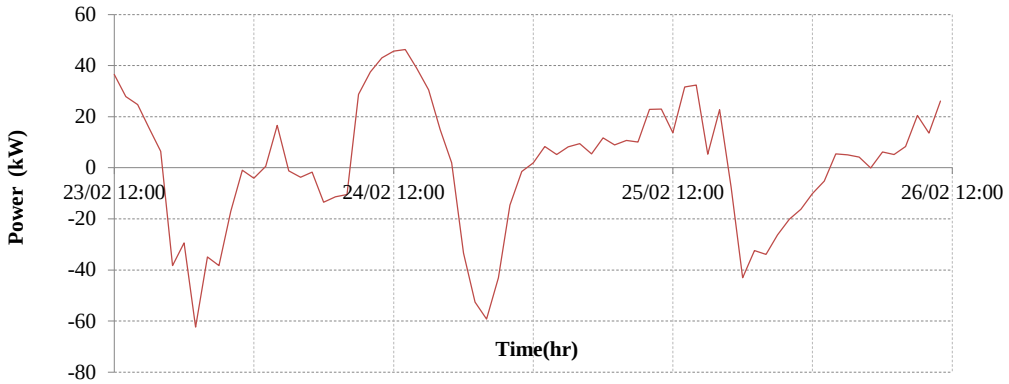

Fig. 4-16. Battery power with energy storage as main supply.

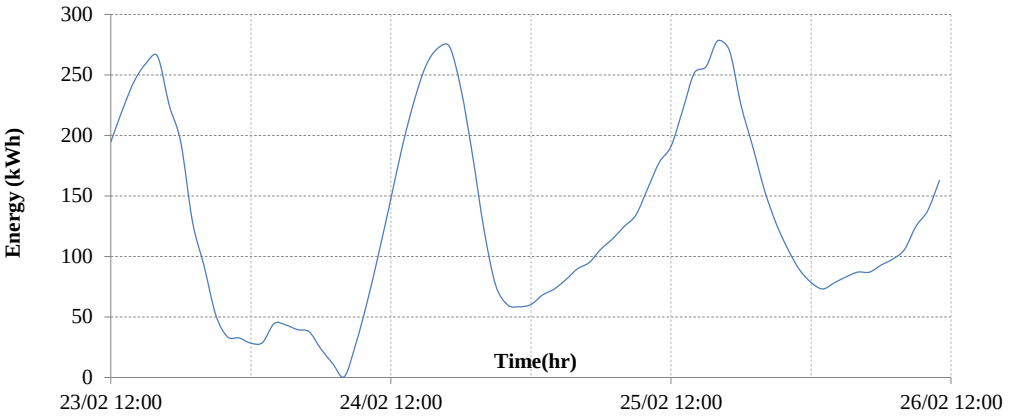

Fig. 4-17. Battery curve with energy storage as main supply.

4.8 Conclusions

This chapter addresses the problem of optimal dispatching of grid scale battery energy storage systems for peak curtailment and load levelling. The study identifies two adaptive BESS management approaches, optimization based model (APOM) and a simple rule based model (DFTM) for scheduling of BESS in smart grid.

Optimization procedure minimizes a cost function derived in terms of costs of battery, energy and peak demand for optimal asset and power flow management. Rule based approach is modelled using discrete Fourier series representation of the aggregated distribution load. Scheduling by both dispatch management strategies are updated at a six hour time scale to adapt to variations in the forecasted conditions. It must be noted that the frequency of the re-optimization could vary from few minutes to few times a day. Compared to APOM, the DFTM will require much less overhead

to develop and implement as it does not require meta-heuristic optimization. Transformer loadings are usually an aggregated load response with dominant low frequency components, thus DFTM approach is able to produce similar results as with the APOM.

Real time measured load data from a real feeder studied under the Solar City PV Saturation Trail in Western Australia are used to develop and validate the proposed models. Results show the robustness of the approaches. Optimal battery parameters very closely follow the anticipated values from the ideal scenario. Numerical results reveal the ability of the proposed models to reduce the peak while achieving a smoothed demand curve. Realized economic gains are attributed to reduced peak demand charges and increased battery cycle life. Amount of peak reduction would increase with more DG due to reduced energy requirements from the grid. BESS with an optimal management strategy can effectively capture reverse power flow and coordinate the power dispatch for best outcomes. A case study also shows that the conventional grid can become a secondary supply in the presence of intelligently managed BESS in the next generation grid with high penetrations of distributed renewable resources.

Chapter 5. BESS for the Optimization of Distribution Network Load and Generation Hosting Capability

5.1 Introduction

This chapter proposes a strategy for optimal integration of BESS to improve the load and DG hosting ability of the utility grid. An effective approach that determines the optimal capacity and day-ahead operation strategy for deployment of distribution network operator (DNO) owned and controlled BESSs is presented. It is a cost based multi-objective optimization strategy that considers two primary factors; distribution system cost and battery linear cycling cost. Quantitative analyses on the benefits and tradeoffs of BESS installations are carried out considering different service options. BESS is investigated for three main service options; (1) voltage regulation, (2) loss reduction, and (3) peak reduction. The performance and benefits of the optimized BESS to control one service option exclusively or multiple services simultaneously is compared. The analysis is further extended to study the effect of installation site on the size, management strategy and the service option. The approach developed using MatLab IP algorithm. Simulations are conducted for the MV IEEE 33 bus system and a LV distribution network in Western Australia studied during the Perth Solar City Trial.

5.2 Problem Formulation

5.2.1 Objective Function

The cost function in (5-1) is constructed to minimize distribution system costs (C_{system}) in terms of costs incurred due to system losses (C_{Loss}), peak demand (C_P) and voltage regulation (C_{VR}). Planning problem should contain the investment and operating costs of battery to optimize benefit tradeoffs.

Hence, a cost factor that represents BESS capital and O&M expenditures ($C_{battery}$) in a form of a daily cost is included in the objective function:

$$f(C_{iF}) = \sum_{l=1}^{4} \gamma_l . f_l = \gamma_1 C_{battery} + \gamma_2 C_{Loss} + \gamma_3 C_{VR} + \gamma_4 C_P \quad (5\text{-}1)$$

Where, $C_{system} = \gamma_2 C_{Loss} + \gamma_3 C_{VR} + \gamma_4 C_P$

$$C_{Loss} = \int_{t=1}^{T} \int_{nbranch=1}^{nbus-1} |\{V_j{}^2(t) + V_i{}^2(t) - 2V_i(t)V_j(t)\, cos(\delta_i(t) - \delta_j(t))\}| . G_{ij} . \Delta t \, . r_{loss}(t) . dt$$

$$C_{VR} = \int_{t=1}^{T} \int_{i=1}^{nbus} |V_i(t)|^2 - V_1{}^2|^{1/2} . \Delta t . r_{VR}(t)\, dt$$

$$C_P = P_{max} . \Delta t . r_p$$

$$\gamma_l = w_l / \zeta_l .$$

In the above equations, $nbranch$, V_i, δ_i, G_{ij}, $V_1 = 1p.u.$, $r_{loss} = 28.4\ c/kWh$, r_{VR}, γ_l, w_l and ζ_l are the branch number, voltage magnitude, voltage angle, conductance of branch $nbranch$, reference voltage at slack bus, loss cost rate, voltage regulation cost rate, scaling factor, weighting factor ($\sum_{l=1}^{4} w_l = 1$, equally weighted) and ζ_l is the minimum of f_l [126] respectively.

The following points are highlighted about the proposed BESS management strategy:

- The primary inputs to the optimization problem are network characteristics, time variant load and generation forecasts at 15 minutes interval and an initial vector of the control variable, Fourier coefficient vector (C_{iF}). The C_{iF} vector length (n) is set to 8 as discussed in Chapter 3.6. The secondary inputs include battery and network constraints and the cost coefficients (r_{loss}, r_{VR}, r_p and BUC).

- The direct output is the optimized Fourier coefficient vector while BESS

charge/discharge schedule (3-7)-(3-8), BESS energy profile (3-5), power flow coordination (3-20)-(3-21) and optimal BESS size (3-9) can be derived using the optimized C_{iF}. The optimization problem is a nonlinear constrained problem that is solved using a linearized MatLab IP algorithm.

- The r_{loss} is the electricity price taken from [127] for Western Australia. This cost comprises of four main components; retail, wholesale energy, transmission and distribution costs. Out of this, wholesale energy and distribution costs are the major drivers representing more than 70% of the aggregated electricity price. The electricity price also reflects the costs of upgrades, O&M and reinforcements driven by voltage and thermal limit violations as well as recovery costs of incentive schemes and carbon costs [127].

- The factor r_p is the peak demand charge assumed at $\$200/\text{kWh/year}$. This is typically made up of peak support, demand supply capital, maintenance and infrastructure development costs [128].

- Rate of voltage violations due to peak generation and load is represented by $r_{VR} = 14.2c/kWh$. This rate reflects the network charges and is about 50% of the end user electricity price [128]. The C_{VR} encourage voltages to the nominal V_{ref}. Most utility providers prefer near unity voltages; the IEC61000 voltage limits are now supplemented by "preferred ranges".

- Cost function will not consider the transmission costs for two main reasons; i) The transmission cost component is generally a small fraction of the aggregated electricity price seen by consumers and ii) Existing transmission lines have been developed with the aim of transporting electricity produced by centralized large scale generators. Improving the DG hosting ability of the LV grid through optimal integration of BESS reduces the power that needs to come from centralized sources. Hence, minimization of LV distribution cost will coincidentally reduce transmission and carbon emission costs.

Note that the optimal parameters and benefits of BESS depend on the services to be

provided. Therefore, this chapter derives optimal BESS parameters considering the minimization of complete cost function defined in (5-1) and individual cost factors that constitute C_{system}, for benefits and tradeoffs quantification.

5.2.2 Objective Function Constraints

- Voltage constraints

  The optimization is required to comply with the inequality voltage constraint (5-2):

$$V_{min} < |V_i^t| < V_{max} \tag{5-2}$$

  Where, V_{min} and V_{max} are the lower and upper voltage limits, respectively.

  The West Australian Technical Rules and Electricity Act 1945 section 25(1)(d), require the steady state voltage to be within ±6% of the nominal voltage during normal conditions.

- Voltage unbalance factor (VUF) constraint

  For three phase unbalanced systems a voltage unbalance factor (VUF) can be defined as [129]:

$$VUF = \sum_{i=1}^{nbus} \frac{V_i^2}{V_i^1} . 100 \tag{5-3}$$

  Where, V^2 and V^1 are the positive and negative sequence voltages respectively.

  The VUF constraint is expressed as:

$$VUF < VUF_{max} \tag{5-4}$$

Where, $VUF_{max} = 1$ is the maximum VUF.

- Battery constraints

  The battery constraints in (4-4) and (4-5) are established for added security to ensure battery power or energy does not exceed their boundary limits during charge/discharge management.

The above sets of constraints can be added to the cost function as a penalty cost rather than separate constraints if required. The battery constraints were not imposed in the optimization to facilitate the problem of sizing in this chapter.

5.2.3 Linearization of the Cost Function and Constraints

The nonlinear optimization problem (5-1) is solved using a linearized IP method. The standard IP method can be computationally very expensive and the computational burden increases with the size of the problem and network topology. Hence, this chapter uses an analytical gradient based IP method to improve the optimization efficiency [130]. Both the objective function and constraints were linearized by supplying Jacobians (with respect to Fourier coefficients) (5-5)-(5-6). In equations (5-5) and (5-6), $\frac{dV_i}{dP_i}$ is found from the inverse power flow Jacobian.

The addition of the analytical gradient also improves the numerical conditioning of the iterative process.

$$\nabla f = \left[\frac{dC_{system}+C_{battery}}{dx_\rho}\right] = \left[\frac{dC_{system}}{dx_\rho} + \gamma_1 \frac{C_{battery}}{dx_\rho}\right] \tag{5-5}$$

Where, ρ is the Fourier coefficient number $\rho = 1,2 \ldots (nx2)$ and,

$$\frac{dC_{system}}{dx_\rho} = \left[\gamma_2 \frac{dC_{Loss}}{dV_i}.\frac{dV_i}{dP_i} + \gamma_3 \frac{dC_{VR}}{dV_i}.\frac{dV_i}{dP_i}\right].\frac{dP_i}{dx_\rho} + \gamma_4 \frac{dC_P}{dP_i}.\frac{dP_{max}}{dx_\rho}.$$

The Jacobian of the inequality constraints are derived as:

$$J_g = \begin{bmatrix} -\frac{dV_i}{dP_i}\cdot\frac{dP_i}{dx_\rho} & \frac{dV_i}{dP_i}\cdot\frac{dP_i}{dx_\rho} \\ -\frac{dP_B}{dx_\rho} & \frac{dP_B}{dx_\rho} \\ -\frac{dE_B}{dx_\rho} & \frac{dE_B}{dx_\rho} \end{bmatrix}^T \tag{5-6}$$

It was found that cost and constraints linearization improves the optimization speed by over 80% (average from 15 runs).

5.2.4 Summary of the Proposed Management Architecture

This chapter uses the receding horizon hierarchical control approach for BESS management similar to that proposed in Chapter 4.2.2. The structure of the system is presented in Fig. 5-1. Central controller performs the proposed day-ahead predictive optimization to identify the optimal parameters of BESS.

The EMS first carries out the forecasting of the load and generation data 24 hours into the future. The BMS uses the forecasted load data to solve the optimal power flow management problem. BMS returns the optimized C_{iF}. Optimal Fourier coefficient vector determines the dispatch schedule of the BESS in terms of charging/discharging response and energy. The EMS then sends the optimized battery set-points for day-ahead scheduling of the BESS to the local controller in the power electronic interface.

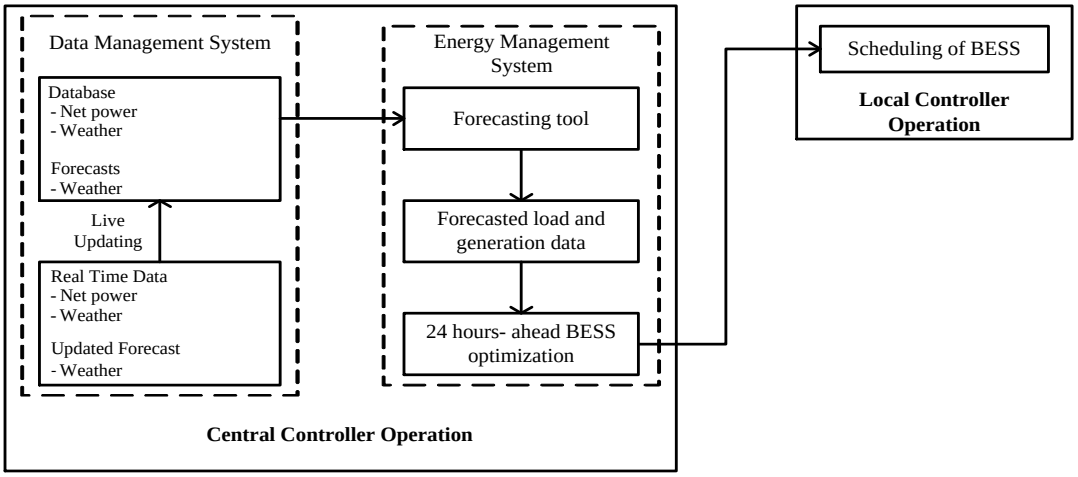

Fig. 5-1. Proposed system architecture.

The control algorithm can be reapplied several times each day to allow the battery energy profile to be progressively updated as new information and trends emerge in the operating distribution network as introduced in Chapter 4.

5.2.5 Summary of the proposed BESS management and sizing approach

The following procedure is adopted for optimal management and sizing of BESS.

Step 1. Determine the candidate buses based on geographical and other planning constraints.

Step 2. Adjust the cost function depending on the optimization objective features required.

a. For multi-objective placement and sizing (5-1);

$$f(C_{iF}) = \gamma_1 C_{battery} + \gamma_2 C_{Loss} + \gamma_3 C_{VR} + \gamma_4 C_P \tag{5-1}$$

b. For pure control of distribution system cost factors, the optimization cost function can be adjusted as:

i. For voltage regulation,

$$f_{VR} = \gamma_3 C_{VR} + \gamma_1 C_{battery} \tag{5-7}$$

ii. For loss reduction,

$$f_{loss} = \gamma_2 C_{Loss} + \gamma_1 C_{battery} \tag{5-8}$$

iii. For peak shaving,

$$f_P = \gamma_4 C_P + \gamma_1 C_{battery} \tag{5-9}$$

Step 3. Run the optimization with BESS at each selected bus, one at a time. The optimization will return,

a. Value of cost function.

b. Corresponding Fourier coefficient vector (C_{iF}).

Step 4. Locate the optimal bus at which cost function is minimal.

Step 5. Obtain the optimized battery energy profile using the optimized Fourier

coefficient vector found for optimal bus in Step 4.

Step 6. Battery size can be evaluated from (3-9).

The approach for sizing and siting should be tested using data for all seasons to capture seasonal variations in the generation and load patterns. Site could be determined as the location that offers maximum tradeoffs and size of the BESS can be determined as the maximum found from optimization for different seasons.

5.3 Test Systems

The proposed approach is tested on a MV and a LV distribution system. The voltage dependency of the loads is modelled using polynomial equations:

$$P_{L-i} = P_{0_i}(a_p + b_p|V_i| + c_p|V_i|^2) \tag{5-10}$$

$$Q_{L-i} = Q_{0_i}(a_q + b_q|V_i| + c_q|V_i|^2) \tag{5-11}$$

Where, $a_p + b_p + c_p = 1$, and $a_q + b_q + c_q = 1$.

In this chapter, load flow calculations are performed using the total current injection method (TCIM) in [131]-[132] and bus 1 is considered as the slack bus with a voltage of 1p.u.

5.3.1 MV Test System-Case 1

In Case 1, the proposed approach is tested on the hypothetical IEEE 33-bus distribution system of Fig. 5-2. Complete system data can be found in Appendix A [133]. The substation voltage of the test system is 12.66kV and the base is 10MVA.

Two wind based DGs and seven PV DGs were allocated to simulate a high DG penetration scenario. PV DGs could represent aggregated generation seen at the installed bus. Two wind DGs of 1MW are sited at buses 18 and 24. Three 400kVA PV DGs are installed at buses 5, 21 and 31 and four 500kVA PV DGs are installed at buses 8, 12, 28 and 33.

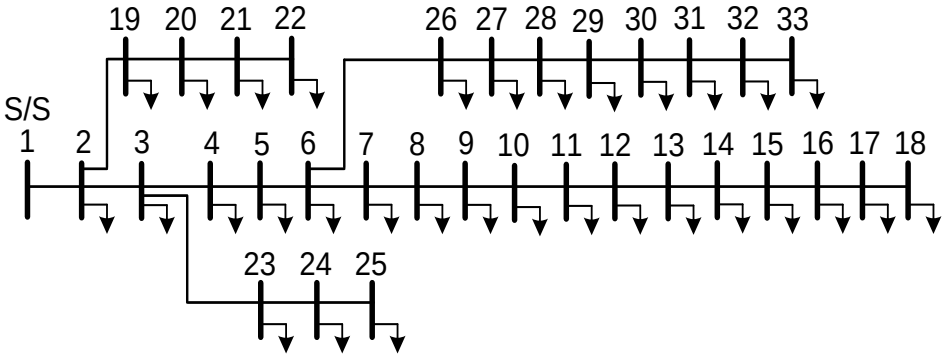

Fig. 5-2. Single-line diagram of IEEE 33 bus distribution system.

It was assumed that the loads follow the IEEE-RTS model as illustrated in Fig. 5-3 [134] and the load composition was set to $a_p = a_q = 0.4$, $b_p = b_q = 0.3$ and $c_p = c_q = 0.3$. Peak active and reactive load power of the system with the above load composition are 3.556MW and 2.191MVar, respectively. The output generation from wind and PV DGs are expected to follow the curves in Fig. 5-3 [135].

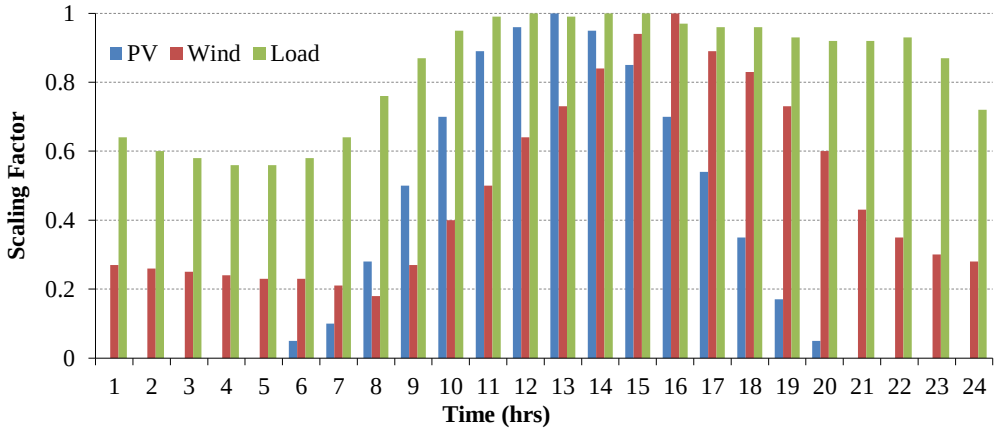

Fig. 5-3. Scaling factors of time variant load and generation.

5.3.2 LV Test System-Case 2

In Case 2, the proposed approach is tested on a LV distribution system studied under the Perth Solar City Trial. System is depicted in Fig. 5-4. Each load is modelled with a co-located rooftop PV system. Network is supplied by a 200kVA 22kV/415V distribution transformer. The consumer mains are of 6mm^2 copper with R=3.7Ω/km and X=0.369Ω/km while the aerial mains are of two all-aluminium conductors (AAC) of types: 7/4.50AAC and 7/3.75AAC. The simulations are conducted assuming balanced conditions.

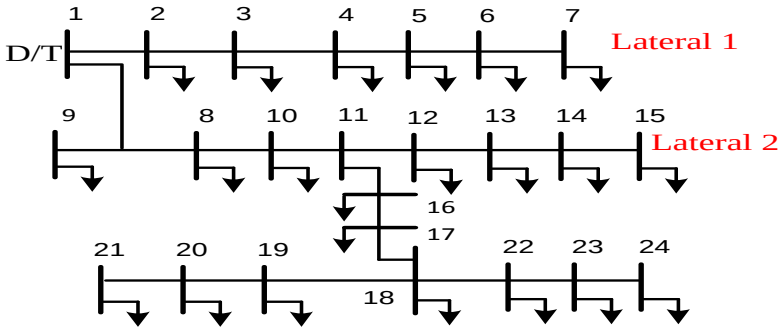

Fig. 5-4. LV test model.

5.4 Results and Discussion

The optimization determines the battery optimal charge/discharge strategy and the size which in turn coordinates the power flows at the interconnection point. Simulations were conducted for the optimization of (i) voltage regulation (f_{VR} defined in (5-7)), (ii) loss reduction (f_{loss} defined in (5-8)), (iii) peak reduction ($f_p$defined in (5-9)), and (iv) multiple services simultaneously (f defined in (5-1)). The installation site is determined as the bus at which the cost function is minimal. A quantitative analysis on the effect of installation site on the optimal battery parameters and grid services to be provided is carried out in this section.

5.4.1 Test Case 1- MV Distribution System

5.4.1.1 Base Operation with no BESS

The Fig. 5-5 and Fig. 5-6 graphically illustrate the net distribution transformer load (without losses) and the voltage profile respectively without BESS. The system clearly experience reverse power flow and overvoltage issues that are recognized as the major limiting factors for the widespread uptake of renewable DG. The peak export power is 1.002MW and the maximum voltage is 1.028p.u at bus 18. The total load energy demand is 71.2005MWh.

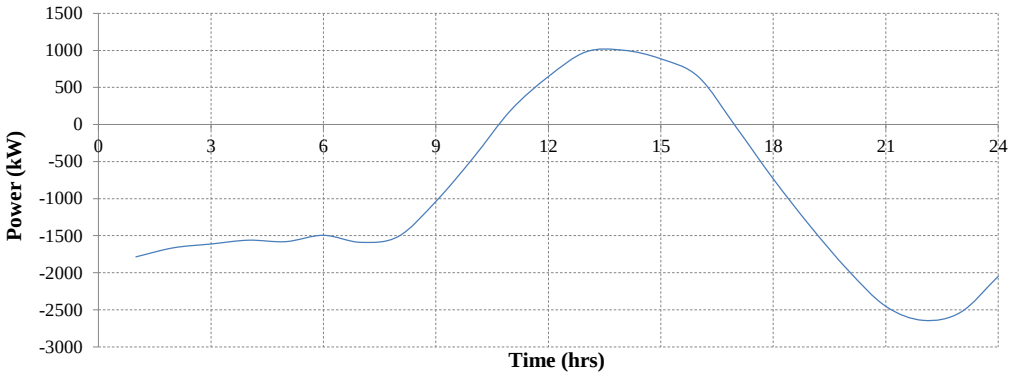

Fig. 5-5. Distribution transformer loading with no BESS.

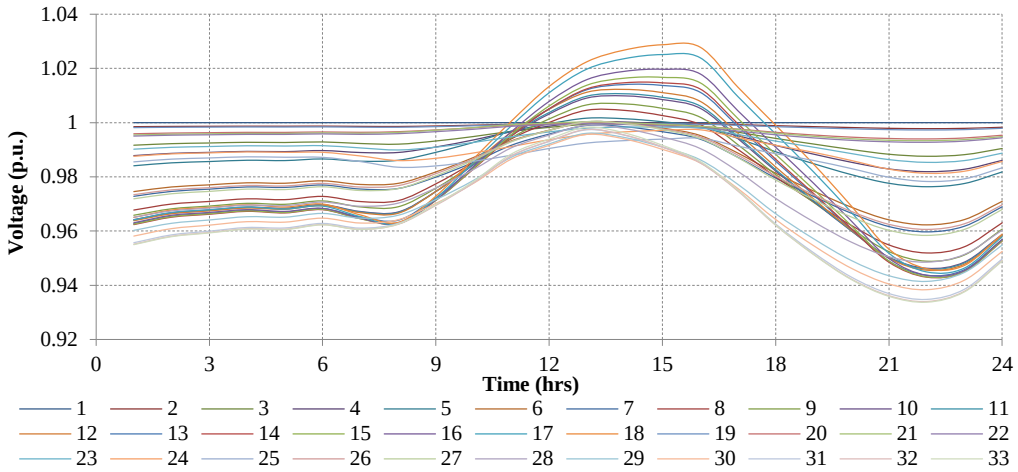

Fig. 5-6. Voltage profile with no BESS.

5.4.1.2 Simulation Results

The Table 5-1 summarizes the simulation results of the optimal size, site, BESS life expectancy, voltages (minimum and maximum), peak power and losses for different service options. The buses 26, 24, 12 and 27 are identified as the installation sites when optimizing for f_{VR}, f_p, f_{loss} and f respectively. Fig. 5-7, Fig. 5-8 and Fig. 5-9 shows the resultant battery profiles, voltage profiles and net distribution transformer loading.

From Table 5-1, bus 26 is the optimal BESS site for maximum voltage regulation. As shown in Fig. 5-7, battery discharges from 1.00am to 8.00am and then operates at a very slow rate until 10.am. This improves the morning voltage profile. During peak generation, the BESS drops the voltage at bus 26 to allow reverse power flow to the BESS. Thus, BESS captures peak DG production effectively and delivers it during

peak demand to enhance the voltages. The maximum and minimum voltages from f_{VR} optimization are 0.960p.u. and 1.006p.u. respectively. The peak is reduced to 1.323MW and energy losses are reduced by 12.22%.

TABLE 5-1: SUMMARY OF RESULTS FOR TEST CASE 1.

Cost Func.	**Site (Bus No.)**	**Voltage (p.u.)**		E_{loss} **(MWh)**	P_{max} **(MW)**	**Battery**	
		Min (Bus#)	**Max (Bus#)**			**Size (MWh)**	**Life (years)**
Base		0.934 (33)	1.028 (18)	1.79	2.642		
f_{VR}	26	0.960 (30,32,33)	1.006 (18)	1.57	1.323	14.42	10.52
f_P	24	0.940 (33)	1.023 (18)	1.94	1.068	14.88	10.53
f_{loss}	12	0.943 (33)	1.000 (1)	1.49	1.997	7.27	10.53
f in (5-1)	27	0.956 (33)	1.007 (18)	1.57	1.091	14.75	10.52

The maximum peak reduction is achieved at bus 24 when controlling peak exclusively (f_P). From Fig. 5-9, both peak import and export power are reduced considerably. The peak is reduced by 59.60% compared to the base case. At bus 24, the charge/discharge of the battery not only achieve peak shaving but also assist load levelling as depicted in Fig. 5-9. During peak PV generation, the battery starts charging and reduces the voltage at bus 24 to allow reverse power flow. During peak demand, the discharge of battery raises the voltage at bus from 6.00pm till midnight while supporting the load. However, no significant improvement in the overall voltage profile is evident and the exclusive peak management has increased the system losses by 8.06%. From Table 5-1, the optimal size of BESS required to

support peak exclusively is greater than for other services.

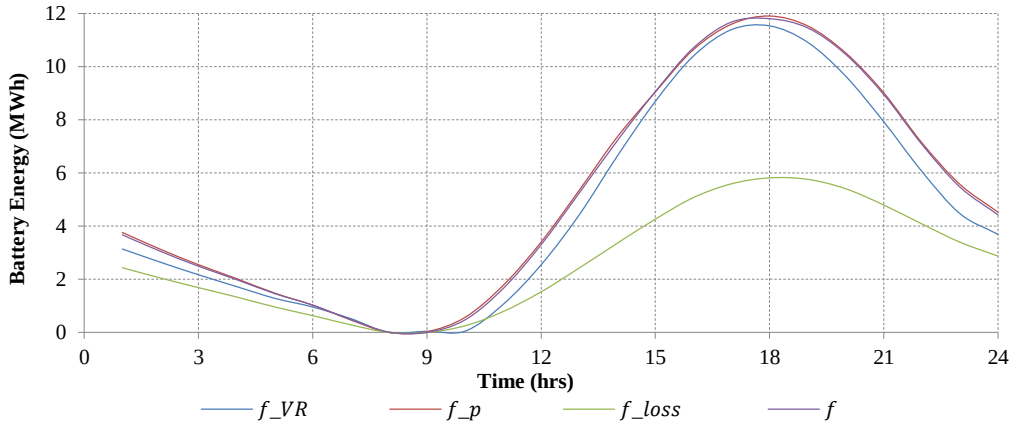

Fig. 5-7. Battery energy profiles for the various service options.

Bus 12 is the optimal site that achieves most loss reductions when controlling the losses exclusively (f_{loss}). From Table 5-1, the BESS capacity required for the pure control of loss is the lowest. System losses are reduced by 16.92%. However, as illustrated in Fig. 5-8(c) and Fig. 5-9 the improvement in the lowest voltage or the peak reduction is not as significant.

Bus 27 is the optimal site from the optimization of the cost function (f) for multiple grid services. The BESS effectively captures the reverse power flow and reduces over voltages. The peak export and import power matches very closely with each other and results from f_P control, thus it is able to achieve peak shaving as well as load levelling. The maximum and minimum voltages are comparable to that of from the optimization for f_{VR}. The system energy losses are reduced by 12.25%.

The size of the battery required for f minimization is 14.75MWh. This matches very closely with the BESS sizes for f_{VR} and f_{loss} control. Therefore, based on Table 5-1 results, the battery is better utilized and maximum tradeoffs are achieved when installed for the simultaneous control of multiple services.

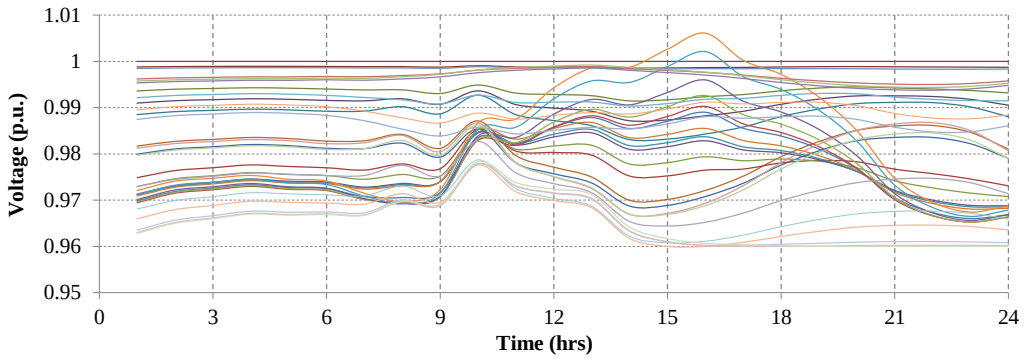

(a)

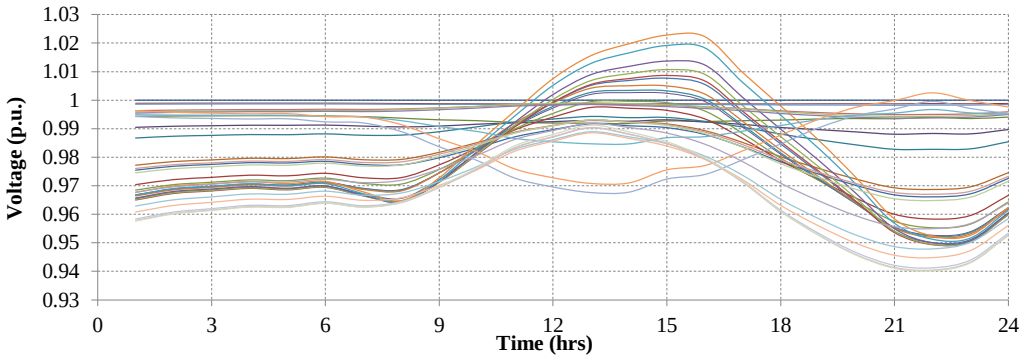

(b)

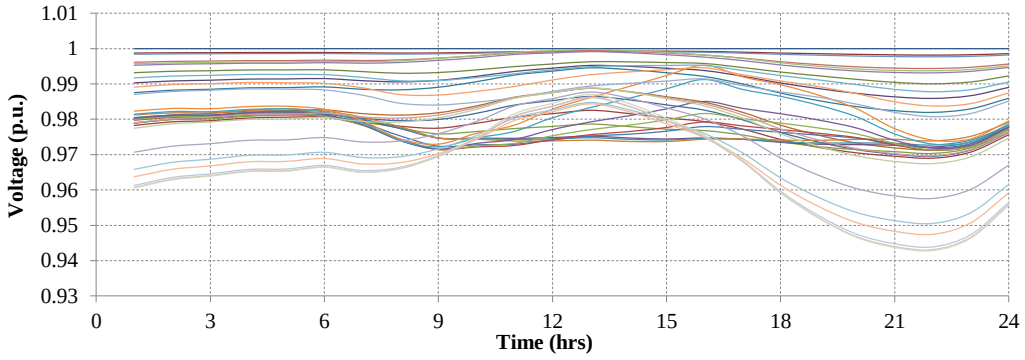

(c)

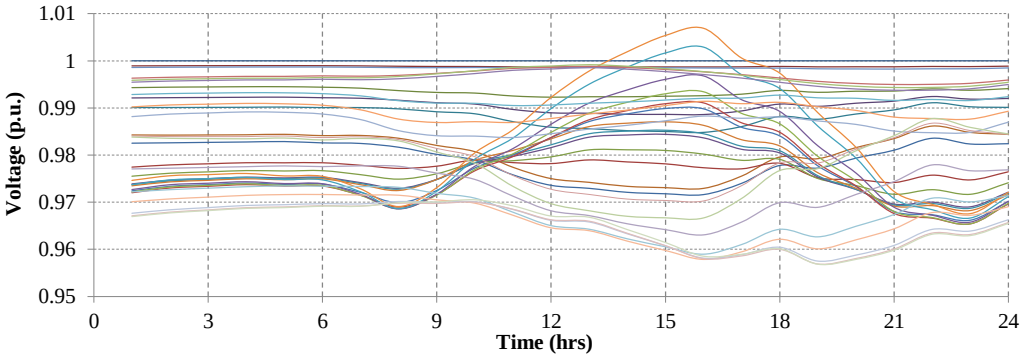

(d)

Fig. 5-8. Voltage profiles for the optimization of (a)f_{VR}, (b)f_p, (c)f_{loss} and (d) f, respectively, legend same as Fig. 5-6.

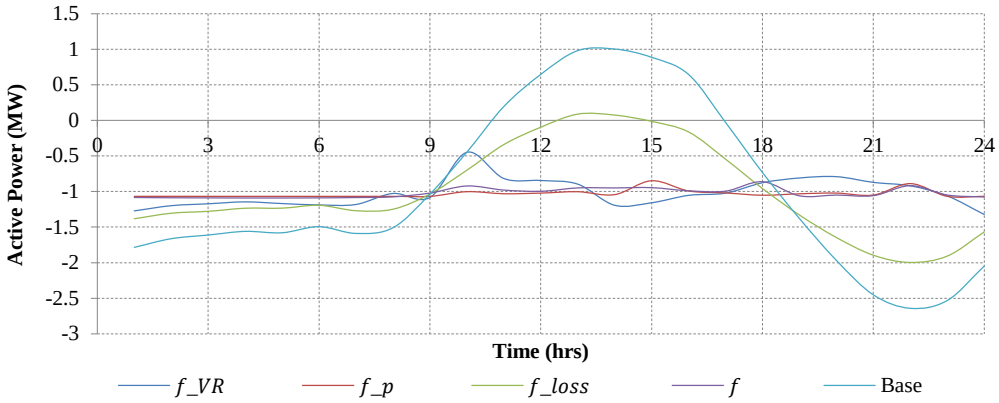

Fig. 5-9. Distribution transformer loading for various service options.

5.4.2 Test Case 2- LV Distribution System

A similar analysis to that presented for Case 1 is carried out in this section. However, only the buses 10, 15, 17, 21 and 24 are chosen as candidate buses for the study due to geographical constraints and easy accessibility. This LV system represents a typical residential feeder with finely distributed rooftop PVs.

5.4.2.1 Base Operation with no BESS

The net transformer loading and the corresponding voltage profile with no BESS are presented in Fig. 5-10 and Fig. 5-11 respectively. From the Fig. 5-4, it can be seen that the lateral 1 is independent and separated by the slack bus supplying fewer loads in comparison to the rest of the system. Hence the voltage deviations and the aggregated load by lateral 1 were not as significant and have no influence on the lateral 2 voltages. Therefore, no battery will be integrated to lateral 1.

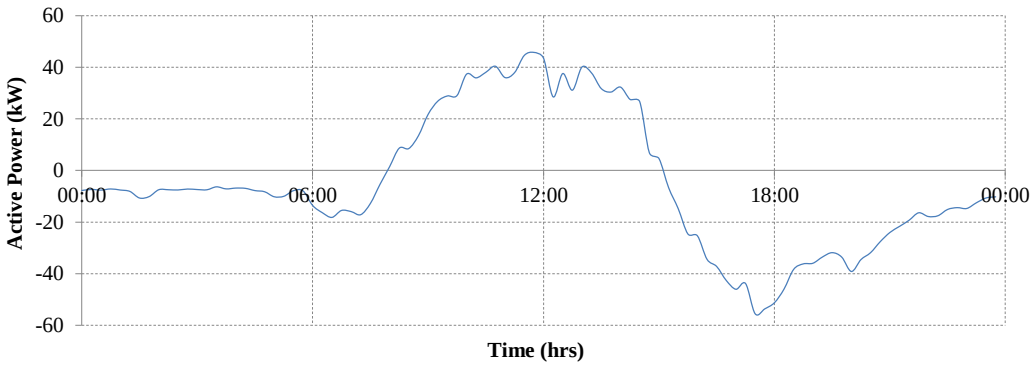

Fig. 5-10. Distribution transformer loading with no BESS.

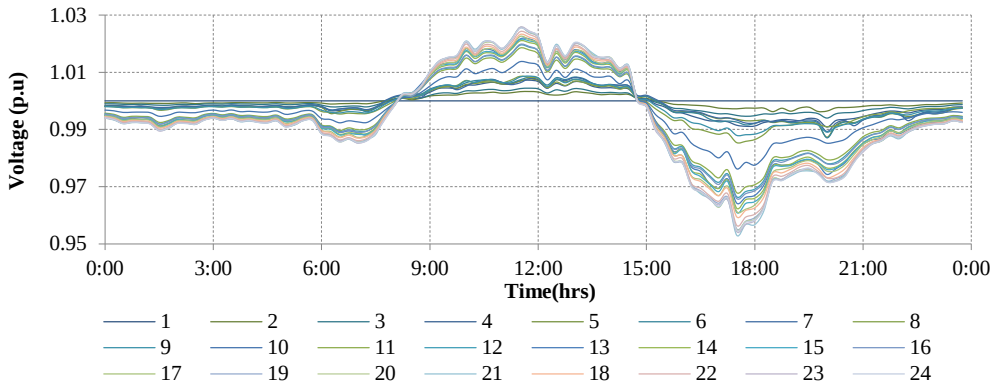

Fig. 5-11. Voltage profile with no BESS.

5.4.2.2 Simulation Results

The Table 5-2 summarizes the simulation results of the optimal size, site, BESS life expectancy, voltages, peak power and losses for different service options. The buses 17, 24, 10 and 24 are identified as the installation sites when optimizing for f_{VR}, f_{loss}, f_p and f respectively. The Fig. 5-12, Fig. 5-13 and Fig. 5-14 shows the corresponding battery profiles, distribution transformer loading and voltage profiles.

From Table 5-2, bus 17 is the optimal BESS site for maximum voltage support. In Fig. 5-12, the f_{VR} BESS discharges from 12.00am to 7.45am. As shown in Fig. 5-14(a) the morning discharge improves the voltage at the bus, consequently improves the overall voltage during this period. Now the power that needs to come from the external grid is nearly zero as shown in Fig. 5-13. During peak PV generation, the BESS drops the voltage at bus 17 to allow reverse power flow to the BESS. Thus, BESS captures peak DG production effectively and delivers it during peak demand to enhance the voltages. The maximum and minimum voltages from f_{VR} optimization are 0.975p.u. and 1.011p.u. respectively. The peak is reduced to 35.08kW and energy losses are reduced by 11.56%.

The optimization shows that the battery at head of feeder enables more peak support while absorbing more PV generation. The maximum peak reduction is achieved at bus 10 when controlling peak exclusively. From Fig. 5-13, both peak import and export power are reduced considerably. The peak is reduced by 49.35% compared to the base case. At bus 10, the charge/discharge of the battery not only achieve peak

shaving but also assist load levelling as depicted in Fig. 5-13. During peak PV generation, the battery starts charging and reduces the voltage at bus 10 to allow reverse power flow. Hence, in Fig. 5-14(b), the minimum voltage of the system is observed at bus 10. During peak demand, the discharge of battery raises the voltage at bus from 3.30pm till midnight while supporting the load. However, no significant improvement in the overall voltage profile is evident and the exclusive peak management has increased the system losses considerably (by 66.74%).

From Table 5-2, the optimal size of BESS required to support peak exclusively is much greater with the lowest life expectancy than for other services.

TABLE 5-2: SUMMARY OF RESULTS FOR TEST CASE 2.

Cost Func.	**Site (Bus No.)**	**Voltage (p.u.)**		E_{loss} **(kWh)**	P_{max} **(kW)**	**Battery**	
		Min (Bus#)	**Max (Bus#)**			**Size (kWh)**	**Life (years)**
Base		0.953 (21)	1.027 (23)	8.30	55.58		
f_{VR}	17	0.975 (17)	1.011 (17)	7.34	35.08	148.85	15.26
f_P	10	0.960 (10)	1.020 (10)	13.84	28.15	228.88	13.22
f_{loss}	24	0.975 (21)	1.014 (13)	5.27	33.96	93.00	16.10
f in (5-1)	24	0.975 (24)	1.013 (24)	6.14	31.60	136.26	16.20

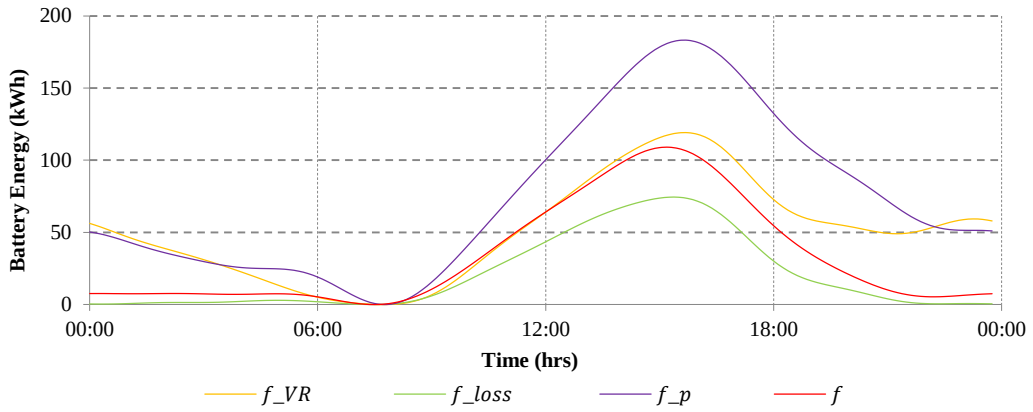

Fig. 5-12. Battery energy profiles for the various service options.

Bus 24 is the optimal site that achieves most loss reductions when controlling the losses exclusively and is also the optimal site from the optimization of the cost function for multiple grid services. From Table 5-2, the BESS capacity required for the pure control of loss is the lowest. The battery is nearly idle from 12.00am to 8.00am. However, the battery for multiple grid services discharges from 5.00am to 7.30am to support the morning peak. During peak PV generation battery charges until 3.30pm and discharges from 3.30pm to 10.00pm. In this case, the reduction in peak export and import power is almost equal. The power from/to utility is significantly reduced and more evenly distributed over 24 hours and managed efficiently. The minimum voltage and maximum voltage observed with battery at bus 24 are 0.975p.u. and 1.013p.u. respectively.

From the battery energy profiles in Fig. 5-12, it can be seen that battery energy at the beginning of the day is closer to that of at the end of the period. The resultant periodicity and continuity are attributable to the Fourier series approach adopted for battery modelling.

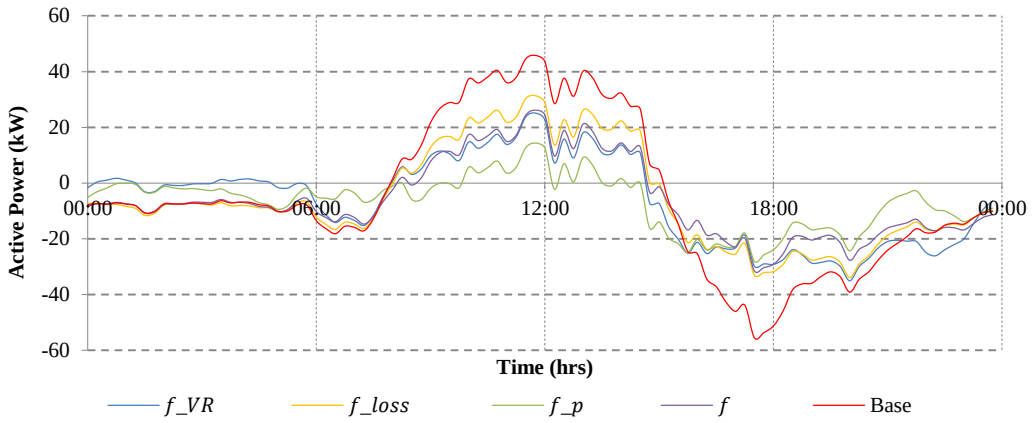

Fig. 5-13. Distribution transformer loading for various service options.

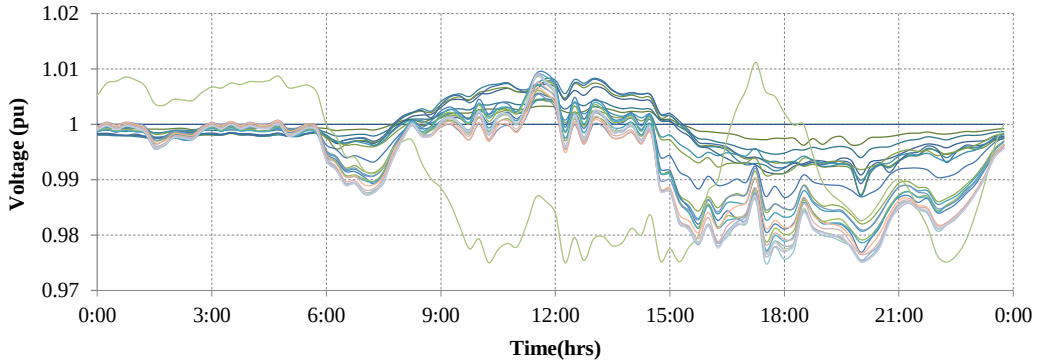

(a)

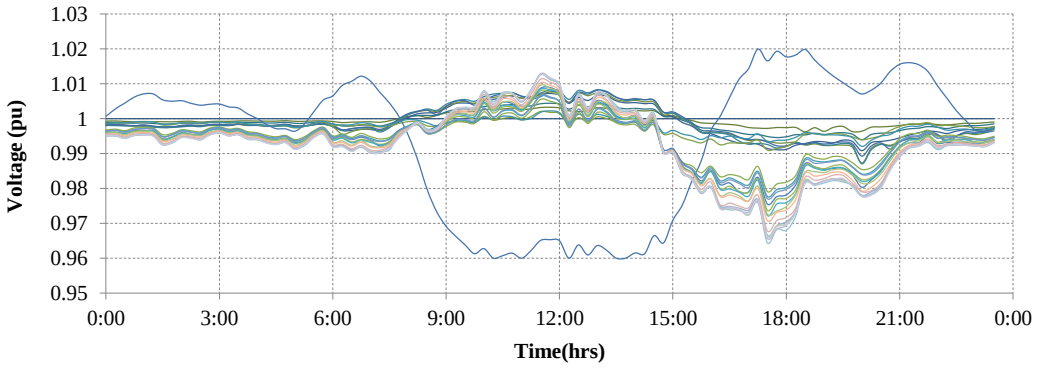

(b)

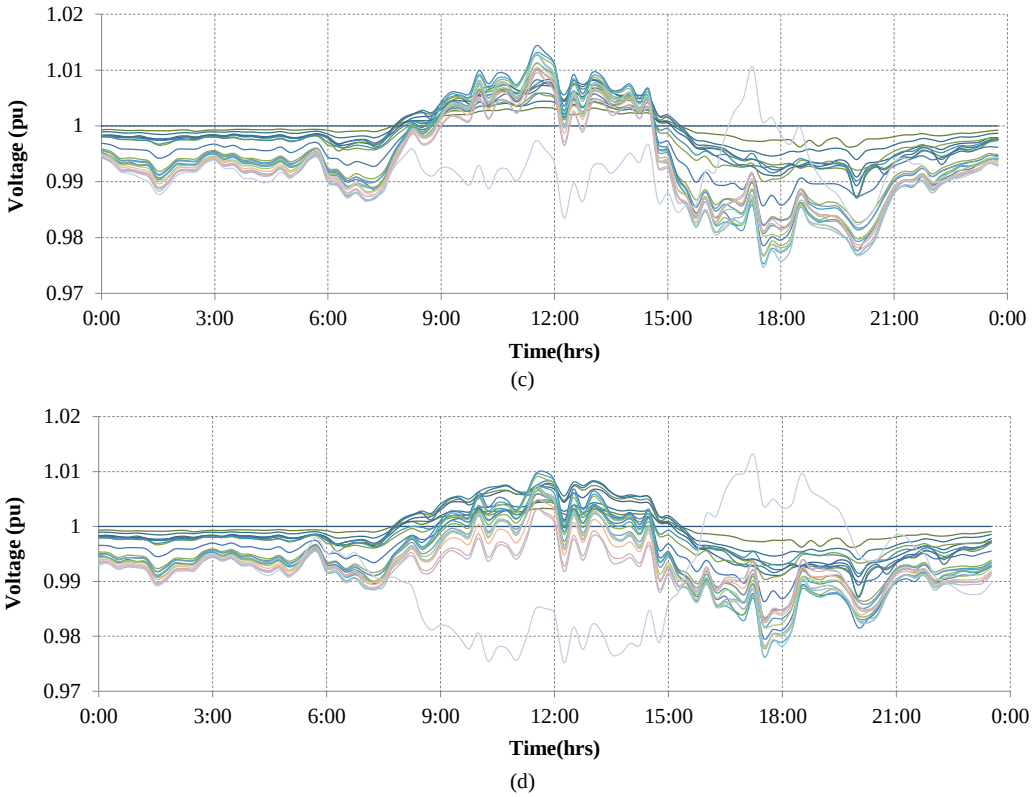

Fig. 5-14. Voltage profiles for the optimization of (a)f_{VR}, (b)f_p, (c)f_{loss} and (d) f, respectively, legend same as Fig. 5-11.

5.5 Conclusions

This chapter proposes a tool that effectively deals with the problem of optimal sizing and dispatch management of BESSs considering various service options. Detailed simulation results show the potential of community level BESS, controlled by DNO, in addressing distribution system overarching concerns including peak shaving, voltage regulation and loss reduction for improving system efficiency. Simulations were carried out for a MV and a LV distribution test system. Based on the quantitative analysis, the main conclusions are:

- Proposed method is able to take the battery daily cycling into consideration, thus optimizes the BESS performance by effectively controlling the cyclic ageing.

- In most literature, battery systems are installed for peak shaving only. However, based on results in Table 5-1 and Table 5-2 installation for peak

support does not reconcile overvoltage (the primary DG limiting factor) or low voltage issues. Moreover, it increases system losses considerably.

- Therefore, the problem needs to be addressed with the aim of improving system voltages to enhance the DG absorption. Maximum tradeoffs are achieved when installing battery considering its ability to simultaneously provide multiple services (Table 5-1 and Table 5-2).

- Amount of tradeoffs in terms of voltage regulation, peak shaving, loss reduction and battery parameters highly depend on the installation site.

- Base on the results, the benefits and battery parameters are primarily characterized by the system topology and the distribution of loads and generation.

- At any stage, the proposed BESS approach did not violate the capacity limit of distribution system as the transformer loading is effectively minimized. Therefore, no upgrades will be required for peak support.

- Adoption and optimal integration of BESS in the next generation grid will enable better utilization and decentralize management of the available resources improving the ability of the grid to support more demand and host larger quantities of DG.

- Therefore, the proposed approach will reduce the supply that needs to come from centralized power sources, transmission losses, carbon emission and related investment costs.

Chapter 6. Optimal Management of Residential BESSs in Unbalanced Distribution Networks with High Penetrations of PV

6.1 Introduction

In this chapter, the approach proposed in Chapter 5 is improved for real and reactive power flow management in three-phase four-wire unbalanced distribution systems with large penetrations of PV. Distributed battery storage devices, under the control of the network operator, are co-located with residential PVs to allow the requisite degrees of freedom while making use of the available PV inverter capacity. Approach assumes the active collaboration of the consumers and utility.

The battery dispatch scheduling algorithm determines which generation unit (grid, PV or battery) operates at any given time interval and the charge/discharge mode of battery. Inverter interfaced batteries can operate either in real (P) or real and reactive (PQ) power mode. Thus assists active management and allocation of available resources. Simulations were carried out for a three-phase four-wire unbalanced network using MATLAB IP algorithm.

6.2 Problem Formulation

6.2.1 Objective Function

The cost function in (5-1) is updated to include a VUF cost component (C_{VUF}) to effectively minimize impacts of imbalances:

$$f(C_{iF}) = \sum_{l=1}^{5} \gamma_l . f_l = \gamma_1 C_{battery} + \gamma_2 C_{Loss} + \gamma_3 C_{VR} + \gamma_4 C_P + \gamma_5 C_{VUF} \quad (6\text{-}1)$$

Where, $C_{VUF} = \int_{t=1}^{T} \int_{i=1}^{nbus} \frac{{V_2}^i}{{V_1}^i} . 100 . \Delta t . r_{VR}(t)\, dt$

6.2.2 Objective Function Constraints

The inequality constraints defined in Chapter 5.2.2 are implemented in this chapter.

6.3 Simulation Results

6.3.1 Test System

The three-phase model based upon the test system presented in Chapter 5.3.2 is used in this chapter. It must be noted that this feeder model, referred to as "Pavetta 1", has been intensively studied within the Perth Solar City high penetration PV trial undertaken by Western Power. The residential data used in this chapter are generated from aggregated consumer data and is useful representation of typical household load and solar over a day. Each residential load is modelled with a local load and a consumer installed rooftop PV systems. The solar array rating varies from 5-6kW, the typical residential load peak varies from 3.5-4.5kW.

Simulations were carried out for the simulation scenarios in Table 6-1. Case 1 shows the base condition of the grid without battery controls. Case 2 and 3 presents the optimized results with real and real/reactive power controls respectively. In Case 4, the optimized battery set points found in Case 2 are assigned to batteries while loads and solar generation data for this case are generated with a forecasting error in comparison to data used in Case 2 to simulate a real-time application. Only phase '*a*' results are discussed in this section for brevity as phase '*b*' and '*c*' results show similar characteristics.

TABLE 6-1: SIMULATION CASES.

Case	Description
1-(Base)	Base case with PV at each load but no battery control
2-(*P Control)*	26 batteries are randomly allocated across all three phases for system in Case 1
3-(*P-Q Control)*	Case 1 system with real and reactive control (0.95 PF)
4–(*Application)*	Case 2 optimized results tested in real-time.

6.3.2 Case 1 - Base

Fig. 6-1 illustrates the phase '*a*' voltage profile with no battery and the net distribution load and generation curve. The peak demand seen at the transformer is 48.8kW. At peak hour, the voltage at the furthest bus is 0.943p.u. Low voltages are observed from 5.00pm till 6.30pm during the evening peak consumption period. This is marginally within the regulatory voltage lower limit. Maximum voltage due to reverse power flow during peak PV generation is 1.031p.u.

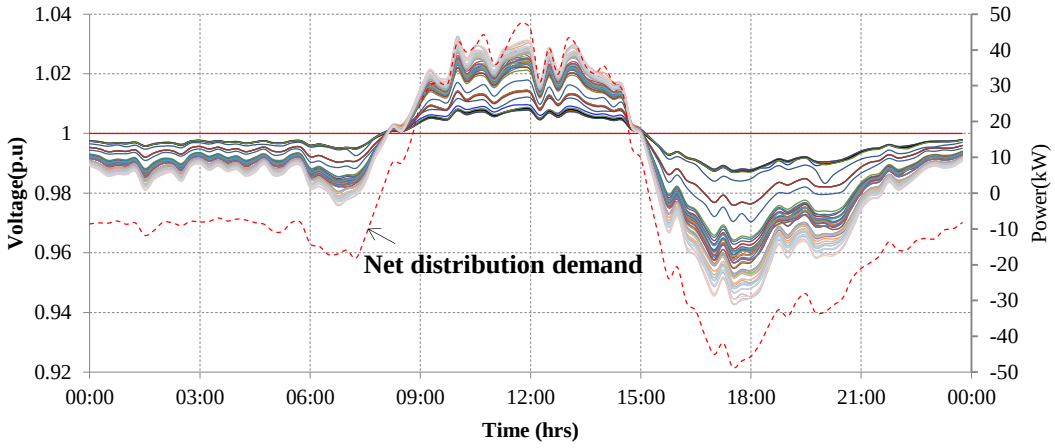

Fig. 6-1. Case 1-Phase '*a*' daily voltage profiles and the distribution transformer loading.

6.3.3 Case 2 - P Control

A total of 26 batteries are randomly allocated along the feeder across all three phases co-located with PV systems. There are 9, 9 and 8 batteries on phase '*a*', '*b*' and '*c*', respectively. Fig. 6-2 gives the optimized energy profile for the batteries on phase '*a*' and the corresponding demand curve as seen at reference bus in dotted line. Fig. 6-3 shows the optimized voltage profile over 24 hours.

As depicted in Fig. 6-2, the batteries charge during the peak PV generation period and the stored battery energy increases from 9.00am until 3.00pm. The batteries at the head of the feeder such as battery 8.1 (on bus 8) are mostly idle during the periods of PV generation but charge off peak. The batteries near the end of the feeder, such as battery 24.1 (on bus 24) charge strongly during the periods of high PV generation and control the feeder voltage rise.

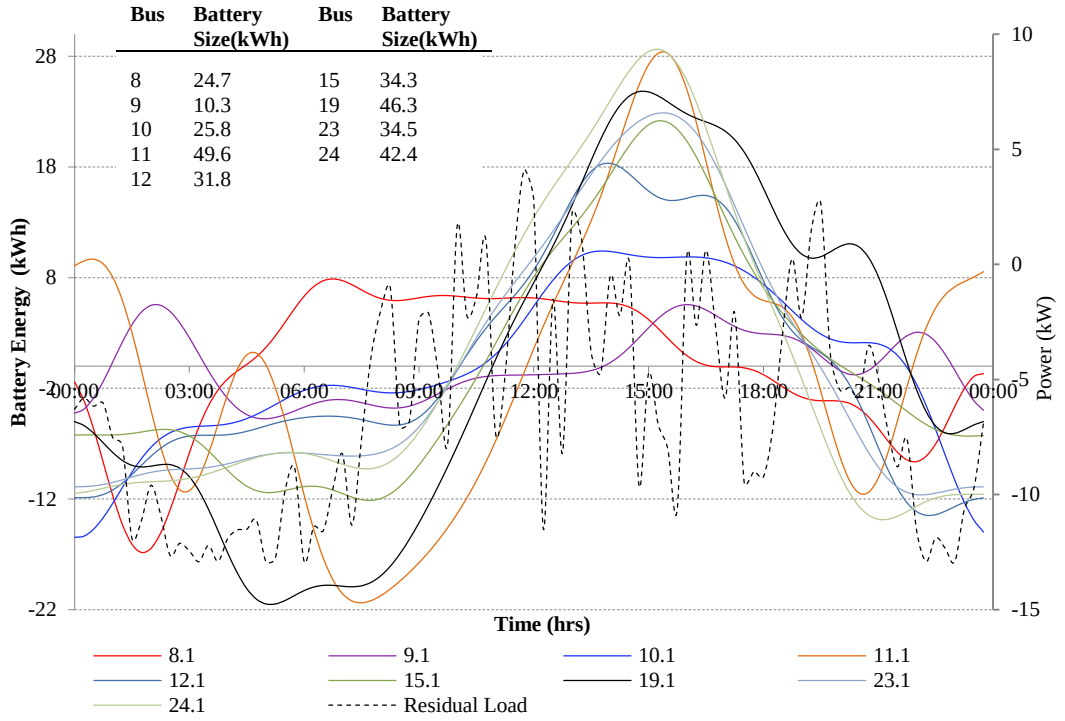

Fig. 6-2. Case 2- Phase '*a*' optimized battery energy profiles and the transformer loading.

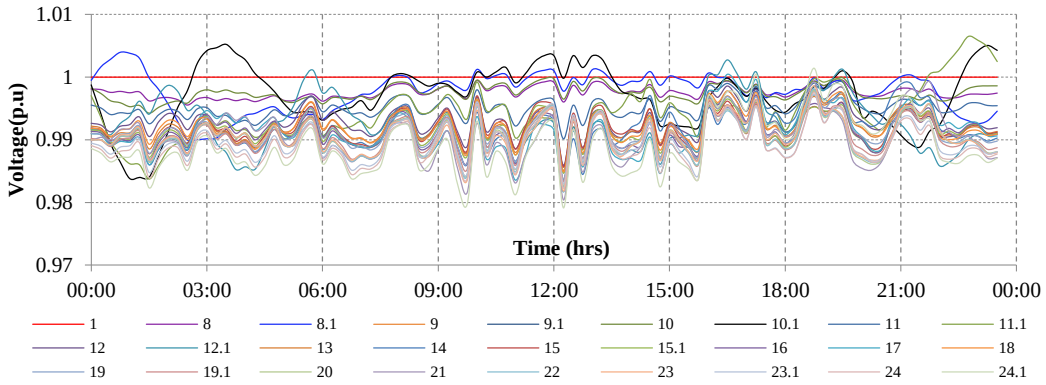

Fig. 6-3. Case 2- Phase '*a*' daily voltage profiles.

The charging and discharging of batteries have significantly reduced the peak import power from 48.8kW to 12.9kW. Similarly, peak export power is reduced from 47.5kW to 4.1kW. Peak shaving is realized by the aggregated discharge of the batteries along the feeder. It is observed that the battery operation is highly dependent on the positioning of the battery with storages near the head of the feeder operating differently from those at the end.

In order to optimally manage the voltage profile, batteries at end of feeder discharge at a relatively high rate than the head of the feeder batteries. During peak PV

generation far end batteries charge more in order to capture more reverse power flow as the voltage rise occurs predominantly at the end buses. Head of the feeder batteries charge at a lower rate or remain flat permitting the rest of the batteries to charge. Therefore, end of the feeder batteries appear to have more influence on the feeder voltage regulation than the batteries installed head of the feeder. However, all the batteries collaboratively control reverse power flow, voltage regulation, peak shaving and load balancing.

The maximum size of the battery required is 49.6kWh at bus 11 and the minimum size is 10.3kWh at bus 9. With battery control, the minimum voltage is improved to 0.976p.u., the maximum voltage is 1.006p.u. and the VUF was improved by 53%.

6.3.4 Case 3- PQ Control

This section explores voltage support by PV/battery systems with inverter reactive power capability enabled for real and reactive power compensation. Standard generator conventions are used to define the inverter PF. A lagging PF indicates that generator is injecting reactive power to the grid.

Since distribution networks require more active power compensation than reactive power compensation, an inverter PF of 0.95 (leading to lagging) magnitude is stipulated in this chapter. During real power import, a lagging PF will accentuate the voltage reduction capability. During real power export a lagging PF will maximize the voltage raising capability.

Fig. 6-4 shows the battery charging profiles on the primary axis and total demand on the secondary axis when the optimization was repeated with a fixed 0.95 PF for PV inverter systems. Addition of reactive support ability in the optimization improves the flexibility of the optimization. Moreover sizing of the batteries have decreased as a consequent of added voltage support ability. Fig. 6-5 depicts the corresponding voltage profile. In this case, the minimum voltage is improved to 0.982p.u., the maximum voltage is 1.004p.u. and the VUF was improved by 59%.

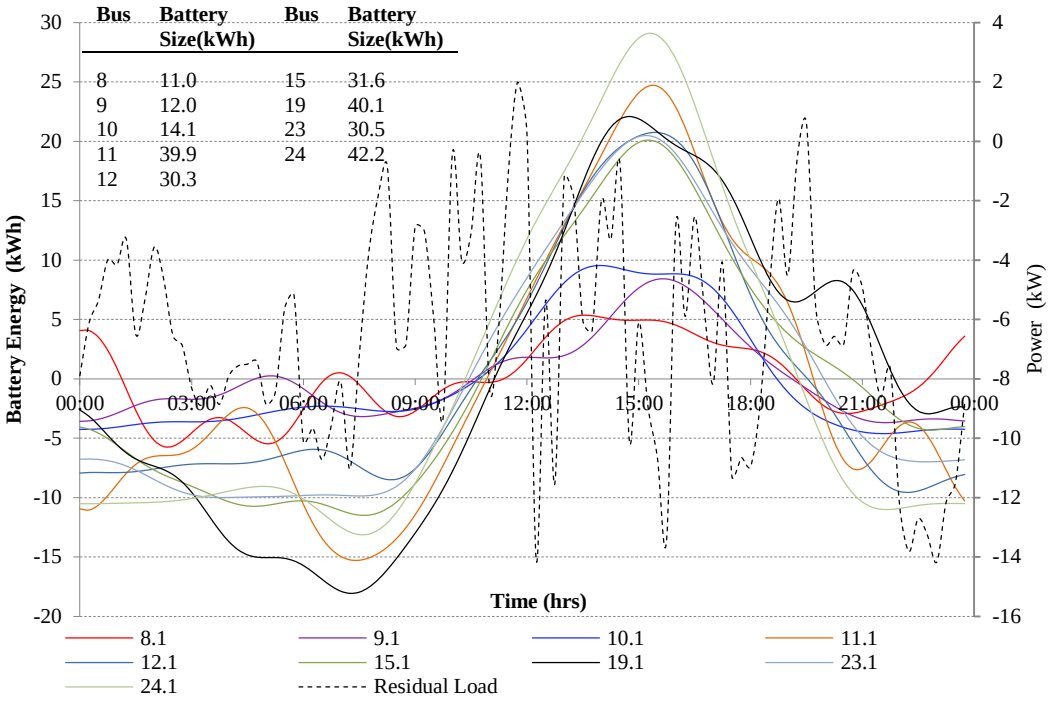

Fig. 6-4. Case 3- Phase '*a*' optimized battery energy profiles and the total demand as seen at slack bus.

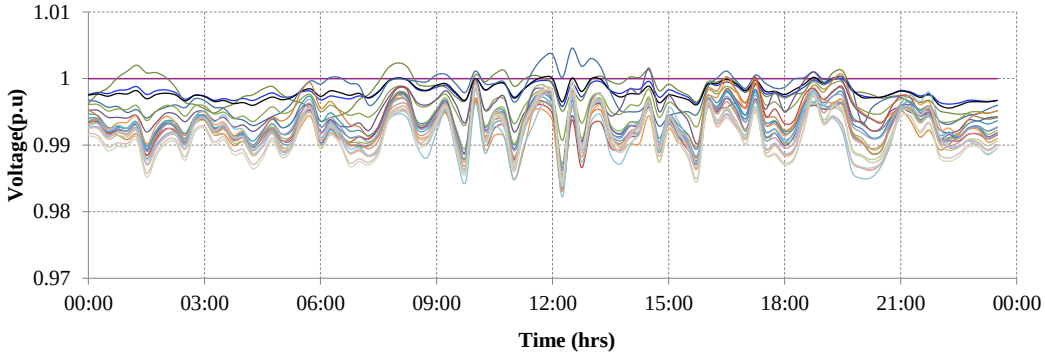

Fig. 6-5. Case 3- Phase '*a*' daily voltage profile (Legend same as Fig. 6-3).

6.3.5 Case 4- Application in Real Time

Case 4 schedules the charge/discharge cycles of the batteries according to optimized battery energy derived in Case 2. Load and PV data were modified by the addition of a uniformly distributed random variable with a range of +-15% of the forecasted load or solar generation at each bus.

Fig. 6-6 shows the voltage profile. Voltage variability increases marginally in comparison to the voltage in the forecasted case. Initial forecast of battery energy

still maintain improved voltage levels with the 15% forecasting error. In this case, the minimum voltage is 0.978p.u., the maximum voltage is 1.004p.u. and the VUF was improved by 41%.

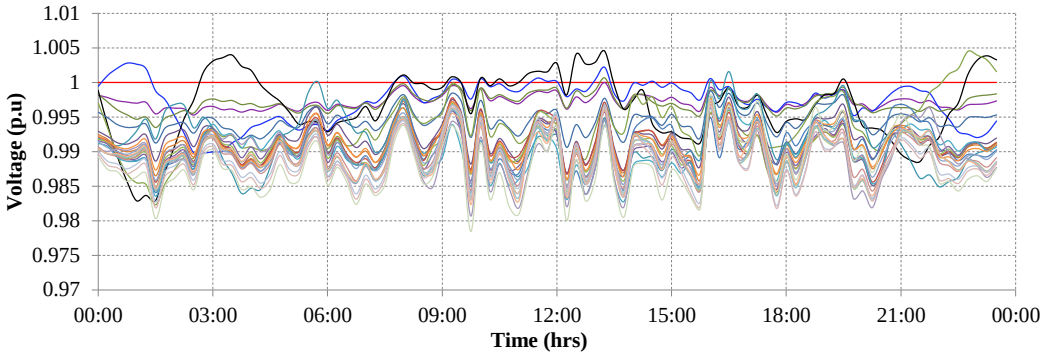

Fig. 6-6. Case 4- Phase '*a*' daily voltage profile (Legend same as Fig. 6-3).

6.3.6 Analysis and Comparison of Results

Fig. 6-7 and Fig. 6-8 present the frequency of voltage occurrences across all three phases for Cases 1 and 4. As it can be seen from the figures the voltages are substantially improved in Case 4 even with the forecasting error. The voltages are now clustered tightly around the nominal voltage. Similar improvements were seen in case with PQ control.

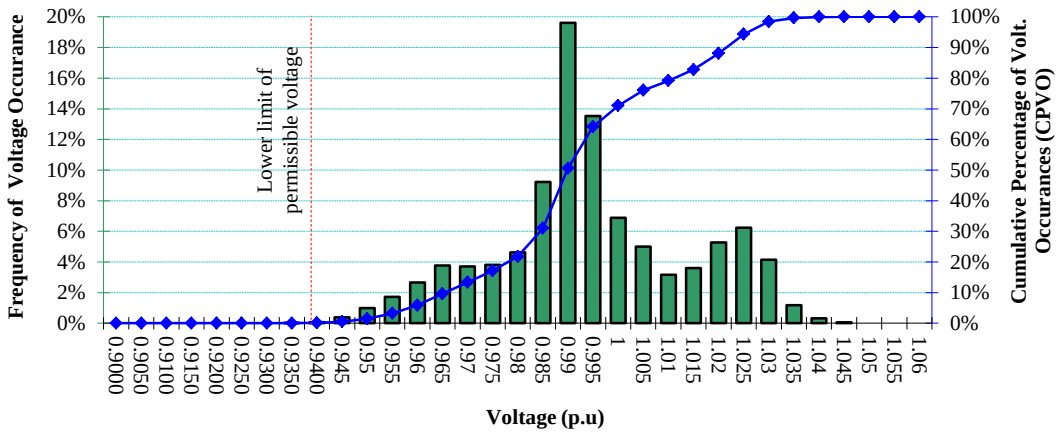

Fig. 6-7. Frequency distribution of voltage- Case 1.

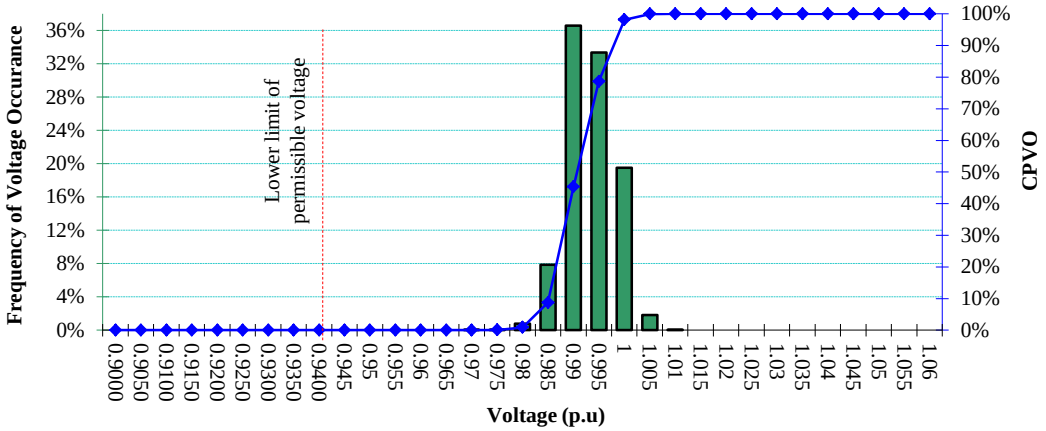

Fig. 6-8. Frequency distribution of voltage- Case 4.

VUF cost component ensures that phase voltages at any given node are balanced with minimal deviations. Low VUF guarantees the safe operation of three phase systems and connected equipment. Fig. 6-9 shows average VUF for each test case.

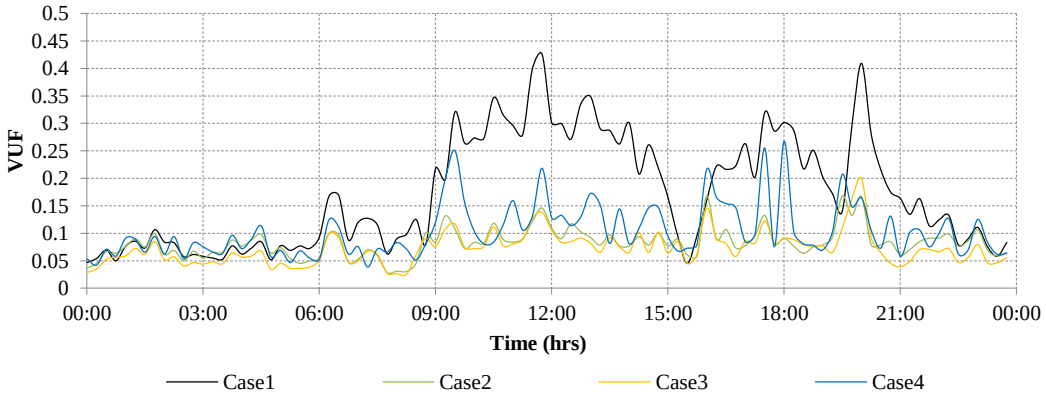

Fig. 6-9. Daily variation of average voltage unbalance factor over 24 hours.

Fig. 6-10 shows the net power drawn from the grid on phase '*a*' for each test scenario. The peak power is significantly reduced and more evenly distributed over 24 hours with battery control. This holds true for *P* control and *PQ* control modes. The peak export and import power is reduced by approximately 90% and 72% respectively in Case 4 in comparison to Case 1.

Fig. 6-11 shows the losses distribution for each case. In Case 2 and Case 4, the losses have reduced by 72%. With *PQ* control in Case 3 the losses have decreased by almost 83%. Operation in *PQ* mode has reduced the losses slightly more than that of with *P* only. Level of voltage correction achieved in *P* and *PQ* modes match very

closely for the LV test system. Reactive power injections reduce reactive requirement of the load and reactive power losses in the lines.

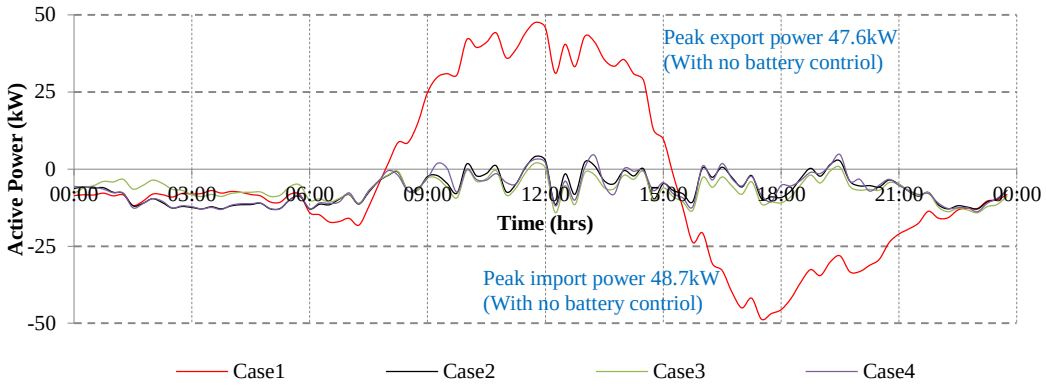

Fig. 6-10. Daily variation of total active power on phase '*a*' as seen at source bus.

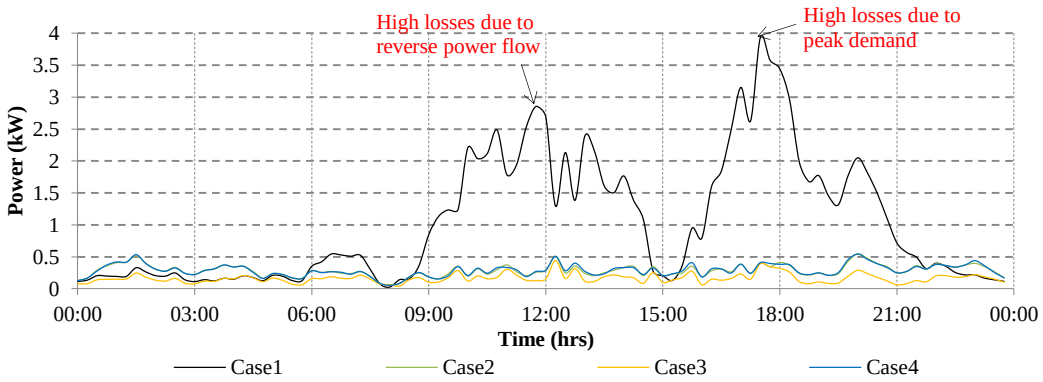

Fig. 6-11. Daily variation of total active power losses on phase '*a*'.

6.4 Conclusion

In this chapter, the distributed battery storage devices are integrated with customer PV systems to coordinate and manage the dispatch of generation. This requires cooperative operation between the utility and customer installed PV/Battery units through advanced communication. Simulations were carried for an unbalanced three phase distribution system. Results highlight the capability of the proposed algorithm to reduce distribution losses, reduce the peak demand and improve the feeder voltage profile with respect to voltage magnitude and phase balance. Deployment of battery storage with PV systems allows for better utilization of available renewable generation and minimizes the import from the external grid.

In addition to the proposed battery management strategy, the chapter makes a major

contribution in highlighting the influence of the battery location on the daily charge profile and grid performance. The battery energy profile varies significantly from the head to the far end of the feeder. For the typical LV test system, the battery operation at the head of the feeder is far more influenced by the peak shaving while those at the far end of the feeder are more influenced by voltage regulation requirements.

Chapter 7. Analytical Approach for Optimal Placement, Sizing and Management of Battery Storage for Voltage Regulation

This chapter proposes a holistic analytical approach to optimally site and size single or multiple BESSs along with a real-time smart charge/discharge management strategy. The proposed method is simple and provides improved levels of voltage support while enhancing the ability of the distribution system to absorb high penetrations of DG. BESSs can provide active and/or reactive power support. Voltage-control zones (VCZs) are identified using voltage sensitivity factors (VSFs) to establish BESS influence zones which in turn determine the optimal locations and maximum numbers of BESS units required. Optimal BESSs capacities and management strategy are evaluated using an augmented load flow (ALF) approach.

BESS will operate in a constant power mode during off peak and in a variable power mode during periods of peak generation and demands. The intervals for varying operating modes are defined through the identification of off peak, peak generation and peak demand time zones based on the net forecasted distribution transformer load. Optimal BESS management strategy controls the battery external parameters; charge/discharge rates, depth of discharge and daily cycling. Offline and real-time dispatch control strategy defines which source or unit (grid or BESS) operates at any given time, the quantum of power exchange and the direction of power flow. The optimal BESSs sizing is derived considering the optimal dispatch management strategy for added accuracy. Detailed simulations are performed using a distribution system in Western Australia studied under the Solar City Trial project.

7.1 Optimal Placing of BESS

The proposed approach determines optimal BESS locations analytically using power flow Jacobian and VSFs. This method ensures maximum voltage support is accomplished with minimal real and reactive power flows from the selected bus. Thus, voltage enhancements can be achieved with minimum BESSs investment costs.

The optimal siting strategy identifies voltage control zones and optimal sites, depending on the voltage sensitivity of buses to variations in active power (dV/dP). The approach is explained below.

The sensitivity coefficients, VSFs, are calculated using the inverse Jacobian:

$$\begin{bmatrix} \frac{d\delta}{dP} & \frac{d\delta}{dQ} \\ \frac{dV}{dP} & \frac{dV}{dQ} \end{bmatrix} = \begin{bmatrix} \frac{dP}{d\delta} & \frac{dP}{dV} \\ \frac{dQ}{d\delta} & \frac{dQ}{dV} \end{bmatrix}^{-1} = J^{-1}; \quad VSF = \left[\frac{dV}{dP}\right] \tag{7-1}$$

Where, P, Q, V, and δ are the active power, reactive power, voltage magnitude and phase angle respectively.

The dV/dP entry of J^{-1} is defined as the VSF, which is a $(nbus-1)X(nbus-1)$ matrix, where n is the number of buses. The diagonal and off diagonal elements of VSF matrix indicate the impact on a particular bus voltage due to its own power variations and the power variations at the rest of the buses respectively.

Optimal BESS sites selections are performed according to the following steps.

Step 1. Obtain the VSF matrix from (7-1) when the demand is at maximum.

Step 2. Identify bus j that returns the maximum dV_i/dP_j value for each bus i. In other words, power variations at bus j influence the bus i voltages the most (Fig. 7-1).

Step 3. Identify VCZs and optimal BESS sites as follow:

a. Cluster the buses that returned the same j.

b. Ensure that $j = i$ is not the only element in a cluster or the size of the cluster is greater than one; otherwise, eliminate the clusters of size one.

c. The remaining j buses are the optimal BESS sites.

d. The remaining clusters are defined as the VCZs. The voltage at the buses belonging to a particular VCZ are influenced by the power variations at the j of the cluster. Therefore, this ensures maximum voltage support with minimum investments.

e. The eliminated buses in Step 3(b) can be clustered into a remaining VCZ that will return the highest dV_i/dP_j for the eliminated bus, where j is one of the optimal sites.

Step 4. The maximum number of BESS units required is equal to the number of identified zones.

For a selected VCZ the highest dV_i/dP_j of the zone occurs when $i = j$. Therefore, the identified optimal sites can be ranked in a descending order based on $\left|dV_j/dP_j\right|$. This ranking is then used to determine the highest priority sites which assist determine the optimal sites in events where other constraints such as budget or geography do not allow the installations of maximum number of BESS found in Step 4. The simplified flow chart of the above steps is presented in Fig. 7-1.

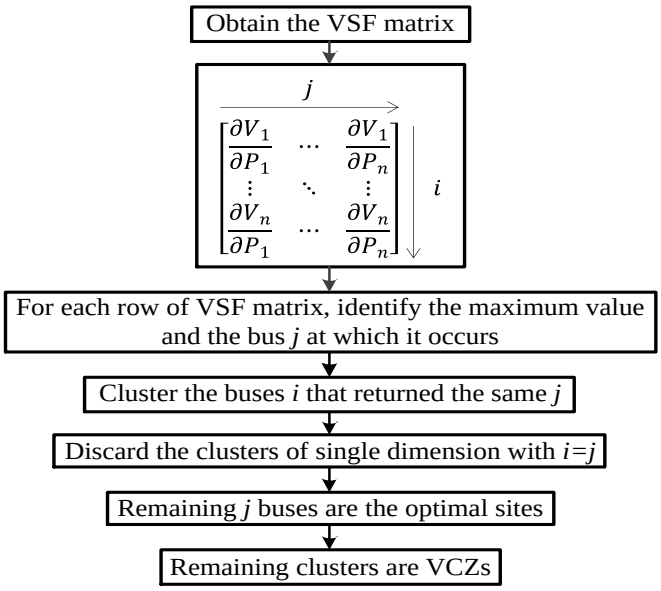

Fig. 7-1. Simplified flow chart for the determination of optimal BESS sites.

7.2 System Architecture of the Proposed Real-Time BESS Smart Management Strategy

Three modes of operation for BESS are proposed in this section; variable power mode (VPM), constant power mode (CPM) and idle mode. Optimal charge/discharge strategy for the operation in the modes VPM and CPM are calculated using an ALF approach. BESS management strategy coordinates the power flow direction and amount of flow between loads, BESSs and generators.

7.2.1 Variable Power Mode (VPM) of BESSs

BESSs operate in the VPM during peak generation and demand periods to ensure voltage at the PCC is maintained at a desired reference voltage level (V_{ref}). Therefore, effectively resolve issues of voltage fluctuations and over voltage. The real-time smart charging/discharging process is accomplished through online monitoring of PCC voltage as depicted in Fig. 7-2. A local controller at PCC interfaced with the BESS will function as the real-time smart charge/discharge controller.

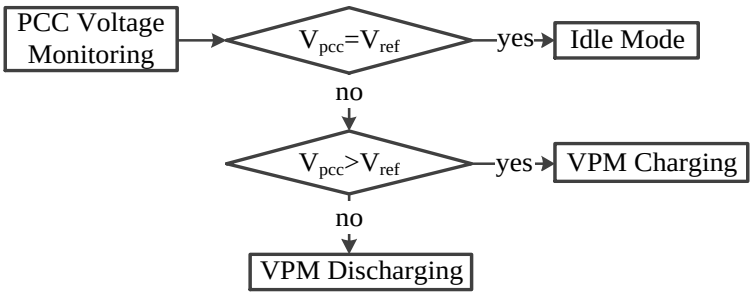

Fig. 7-2. Proposed VPM charge/discharge control strategy.

7.2.2 Constant Power Mode (CPM) of BESSs

BESSs operate in the CPM during identified off peak periods. A constant charge/discharge rate is calculated in real-time so that the battery charge state will return to a predetermined charge state at the end of the cycle. Losses or gains in energy due to forecasting errors are corrected during CPM. This allows the BESS to begin the following day at a charge level consistent with the safe operation of battery. Setting the initial BESS charge state correctly for the day allows the maximum absorption of peak generation and an adequate level of discharge during the evening peak for regulating the voltage.

7.2.3 Idle Mode of BESSs

Battery will switch to the idle mode at times where battery charge level reaches upper or lower limits of its energy constraints in (4-5) or when bus voltages matches the preferred reference voltage tolerance in the VPM. In addition, battery power constraints in (4-4) need to be taken into account to ensure safe operation of the battery devices. Battery rates will be adjusted to the boundary limits, if at any stage battery charge/discharge rates violate the constraints.

7.2.4 Numerical Approach to Determine Battery Bus Reference Voltages and inverter PFs

The battery bus reference voltages are determined using forecasts of load and generation data so that the overall voltage profile can be improved while ensuring energy availability. The optimization problem in (7-2) is minimized using interior-point numerical optimization algorithm in MatLab and proposed ALF.

$$f(V_{ref}, PFs) = \int_{t=1}^{T} \int_{i=1}^{n} ||V_i(t)|^2 - {V_1}^2|^{1/2}.\Delta t.dt \quad (7\text{-}2)$$

The objective function (7-2) locates V_{ref} for battery buses and the power factors (PFs) of BESSs inverters for varying operating intervals during VPM. Minimization of (7-2) encourages system voltages towards the nominal V_1 voltage. It must be noted that (7-2) is flexible and battery PFs can be set to unity if only real power compensation is required.

Furthermore, each BESS will be subjected to the constraint:

$$E_{B-charge} > E_{B-discharge} \quad (7\text{-}3)$$

Where, $E_{B-charge}$ and $E_{B-discharge}$ are battery captured energy and discharged energy respectively during VPM.

The constraint (7-3) will ensure energy availability while avoiding over charging or discharging. Any variations occur during real-time operation due to forecasting errors will be adjusted during CPM.

For three-phase unbalanced systems VUF constraint in (5-4) can be established to minimize effects of imbalances.

7.2.5 Identification of BESS Operating Intervals

The intervals for varying operating modes of BESSs are defined through the identification of off peak, peak generation and peak demand periods for the distribution system under study. Off peak, peak and shoulder periods depend on several factors such as the type of consumers (residential, commercial or mix), location, season and day of the week. This information can be obtained from utility operators and are typically reflected by the tariff structures. BESSs will operate in the VPM during periods of peak demands, shoulder and peak generation. The VPM operation of BESSs will effectively mitigate effects of high frequency variations in

load and generation as BESSs operate in response to PCC voltage. CPM during off peak period is then utilized to correctly set BESSs for the following day operation. A typical winter residential distribution transformer load curve is presented in Fig. 7-3. Based on the Fig. 7-3, t_3 is the peak generation period defined using the mean load. This method is adopted as the normal tariff structures do not identify peak DG production periods.

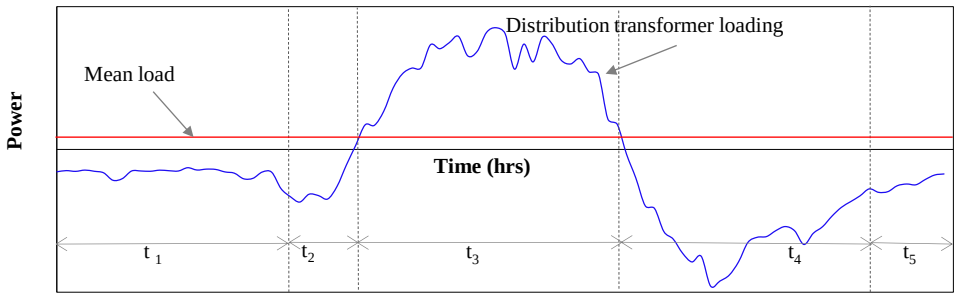

Fig. 7-3. Determination of BESS management intervals.

7.2.6 Hierarchical Communication Strategy

The proposed real-time BESS dispatch management approach adopts a hierarchical control mechanism with two levels of controls; (i) Centralized controller to perform forecasting and the determination of V_{ref} , (ii) Local inverter interfaced controller to manage charge/discharge state of the battery. The control approach is shown in Fig. 7-4.

The central controller DMS establishes a bi-directional communication link with the network and weather stations for online data acquisition. As new information become available, the DMS archives them in a database and process them along with future forecasts of weather. Collected data are then fed to the forecasting tool to produce the 24 hours ahead forecast of the load and generation data. The forecasted data are then used to define the operating intervals and to evaluate V_{ref} set points. The central controller then sends this information to the local controllers through AMI.

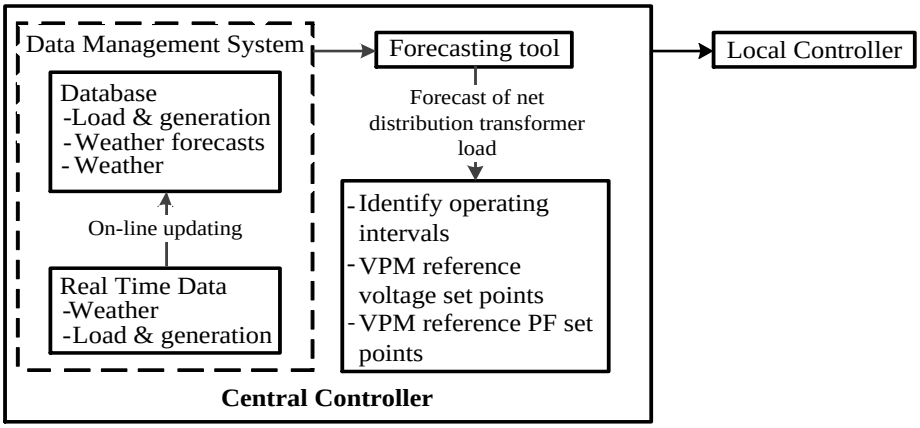

Fig. 7-4. Communication strategy.

7.2.7 Limitations of BESSs

Under exceptional conditions such as upstream grid failures or blackouts, BESSs could be set to operate under different sets of rules. In events of upstream grid failures, BESSs will discharge to provide the required levels of voltage support, given that the battery constraints are not violated. In the VPM, BESSs operate in response to PCC voltage. Therefore, a drop in PCC voltage will cause the battery to discharge to ensure PCC voltage matches the reference voltage. However, in the CPM, BESSs could be charging to adjust for forecasting errors. Therefore, it is advisable to set these BESSs to the idle mode to minimize the burden on the network. Even during the nominal VPM periods, batteries could be set to discharge at a constant rate. These new conditions can be communicated to the BESSs local controllers upon detection of an exceptional situation.

7.3 Proposed Approach for Optimal Management and Sizing of BESS

Optimized BESS management strategy defines the battery external parameters; depth of discharge, energy state and daily cycling. An ALF approach is developed in this chapter to derive the optimal BESS charge/discharge management strategy using the numerically found V_{ref} and PFs. The battery inverter can function at unity PF for real power support only or at optimized PFs for real and reactive power support.

7.3.1 Proposed Augmented Load Flow

To achieve voltage regulation, a new bus type, named the "QV" bus, is introduced. The bus voltage (V_{ref}) and the reactive power (or the PF) of the inverter at a QV bus are considered as independent variables.

The ALF approach is a development of the total current injection method (TCIM) proposed in [131]. Only the modification of the power flow approach to accommodate QV buses is presented here. References [131] provide the PV and PQ bus nodal admittance matrix derivations.

From [131], the current injection mismatch equations for PQ type bus can be expressed as;

$$\begin{bmatrix}\Delta I_{m_i}\\ \Delta I_{r_i}\end{bmatrix}=\begin{bmatrix}\frac{V_{m_i}}{{V_i}^2}\Delta P_i-\frac{V_{r_i}}{{V_i}^2}\Delta Q_i\\ \frac{V_{r_i}}{{V_i}^2}\Delta P_i+\frac{V_{m_i}}{{V_i}^2}\Delta Q_i\end{bmatrix}=\begin{bmatrix}{B'}_{ii} & {G'}_{ii}\\ {G''}_{ii} & {B''}_{ii}\end{bmatrix}\begin{bmatrix}\Delta V_{r_i}\\ \Delta V_{m_i}\end{bmatrix} \tag{7-4}$$

Where, V_i, V_r and V_m are the magnitude, real and imaginary component of voltage E_i, respectively. ${B'}_{ii}$, ${G'}_{ii}$, ${G''}_{ii}$ and ${B''}_{ii}$ are defined in [131]. ΔI_{m_i} and ΔI_{r_i} are the imaginary and real components of the current mismatch at bus i.

For a QV bus, the active power mismatch ΔP_i becomes a dependent variable. Therefore, from (7-4), ΔI_{r_i} and ΔI_{m_i} components for a QV bus are derived as:

$${\Delta I^*}_{m_i}=-\frac{V_{r_i}}{{V_i}^2}\Delta Q_i \tag{7-5}$$

$${\Delta I^*}_{r_i}=\frac{V_{m_i}}{{V_i}^2}\Delta Q_i \tag{7-6}$$

Equation (7-4) can be modified to contain the dependent variable (ΔP_i). However, another equation is needed to avoid matrix over-determination. Thus, an equality

constraint is established in (7-7) considering that for QV buses $\Delta V_i = 0$:

$$\Delta V_i = \frac{V_{r_i}}{V_i}\Delta V_{r_i} + \frac{V_{m_i}}{V_i}\Delta V_{m_i} = 0 \tag{7-7}$$

Therefore, by combining (7-4) and (7-7):

$$\begin{bmatrix} -\frac{V_{r_i}}{{V_i}^2}\Delta Q_i \\ \frac{V_{m_i}}{{V_i}^2}\Delta Q_i \\ 0 \end{bmatrix} = \begin{bmatrix} B'_{ii} & G'_{ii} & -\frac{V_{m_i}}{{V_i}^2} \\ G''_{ii} & B''_{ii} & -\frac{V_{r_i}}{{V_i}^2} \\ \frac{V_{r_i}}{V_i} & \frac{V_{m_i}}{V_i} & 0 \end{bmatrix} \begin{bmatrix} \Delta V_{r_i} \\ \Delta V_{m_i} \\ \Delta P_i \end{bmatrix} \tag{7-8}$$

Equation (7-7) establishes that,

$$\Delta V_{r_i} = -\frac{V_{m_i}}{V_{r_i}}\Delta V_{m_i} \tag{7-9}$$

By substituting (7-9) into first two equations in (7-8) yields;

$$\begin{bmatrix} -\frac{V_{r_i}}{{V_i}^2}\Delta Q_i \\ \frac{V_{m_i}}{{V_i}^2}\Delta Q_i \end{bmatrix} = \begin{bmatrix} (G'_{ii} - \frac{B'_{ii}V_{m_i}}{V_{r_i}}) & -\frac{V_{m_i}}{{V_i}^2} \\ (B''_{ii} - \frac{G''_{ii}V_{m_i}}{V_{r_i}}) & -\frac{V_{r_i}}{{V_i}^2} \end{bmatrix} \begin{bmatrix} \Delta V_{m_i} \\ \Delta P_i \end{bmatrix} \tag{7-10}$$

Hence, the diagonal elements of the augmented nodal admittance matrix (Y) related to bus i that is of QV type can be expressed as:

$${Y_{ii}}^* = \begin{bmatrix} (G'_{ii} - \frac{B'_{ii}V_{m_i}}{V_{r_i}}) & -\frac{V_{m_i}}{{V_i}^2} \\ (B''_{ii} - \frac{G''_{ii}V_{m_i}}{V_{r_i}}) & -\frac{V_{r_i}}{{V_i}^2} \end{bmatrix} \tag{7-11}$$

The generic off-diagonal element for a branch ij is:

$$Y_{ij}{}^{*} = \begin{bmatrix} (G_{ij} - \frac{B_{ij}V_{m_i}}{V_{r_i}}) & 0 \\ (-B_{ij} - \frac{G_{ij}V_{m_i}}{V_{r_i}}) & 0 \end{bmatrix} \tag{7-12}$$

Therefore, the proposed augmented TCIM algorithm can be summarized as in (7-13); where node i of QV type is connected to two PQ nodes l and j.

$$\begin{bmatrix} \vdots \\ \overline{\Delta I_{m_l}} \\ \Delta I_{r_l} \\ \overline{\Delta I^{*}{}_{m_l}} \\ \Delta I^{*}{}_{r_i} \\ \overline{\Delta I_{m_j}} \\ \Delta I_{r_{lj}} \\ \overline{\vdots} \end{bmatrix} = \begin{bmatrix} \vdots & \vdots & \vdots & \vdots & \vdots \\ \cdots & Y_{ll} & Y_{li}{}^{*} & Y_{lj} & \cdots \\ \cdots & Y_{il} & Y_{ii}{}^{*} & Y_{ij} & \cdots \\ \cdots & Y_{jl} & Y_{ji}{}^{*} & Y_{jj} & \cdots \\ \vdots & \vdots & \vdots & \vdots & \vdots \end{bmatrix} \begin{bmatrix} \vdots \\ \overline{\Delta V_{r_l}} \\ \Delta V_{m_l} \\ \overline{\Delta V_{m_i}} \\ \Delta P_i \\ \overline{\Delta V_{r_j}} \\ \Delta V_{m_j} \\ \vdots \end{bmatrix} \tag{7-13}$$

Equation (7-13) can be compactly presented as:

$$\Delta I_{mr} = Y \Delta V_{rm}{}^{*} \tag{7-14}$$

The solution algorithm for BESS charge/discharge rate determination is summarized below.

Step 1. Initialize iteration counter ($iteration = 0$). Identify optimal BESS nodes. Define BESS nodes as "QV" buses. Initialize voltage magnitudes and phase angles (For QV buses set the voltage magnitude to (V_{ref}).

Step 2. Construct the Y matrix (Eqs. (7-11)-(7-12)) and determine current injections (for QV buses Eqs. (7-5)-(7-6) and for PV and PQ buses as defined in [131]).

Step 3. Calculate subsequent power mismatches.

$$\Delta P_i = P_i^{sp} - P_i^{calc} \tag{7-15}$$

$$\Delta Q_i = Q_i^{sp} - Q_i^{calc} \tag{7-16}$$

Where, P_i^{sp} and Q_i^{sp} are the specified active and reactive power at bus i while P_i^{calc} and Q_i^{calc} are the calculated bus powers as defined in [131].

Step 4. If $max(\Delta P, \Delta Q) \leq tolerance$, then go to Step 5; otherwise, determine the bus voltages and power corrections using (7-13), update the bus voltages and go back to Step 2.

Step 5.

- For PQ buses, update voltages using (7-17) and (7-18):

$$V_i = V_i^h + \Delta V_i = V_i^h + (\frac{V_{r_i}}{V_i}\Delta V_{r_i} + \frac{V_{m_i}}{V_i}\Delta V_{m_i}) \tag{7-17}$$

$$\theta_i = \theta_i^h + \Delta\theta_i = \theta_i^h + (\frac{V_{r_i}}{V_i^2}\Delta V_{m_i} - \frac{V_{m_i}}{V_i^2}\Delta V_{r_i}) \tag{7-18}$$

- For PV buses, voltage angles are updated using (7-18).
- For QV buses, voltage angles are updated using (7-18), while P_i^{calc} is calculated with updated voltages.

Step 6. Therefore, BESS system inverter active and reactive power can be calculated as shown in (7-19) and (7-20) respectively.

$$P_{inv-i} = P_i^{calc} + P_{L-i} \tag{7-19}$$

$$Q_{inv-i} = P_{inv-i}.tan(\theta_{PF_i}) \tag{7-20}$$

Where, θ_{PF_i} is the optimized inverter PF angle at battery bus i. A positive P_{inv-i} would indicate an export to the grid and negative indicate import from the grid.

Step 7. Then, battery instantaneous power can be found as,

$$P_{B-i} = P_{inv-i}/\eta_{inv} - P_{DG-i} \tag{7-21}$$

7.3.2 Optimal Battery Management Strategy and Sizing

Optimized battery management strategy achieves the optimal coordination between supply and demand for required levels of voltage regulation. Fig. 7-5 provides a summary of the proposed procedure for optimal BESSs integration.

- Real-time smart charging/discharging rates in the VPM are calculated by running the above ALF solution algorithm at Δt sampling interval with the preferred reference voltages.
- The constant charge/discharge rate in the real-time CPM is derived using the expression in (7-22) at the end of VPM operation.

$$P_{B-i} = (E_{B-i}(t_{vpm}) - {E_{B-i}}^{int})/\Delta t_{cpm} \tag{7-22}$$

Where, t_{vpm}, Δt_{cpm}, and ${E_{B-i}}^{int}$ are the time at the end of VPM, period of CPM, and battery fixed charge state required at the end of the period of CPM respectively.

- Battery energy (E_{B-i}) is calculated as:

$$E_{B-i}(t) = E_{B-i}(t-1) - \Delta E_{B-i}(t) \tag{7-23}$$

Where,

$$\Delta E_{B-i}(t) = P_i^{bat}(t) * (\Delta t \times \eta_c) \quad if\ charging,\ \text{and}$$

$$\Delta E_i^{bat}(t) = P_i^{bat}(t) * \frac{\Delta t}{\eta_d} \quad if\ discharging.$$

- Therefore, optimal sizes of BESS can be yielded from (3-9). This proposed method achieves financial benefits by deriving the minimal sizing required for BESSs.

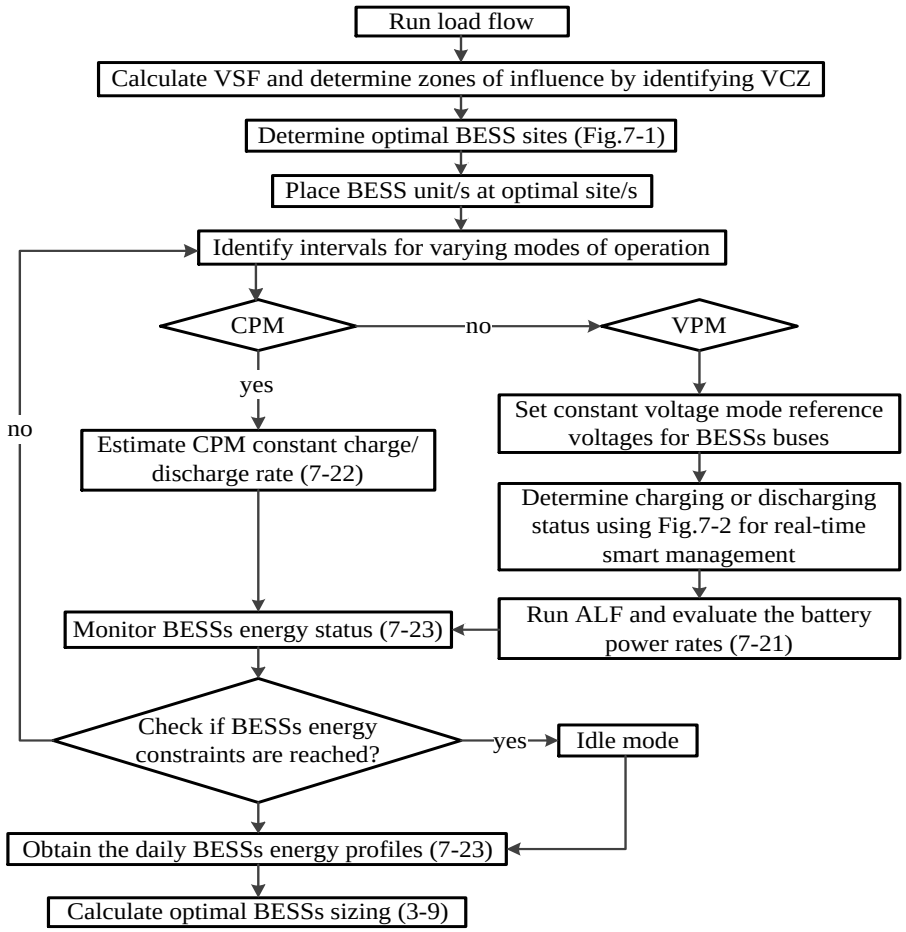

Fig. 7-5. Flowchart of the proposed optimal siting, sizing and management of BESS for voltage support.

For MV or large scale systems where aggregated load is greatly dominated by the low frequency diurnal variations, the daily BESS management may be achieved through scheduling using forecasted load data. The proposed management strategy can be used to analytically solve the dispatch schedules of BESSs.

7.4 Test System

The proposed approach for optimal siting, sizing and management of BESS is tested on a distribution system presented in Chapter 5.3.2.

The system voltage profile and the distribution transformer loading are illustrated graphically in Fig. 7-6 and Fig. 7-7 respectively. In Fig. 7-7, import power from the grid is negative while export is positive and data are sampled at 15 minutes intervals. The minimum and maximum system voltages are 0.953p.u. at bus 21 and 1.03p.u. at bus 23 respectively.

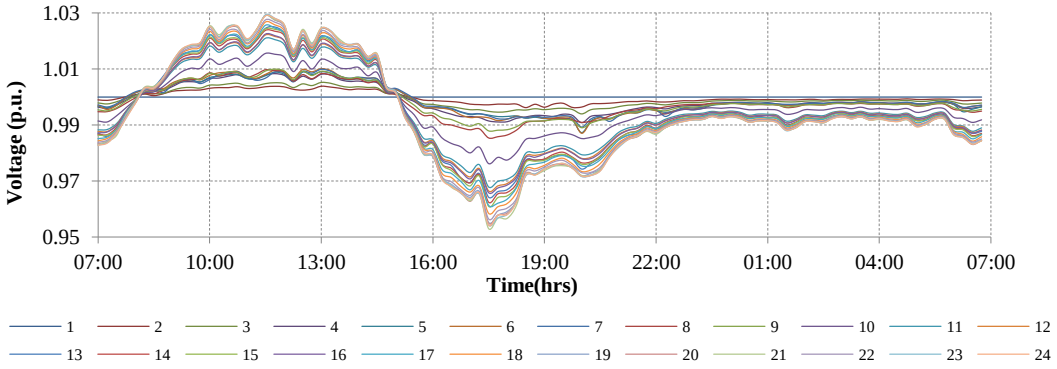

Fig. 7-6. Voltage profile with no BESS.

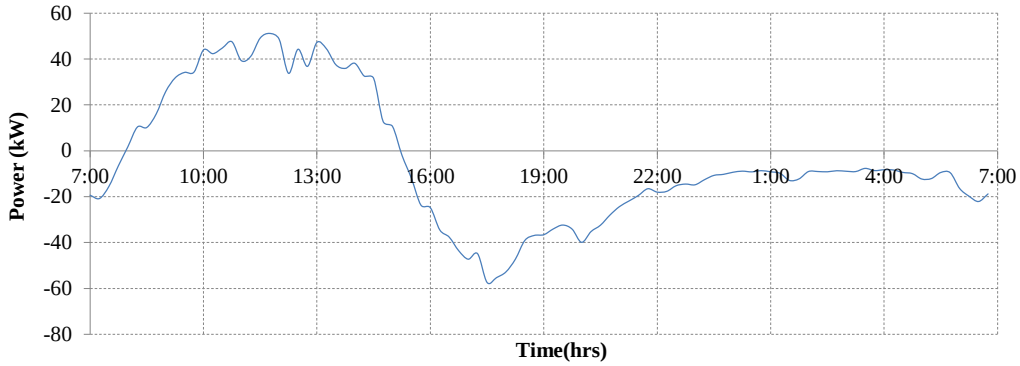

Fig. 7-7. Distribution transformer loading with no BESS.

7.5 Simulation Results

Testing of the proposed approach was carried out for varying number of zones of influence. Four voltage control zones of influence were identified as depicted in Fig. 7-8. Optimal sites and the zones were identified as buses 21 (zone 1), 24 (zone 2), 15 (zone 3) and 7 (zone 4) in a descending order from highest to lowest priorities.

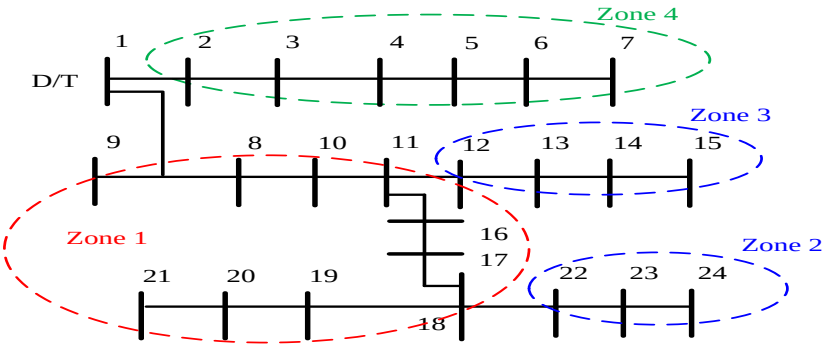

Fig. 7-8. Voltage control zones that define zones of BESS influence.

From the Fig. 7-8 it can be seen that the feeder supplying zone 4 is separated by the slack bus. Hence, the voltages along that feeder are not influenced by the rest of the network or vice versa. The voltages in zone 4 are within 1.015-0.985p.u. Thus, it was decided not to add a BESS at zone 4 optimal site (bus 7) as the deviations in the voltage levels are relatively low.

The distribution test system of Fig. 5-4 is a West Australian (WA) residential feeder and the data reflects winter variations. Therefore, based on the relevant tariff structure, the off peak, peak and shoulder periods are classified as shown in Table 7-1 [136]. The peak generation period is identified using the forecast mean distribution transformer loading. Peak generation period intercept the typical morning peak and shoulder periods. The modes of BESS operations are also indicated in Table 7-1.

TABLE 7-1: BESS OPERATING INTERVALS AND MODES.

Duration (hours)		**Classification**	**BESS Mode**
Typical [136]	**For Proposed Approach**		
07:00-11:00	07:00-07:45	Morning peak period (MPP)	VPM
11:00-17:00	15:30-17:00	Shoulder period (SP)	VPM
17:00-21:00	17:00-21:00	Evening peak period (EPP)	VPM

21:00-07:00	21:00-07:00	Off peak period (OPP)	CPM
	07:45-15:15	Peak generation period (PGP)	VPM

7.5.1 With Active Power Control Only

During peak generation and demands, BESS operates in the VPM facilitating the real-time regulation of the PCC voltage. Optimized reference voltages for respective VPM periods are presented in Table 7-2. As the number of BESSs increase the reference voltages for respective periods at battery buses improves as shown in Table 7-2. CPM charge or discharge powers are estimated based on the available energy at the end of evening peak using (7-22).

TABLE 7-2: V_{ref} WITH VARYING NUMBER OF BESS.

No. of BESS	**V_{ref} during MPP (p.u)**			**V_{ref} during PGP (p.u)**			**V_{ref} during SP/EPP (p.u)**		
	Bus 21	**Bus 24**	**Bus 15**	**Bus 21**	**Bus 24**	**Bus 15**	**Bus 21**	**Bus 24**	**Bus 15**
1	1.010			0.975			1.010		
2	1.004	1.004		0.982	0.982		1.006	1.006	
3	1.000	1.000	1.000	0.991	0.989	0.989	1.000	1.000	1.000

The Table 7-3 presents the resultant BESS sizes and system energy losses as well as minimum and maximum voltages during VPM BESS operation with varying number of BESS using the proposed strategy. Battery and voltage profiles are graphically demonstrated in Fig. 7-9, Fig. 7-10 and Fig. 7-11 for one, two or three BESS installations respectively.

TABLE 7-3: SUMMARY OF RESULTS WITH VARYING NUMBER OF BESS.

No. of BESS	**BESS Size (kWh)**			**Total Size (kWh)**	**Energy loss (kWh)**	**Voltage (Bus No.)**	
						Min. (p.u.)	**Max. (p.u.)**
No BESS					9.52	0.953 (21)	1.030 (23)
	Bus 21	**Bus 24**	**Bus 15**				
1	151.2			151.2	8.31	0.975 (21)	1.012 (13)
2	84.5	108.2		192.7	6.02	0.982 (21)	1.007 (13)
3	58.9	75.5	61.4	195.7	4.41	0.988 (19)	1.004 (9)

Proposed approach offers enhanced voltages with significant reductions in the system losses as indicated in Table 7-3.

Improvement in the voltage profile and reduction in the system losses increase with increased number of BESS units. With three BESS systems losses are reduced by 53.7% and voltages vary between 1.004p.u. and 0.988p.u.

The battery profiles in Fig. 7-9, Fig. 7-10 and Fig. 7-11 evidently show that the BESSs energy profiles reach the initial energy state at the end of the day. Therefore, proposed strategy prevents BESSs from unnecessarily over-charging or over-discharging and sets the battery state correctly for the following day management.

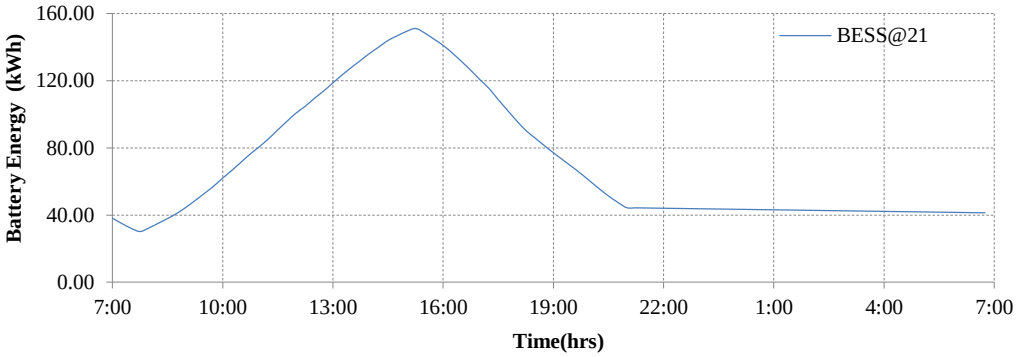

(a)

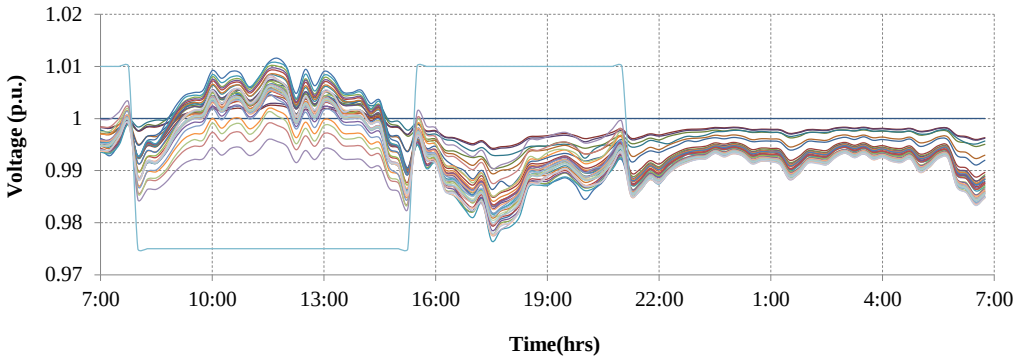

(b)

Fig. 7-9. (a) Battery profile (b) Voltage profile with one BESS, legend same as Fig. 7-6.

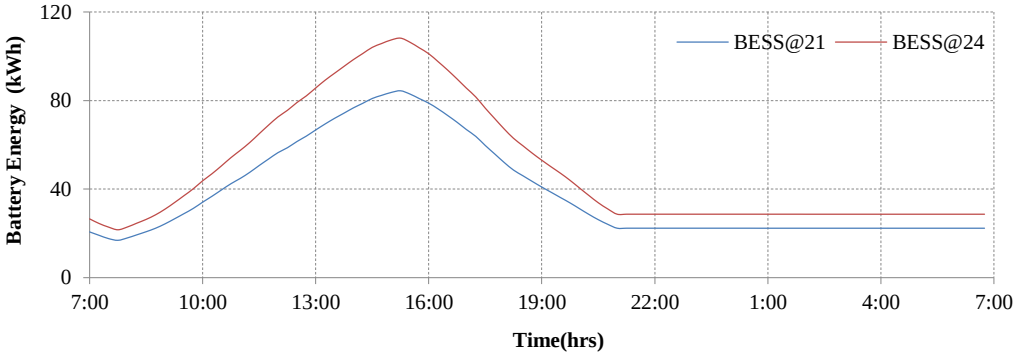

(a)

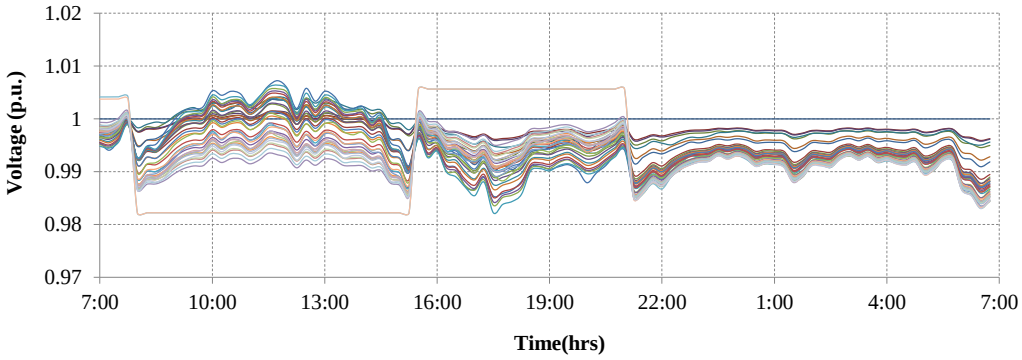

(b)

Fig. 7-10. (a) Battery profile (b) Voltage profile with two BESSs, legend same as Fig. 7-6.

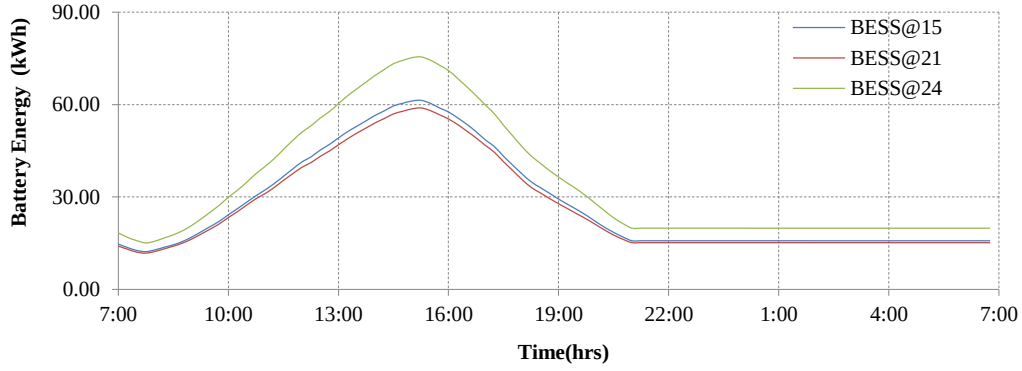

(a)

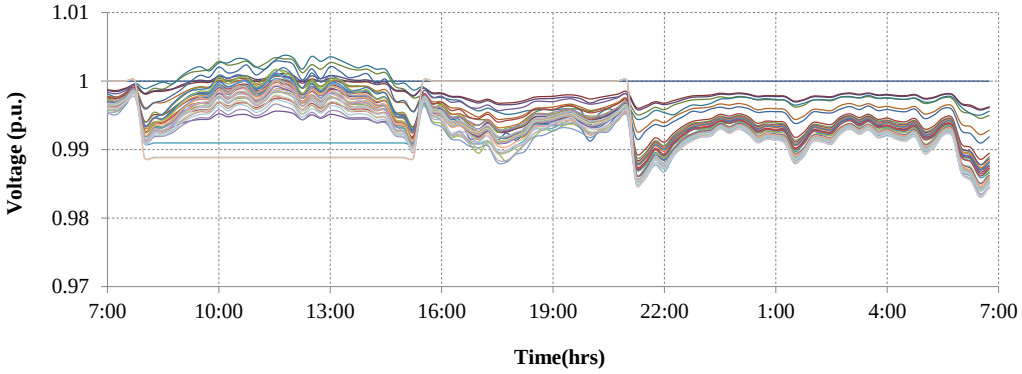

(b)

Fig. 7-11. (a) Battery profile (b) Voltage profile with three BESSs, legend same as Fig. 7-6.

Fig. 7-12 shows the distribution transformer loading inclusive of zone 4 loads with varying number of BESSs. Reduction in the peak increases with the addition of a BESS. With three BESS peak export is reduced by 64.4% and import by 62.8%.

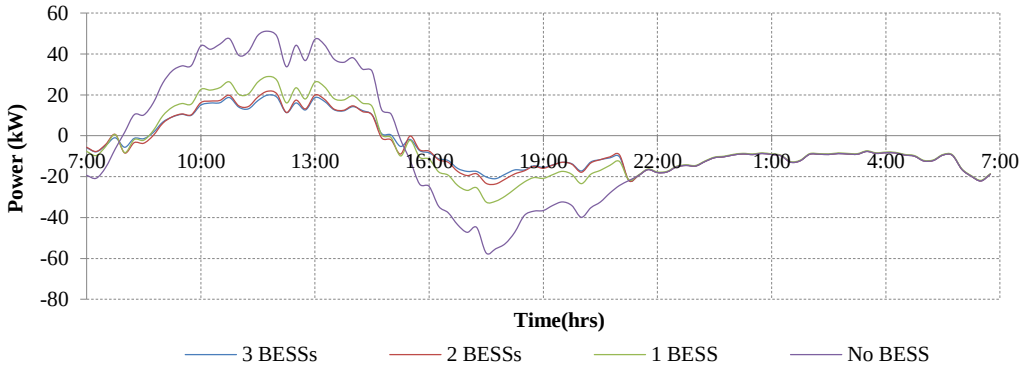

Fig. 7-12. Distribution transformer loading with varying number of BESS.

7.5.2 With Active and Reactive Power Control

Optimized reference voltages and PFs of BESSs inverters for respective VPM periods are presented in Table 7-4. Based on Table 7-4, similar to the case with active power control only, as the number of BESSs increases the reference voltages for respective periods at battery buses improves. According to PF information in Table 7-4, reactive power compensations required during SP/EPP are much greater than during MPP. PF vary from lagging to leading (reactive power export) during PV generation and peak demand respectively. With three BESSs, reactive power injections during SP/EPP are primarily from the battery at bus 21 and reactive power compensation during MPP and PGP are very marginal.

TABLE 7-4: V_{ref} AND PFS WITH VARYING NUMBER OF BESS.

No. of BESS		**During MPP**			**During PGP**			**During SP/EPP**		
	Bus #	**21**	**24**	**15**	**21**	**24**	**15**	**21**	**24**	**15**
1	V_{ref} (p.u)	1.001			0.982			1.009		
	PF	0.942			0.707			0.949		
2	V_{ref} (p.u)	1.006	1.003		0.988	0.989		1.009	1.008	
	PF	0.966	1		1	1		0.707	0.870	

3	V_{ref} (p.u)	1.002	0.994	1.002	0.992	0.992	0.991	1.003	0.999	1.000
	PF	1	1	1	0.993	1	0.996	0.707	1	1

The Table 7-5 presents the resultant BESS sizes and system energy losses as well as minimum and maximum voltages during VPM BESS operation with varying number of BESS using the proposed strategy. Battery and voltage profiles are graphically demonstrated in Fig. 7-13, Fig. 7-14 and Fig. 7-15 for one, two or three BESS installations respectively.

A trend similar to that with active power control only can be seen in voltages and system loss reductions. Improvement in the voltage profile and reduction in the system losses increase with increased number of BESS units. With three BESS systems losses are reduced by 57.8% and voltages vary between 1.004p.u. and 0.988p.u.

TABLE 7-5: SUMMARY OF RESULTS WITH VARYING NUMBER OF BESS.

No. of BESS	**BESS Size (kWh)**			**Total Size (kWh)**	**Energy loss (kWh)**	**Voltage (Bus No.)**	
						Min. (p.u.)	**Max. (p.u.)**
No BESS					9.52	0.953 (21)	1.030 (23)
	Bus 21	**Bus 24**	**Bus 15**				
1	113.3			113.3	8.01	0.978 (15)	1.012 (13)
2	72.1	86.1		158.2	5.64	0.985 (15)	1.009 (13)
3	49.1	70.9	57.0	177.0	4.01	0.988 (24)	1.004 (9)

Based on Table 7-4, the reactive power control was less effective for two and three battery installations during PGP than during SP/EPP. Availability of reactive power during SP/EPP has lessened the active power compensation required. Therefore, a 25.06%, 17.9% and 9.55% reduction in total battery sizes with one, two and three BESSs respectively can be seen in Table 7-5. Reactive power control, therefore, has not only improved the voltage profile but also further minimized the required battery capacity. It must be noted that the test system is a highly resistive system with high R/X ratios (Chapter 5.3.2).

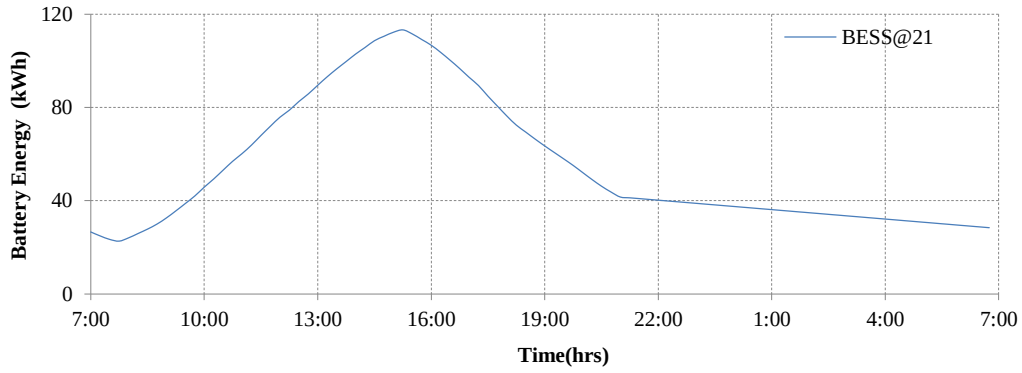

(a)

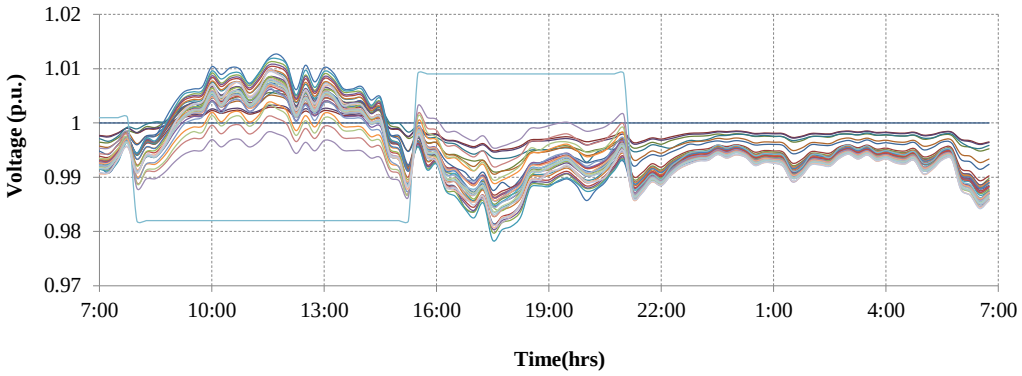

(b)

Fig. 7-13. (a) Battery profile (b) Voltage profile with one BESS, legend same as Fig. 7-6.

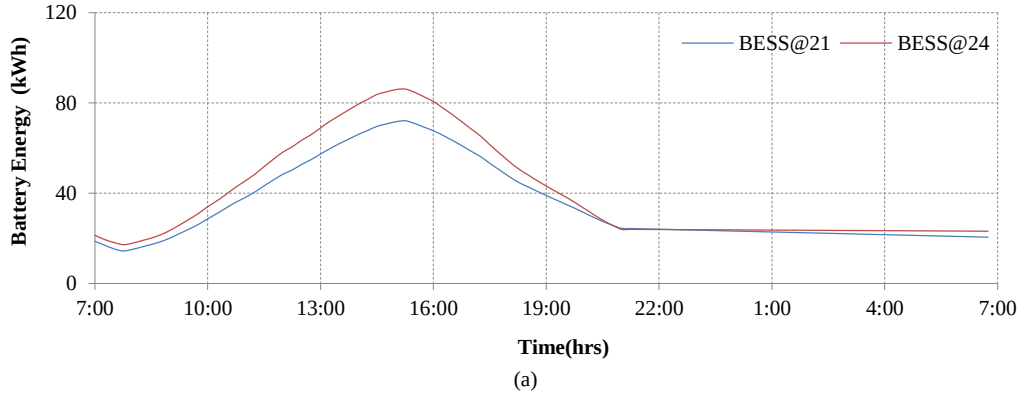

(a)

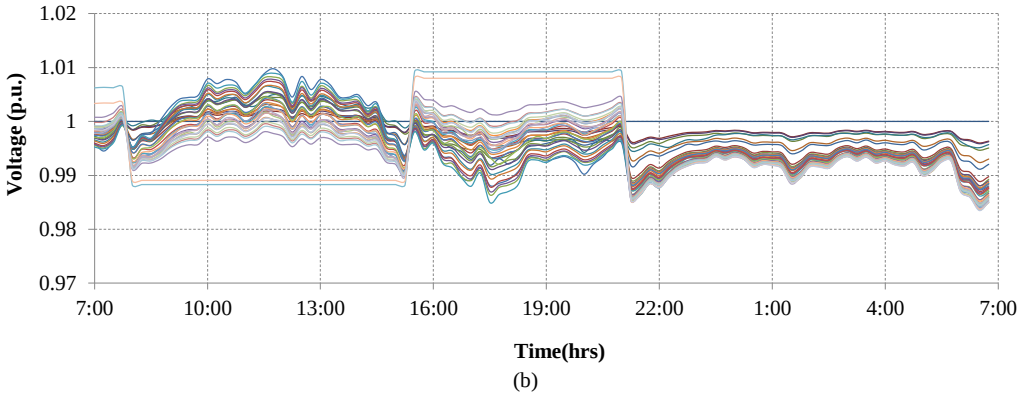

(b)

Fig. 7-14. (a) Battery profile (b) Voltage profile with two BESSs, legend same as Fig. 7-6.

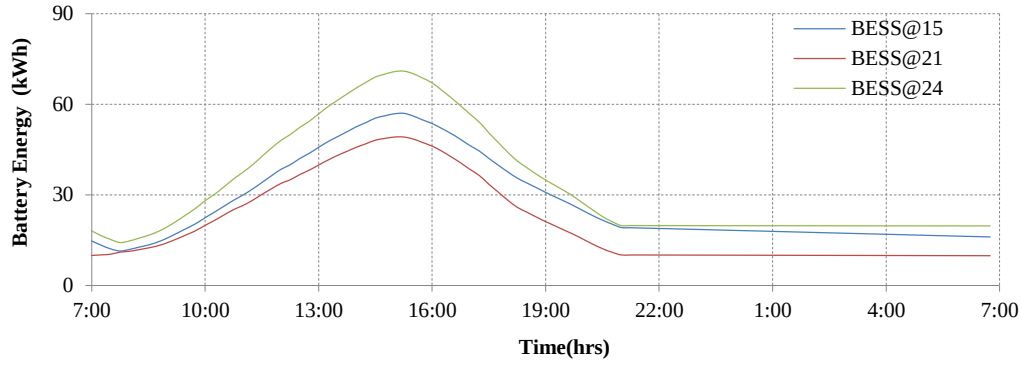

(a)

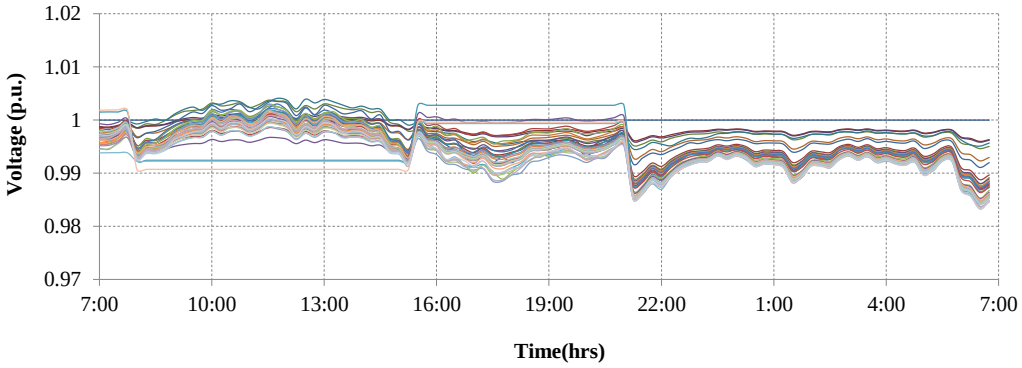

(b)

Fig. 7-15. (a) Battery profile (b) Voltage profile with three BESSs, legend same as Fig. 7-6.

The distribution transformer active power loading is presented in Fig. 7-16. Based on Fig. 7-16, reduction in the peak increases with the addition of a BESS. With three BESSs peak export is reduced by 55.8% and import by 63.5%.

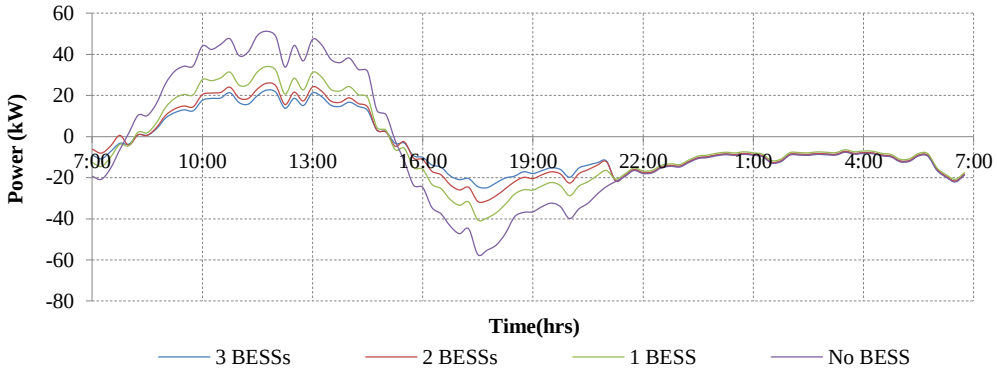

Fig. 7-16. Distribution transformer loading with varying number of BESS.

From the analysis, real-time smart charging during high generation effectively captures the excess energy that dynamically varies with environmental factors. Dispatch control using the real-time smart discharging during peak demand effectively improves the voltage quality while shaving the demand that is highly variable. The proposed approach effectively enhances the performance of the grid, enabling decentralized management of available resources. Optimal deployment and management of multiple BESS shows high potential in maintaining requisite voltage levels compared to those observed with single BESS.

7.5.3 Conclusions

A novel analytical approach for optimal placement, sizing and management of single or multiple BESS is proposed in this chapter. The approach is developed with the main objective of improving voltage regulation while improving DG absorption ability of the grid. Method shows superior performance in terms of simplicity, accuracy and speed, avoiding the need for exhaustive optimization algorithms.

- Results demonstrate the ability of the approach to maintain the BESS bus voltage at predetermined voltage levels while achieving significant reductions in system losses and peak load due to enhanced voltages.

- Improvements in the quality of supply translate to high performance levels that enable decentralized smart energy management, reducing the supply that needs to come from centralized power sources and consequent transmission losses and carbon emissions.

- In comparison to single BESS installation, integration and management of multiple BESSs shows further enhanced performance levels with more flexibility to manage feeder voltage profile and absorb mass quantities of DG (Table 7-3 and Table 7-5).

- CPM real-time management during light load simplifies the calculations and improves the BESSs system performance due to single-rate control. This is suitable as the voltage distributions are nearly even during the periods of low load.

- Real-time smart management of the VPM during peak generation and peak demands maintains the voltage profile within desirable limits by controlling the BESS bus voltages. As only the reference voltage and PF set points are communicated to local BESS units, minimal smart grid infrastructure is required.

- The BESSs sizing can be reduced while achieving further improved voltage profiles by enabling reactive power capability of BESSs inverters (Table 7-5).

- BESS management approach can be used as an effective tool for scheduling real power dispatch of storage in MV feeder where forecasting errors are low.

- Optimal siting, sizing and management of BESSs enable smart utilization of available resources, minimize feeder congestion and improve the quality of the voltage supplied to the consumers. Therefore, the method will effectively improve the efficiency of the decentralized energy management in the future grid.

- Optimal integration of BESSs will improve the value in terms of the performance and economy of the entire system supporting the evolution towards a smart grid.

Chapter 8. Distributed Generation Planning for Decentralized Systems

8.1 Introduction

This chapter includes two analytical approaches for optimal siting and sizing of multiple DG units in distribution systems. Approaches can readily be applied for radial and mesh systems; independent of the configuration. The first proposed technique is developed with the primary focus of power system loss reduction. Optimal DG siting and sizing are analytically determined using the loss sensitivity factors (LSFs) and a LSF-based linearized loss function, respectively. The effectiveness of the LSF method for multiple DG placements is assessed using a performance index (PI) method. The main goal of the second approach is to optimally site and size DG units to provide voltage support. Voltage-control zones are identified to establish DG-influence zones using voltage sensitivity factors (VSFs) which in turn determine the optimal locations and numbers of DG units. Optimal DG capacities are evaluated using the proposed augmented load flow (ALF) of Chapter 7. The ALF is executed twice; once for the base case of DG siting and the secondly for computing the optimal DG sizes. Detailed simulations are performed to assess the performance of the two analytical approaches.

8.2 Types of Distributed Generation

DGs can be categorized based on their ability to generate or absorb active (P) and reactive (Q) power as shown below:

- ***Type 1 DG (Generating +P)*** **-** This type of DG only generates active power, PF = 1.

- ***Type 2 DG (Generating +P with +/-Q)*** **-** This type of DG are capable of generating active and reactive power, as well as absorbing reactive power (0 < PF < 1).

- ***Type 3 DG (Generating +/-P with +/-Q)*** **-** These are mostly distributed energy storage units capable of exporting and importing active or reactive power ($0 < PF < 1$).

Typically, DG units that generate reactive power have the ability to absorb reactive power. This is achieved by controlling a grid interface inverter or by controlling the excitation for synchronous generators [137] or doubly fed induction generators. Examples of Types 1, 2 and 3 DG units are PV systems with no *Q* injections, wind power generation, and distributed (battery) storage units, respectively.

8.3 Test System and Data Modelling

8.3.1 Test System

The proposed two approaches for optimal siting and sizing of DGs are tested on the base IEEE 33-bus distribution system of Chapter 5.3.1 (without the assumed DGs). The test system is presented again in Fig. 8-1. The TCIM is employed for power flow calculations [131].

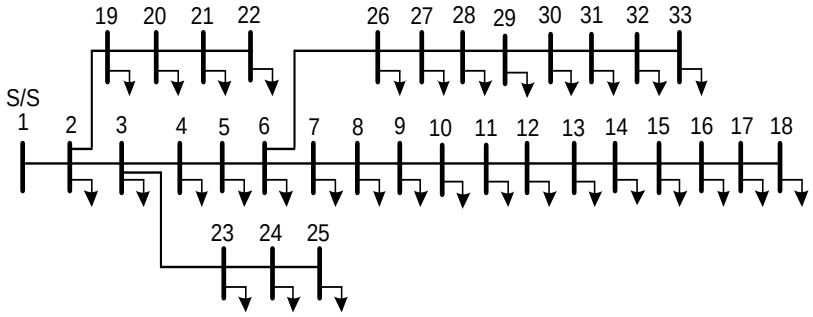

Fig. 8-1. Single-line diagram of IEEE 33 node distribution system used in simulations.

8.3.2 Generalized Load Modelling

The voltage dependency of the loads is mathematically expressed using the second order polynomial equations in (5-10) and (5-11).

8.3.3 Load Variability

The DG sizing and siting problem is typically solved at system peak as the added support by DG is mostly required if the system is not operating under normal

conditions [20],[90],[91],[94],[99]. However, according to [49] system peak is rarely experienced by utility grids. Reference [49] states that the peak events in Australia in 2011/2012 occurred over a period of less than 40 hours per year or less than 0.5% of time. Thus, planning and investing in DG resources by considering only the extreme conditions is questionable. Therefore, a load duration curve (LDC) based method is used to fully characterize the load in [138]. The LDC provides an adequate representation of the distribution system load under its actual operating conditions while considering the probabilistic seasonal and time dependency.

In this study, a method that is similar to [139]-[140] is proposed to consider statistics of maximum, minimum and median demand by means of LDC for analysing annual energy loss. LDC can be partitioned into several load blocks. The median of each load block would represent the load characteristics within the block. The annual energy loss can be calculated using the weighted sum across all load blocks.

8.3.4 Generation Modelling

In many publications the problem of optimal DG sizing allocation is solved through minimization of series of capital and operating costs. It is essential to consider the cost aspect during DG planning. The proposed methods are developed considering the technical aspects of loss minimization and voltage regulation. Cost minimization is achieved by deriving the minimal DG ratings required for improving the aforementioned technical aspects. Testing of the methods are carried out for DGs of various types; based on their active and reactive power capabilities. While this is a common approach to define DG, they can be further categorized considering the technology.

This study is not aimed at making the decision regarding what DG technology to be selected for installation. However, a commonly used practice by many utilities is briefly presented here. DG technology to be selected predominantly depends on the geographical location. Depending on the availability of resources, dispatchable DG (e.g., biomass) or non-dispatchable renewable DG such as PV/wind generation could be chosen.

If the optimal size of DG at bus i found by the proposed technique is S_{DG-i} then the rated size (rated apparent power) of dispatchable DG ($S_{dispatchable\ DG-i}$) is determined as:

$$S_{dispatchable\ DG-i} = S_{DG-i} \tag{8-1}$$

The generation by dispatchable DG has no uncertainties and has the ability to deliver a constant output. Traditionally, these units are dispatched so that capacity factor (CF) of DG is equal to the load factor [141]. The CF is the actual energy generated over a period of time expressed as a ratio of the actual energy that may have been generated if DG was running at its rated power for that period:

$$CF = \sum_{t=t_1}^{T} S_{out-DG-i}(t) / S_{Rated-DG-i}t) \tag{8-2}$$

Where, $S_{out-DG-i}$ and $S_{Rated-DG-i}$ are DG output and DG rated power, respectively at bus i.

Due to current trend towards decentralized networks with high penetrations of greener generation sources, renewable DG technologies such as PV and solar are becoming increasingly popular. However, a number of issues need to be taken into account under renewable DG planning including the variability, stochastic nature and correlation between DG outputs and loads. Outputs of PV and wind based DGs strongly depend on the time varying solar irradiance and wind speed, respectively.

Historical and forecast data bases of wind speed (wind DG) or sun shine (PV) for the site under investigation determines the amount of energy that can be generated and the corresponding CFs. Approaches for modelling PV and wind generation for a given site can be found in [100],[142],[143]. Based on the production information, CF which is dependent on the intermittent nature of renewable DG can be estimated. Therefore, the relationship between the required size of non-dispatchable DG unit and the optimal size found can be established as:

$$S_{non-dispatchable\ DG-i} = S_{DG-i}/CF \tag{8-3}$$

Where, $S_{non-dispatchable\ DG-i}$ is the rated apparent power of the non-dispacthable DG unit at bus i.

To overcome the challenges associated with variable renewable generation a few operational and infrastructure measures can be taken into consideration including integration of storage co-located with DG, balancing fluctuations using disptachable DG and demand-side integration to modify usage to match the generation [28]. These measures can significantly improve the dispatch management of DG, while the co-ordination among the measures can offer maximum benefits to the grid.

8.3.5 Test Cases and Assumptions

The testing of the proposed methods was carried out for the following two cases:

- Case 1: Constant power loads (Eqs. (5-10) and (5-11); $a_p = a_q = 1$) with constant current and constant impedance terms set to zero. Total active and reactive power of system loads are 3.715MW and 2.300MVar, respectively. Note that while modelling loads as constant power terms is a conservative approach used in many publications, this may not be a correct representation of typical distribution systems [94].

- Case 2: Therefore, in Case 2, optimal sizing and siting are carried out considering a load composition of $a_p = a_q = 0.4$, $b_p = b_q = 0.3$ and $c_p = c_q = 0.3$. This study aims to demonstrate the robustness of the proposed approaches and the effects of load models on DG planning. Total active and reactive load power of the system with the above load composition are 3.556MW and 2.191MVar, respectively.

This research does not concern issues related to selection of the DG technology.

8.4 Proposed LSF-Based Optimal DG Placement and Sizing to Reduce System Losses

The first proposed analytical approach for optimal DG siting and sizing is designed to primarily reduce system power losses. DG locations are determined using a LSF approach while DG capacities are determined using a linearized loss function.

8.4.1 Optimal DG Siting Based on Loss Sensitivity Factor (LSF)

Active and reactive power losses (P_{loss} and Q_{loss}) due to load and line active and reactive power requirements constitute the network losses. Increasing active power (P) requirements not only increases system losses but also affects the efficiency of energy delivered and the voltage profile. Even if the loads reactive power demand (Q) are insignificant, some reactive power flow has to be maintained to compensate the reactive power requirements of the lines particularly for high voltage feeders and transmission lines with high X/R ratios. Q control enables smooth active power transition while maintaining voltages within satisfactory levels. Poor Q compensation can elevate bus voltages beyond their permissible limits affecting the quality of supply. The total active and reactive power losses can be calculated from (8-4) and (8-5), respectively.

$$P_{loss} = -\sum_{nbranch=1}^{nbus-1}\{2.V_i.V_j.cos(\delta_i - \delta_j) - {V_i}^2 - {V_j}^2\}.G_{ij} \quad (8\text{-}4)$$

$$Q_{loss} = -\sum_{nbranch=1}^{nbus-1}\{2.V_i.V_j.cos(\delta_i - \delta_j) - {V_i}^2 - {V_j}^2\}.B_{ij} \quad (8\text{-}5)$$

Where, V_i, δ_i, $nbranch$ and G_{ij} are as defined in Chapter 5.2.1; B_{ij} is the susceptance of branch $nbranch$.

LSFs are derived in terms of voltages, angles, conductance and susceptance, therefore, can be effectively applied for radial or meshed power systems. The LSF equations are further supplemented for the DG sizing strategy.

8.4.2 Loss Sensitivity Factor (LSF)

The LSF contains the sensitivities of total active power losses w.r.t bus active and reactive power variations, as well as total reactive power losses w.r.t bus active and reactive power variations. The derivation for the active power LSF is illustrated below.

The derivative of P_{loss} with respect to P and Q are:

$$\begin{bmatrix} \frac{d\,P_{loss}}{dP} \\ \frac{d\,P_{loss}}{dQ} \end{bmatrix} = \begin{bmatrix} \frac{dV}{dP} & \frac{d\delta}{dP} \\ \frac{dV}{dQ} & \frac{d\delta}{dQ} \end{bmatrix} \cdot \begin{bmatrix} \frac{d\,P_{loss}}{dV} \\ \frac{d\,P_{loss}}{d\delta} \end{bmatrix} \tag{8-6}$$

Where, $\frac{dV}{dP}$, $\frac{d\delta}{dP}$, $\frac{dV}{dQ}$ and $\frac{d\delta}{dQ}$ are derivatives of voltage magnitude and angle with respect to P and Q, respectively.

Equation (8-6) can be reorganized using the power flow Jacobian matrix:

$$\begin{bmatrix} \frac{d\,P_{loss}}{dV} \\ \frac{d\,P_{loss}}{d\delta} \end{bmatrix} = \begin{bmatrix} \frac{dP}{dV} & \frac{dQ}{dV} \\ \frac{dP}{d\delta} & \frac{dQ}{d\delta} \end{bmatrix} \cdot \begin{bmatrix} \frac{d\,P_{loss}}{dP} \\ \frac{d\,P_{loss}}{dQ} \end{bmatrix} = \begin{bmatrix} J_1 & J_2 \\ J_3 & J_4 \end{bmatrix} \cdot \begin{bmatrix} \frac{d\,P_{loss}}{dP} \\ \frac{d\,P_{loss}}{dQ} \end{bmatrix} \tag{8-7}$$

By applying Cramer's rule, equation in (8-7) can be presented in terms of the power flow Jacobian entries:

$$\begin{bmatrix} {S_P}^{Ploss} \\ {S_Q}^{Ploss} \end{bmatrix} = \begin{bmatrix} \frac{d\,P_{loss}}{dP} \\ \frac{d\,P_{loss}}{dQ} \end{bmatrix} = \begin{bmatrix} \begin{vmatrix} \frac{H_1}{J_2} - \frac{H_2}{J_4} \end{vmatrix} & \begin{vmatrix} \frac{H_1}{J_3} - \frac{H_2}{J_1} \\ \frac{J_1}{J_2} - \frac{J_3}{J_4} \end{vmatrix} \\ & \begin{vmatrix} \frac{J_4}{J_3} - \frac{J_2}{J_1} \end{vmatrix} \end{bmatrix}^T \tag{8-8}$$

Where, ${S_P}^{Ploss}$ and ${S_Q}^{Ploss}$ are the active power LSF w.r.t active and reactive power variations, respectively. The terms H_1 and H_2 are derived from (8-4);

$H_1 = \frac{d\,P_{loss}}{dV_i} = -\sum_{k=1}^{n-1}\{2.V_j\,cos(\delta_i - \delta_j) - 2.V_i\}.G_{ij}$ and

$$H_2 = \frac{d\,P_{loss}}{d\delta_i} = \sum_{k=1}^{n-1}\{2.V_i.V_j.sin(\delta_i - \delta_j)\}.G_{ij}.$$

By adopting a similar procedure, the reactive power LSF terms w.r.t active and reactive power variations can be calculated as:

$$\begin{bmatrix} {S_P}^{Qloss} \\ {S_Q}^{Qloss} \end{bmatrix} = \begin{bmatrix} \frac{d\,Q_{loss}}{dP} \\ \frac{d\,Q_{loss}}{dQ} \end{bmatrix} = \begin{bmatrix} \begin{vmatrix} \frac{H_3}{J_2} & \frac{H_4}{J_4} \\ \frac{J_1}{J_2} & \frac{J_3}{J_4} \end{vmatrix} & \begin{vmatrix} \frac{H_3}{J_3} & \frac{H_4}{J_1} \\ \frac{J_4}{J_3} & \frac{J_2}{J_1} \end{vmatrix} \end{bmatrix}^T \tag{8-9}$$

Where,

$H_3 = \frac{d\,Q_{loss}}{dV_i} = -\sum_{k=1}^{n-1}\{2.V_j\cos(\delta_i - \delta_j) - 2.V_i\}.B_{ij}$, and

$H_4 = \frac{d\,Q_{loss}}{d\delta_i} = \sum_{k=1}^{n-1}\{2.V_i.V_j.\sin(\delta_i - \delta_j)\}.B_{ij}.$

Therefore, based on (8-8) and (8-9), the LSF is defined as:

$$LSF = \begin{bmatrix} {S_P}^{Ploss} & {S_P}^{Qloss} \\ {S_Q}^{Ploss} & {S_Q}^{Qloss} \end{bmatrix} \tag{8-10}$$

To determine the optimal locations of DG units, the above LSF matrix is calculated and buses with the highest ${S_P}^{Ploss}$ values are identified as the optimal DG locations. In the above calculations the power flow Jacobian is developed taking into account the voltage dependency of loads.

8.4.3 Optimal DG Sizing Based on Linearized Loss Function

In general, the optimal size of DG should be determined based on its ability to simultaneously reduce both active and reactive power losses. Therefore, the nonlinear loss function defined in (8-11) is minimized to find the optimal sizes of DG units and their PF;

$$F_{loss} = \alpha . P_{loss} + \beta . Q_{loss} \tag{8-11}$$

Where, α and β are weighting factors for active and reactive power losses, respectively.

In order to demonstrate the effectiveness of the proposed approach against established methods, simulations are carried out assuming data available with the IEEE 33 bus system. However, (8-11) can be modified using a weighted sum approach to include the effects of various load bands as discussed in Chapter 8.3.3. The proposed method can handle various planning levels for discrete or simultaneous minimization of losses.

Assuming that bus i is integrated with a DG unit injecting active (P_{DG-i}) and reactive (Q_{DG-i}) powers, the power balance at this bus will be adjusted as:

$$P_i = P_{DG-i} - P_{L-i} \tag{8-12}$$

$$Q_i = Q_{DG-i} - Q_{L-i} \tag{8-13}$$

Equation in (8-11) is optimized using the numerical IP algorithm to find the optimal values of P_{DG-i} and Q_{DG-i} and the required DG PF and apparent power capacity are established as:

$$PF_i = \frac{P_{DG-i}}{\sqrt{{P_{DG-i}}^2 + {Q_{DG-i}}^2}} \tag{8-14}$$

$$S_{DG-i} = \sqrt{{P_{DG-i}}^2 + {Q_{DG-i}}^2} \tag{8-15}$$

The nonlinear loss function (8-11) is linearized using the sensitivity factors from the LSF matrix (8-10). This will minimizes the search space while improving the search

direction, computational efficiency and the accuracy.

Sensitivity matrix of the objective function (J_f) in (8-16) composes of two components; objective function with respect to active and reactive power components of DG:

$$J_f = \left[\frac{d\, f_{loss}}{dP_{DG-i}} \quad \frac{d\, f_{loss}}{dQ_{DG-i}}\right] \tag{8-16}$$

Where,

- $\frac{d\, f_{loss}}{dP_{DG-i}} = \alpha.\frac{d\, P_{loss}}{dP_{DG-i}} + \beta.\frac{d\, Q_{loss}}{dP_{DG-i}} =$
  $\alpha\left[\frac{d\, P_{loss}}{dP_i}.sign(P_{DG-i})\right] + \beta[\frac{d\, Q_{loss}}{dP_i}.sign(P_{DG-i})].$
- $\frac{d\, f_{loss}}{dQ_{DG-i}} = \alpha.\frac{d\, P_{loss}}{dQ_{DG-i}} + \beta.\frac{d\, Q_{loss}}{dQ_{DG-i}} =$
  $\alpha\left[\frac{d\, P_{loss}}{dQ_i}.sign(Q_{DG-i})\right] + \beta\left[\frac{d\, Q_{loss}}{dQ_i}.sign(Q_{DG-i})\right].$

The weighting factors of (8-11) are set to $\alpha = 1.0$ and $\beta = 0$. The optimization is carried out using a linearized IP algorithm and the PS algorithm in MATLAB is used to verify that solution approaches a near global minimum. It is worth highlighting that even with $\beta = 0$ there will still be some level of DG reactive power support and Q_{loss} compensations.

8.4.4 Flow Chart of LSF-Based Optimal Siting & Sizing of DGs

The first proposed optimal DG siting and sizing approach is depicted in (Fig. 8-2).

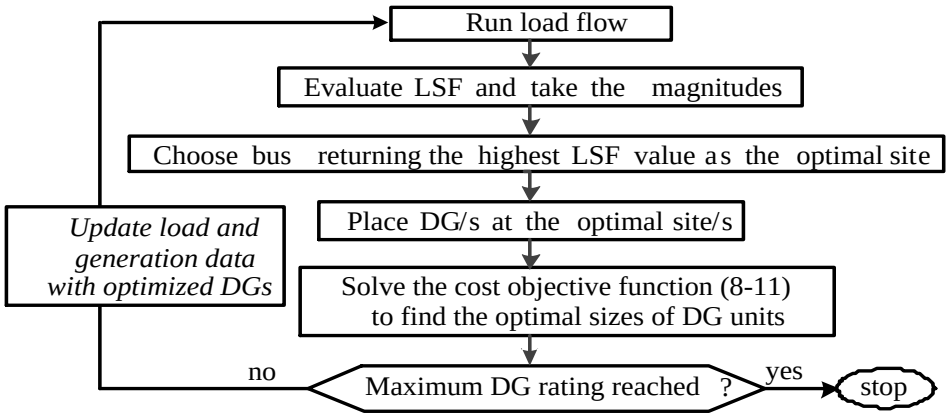

Fig. 8-2. Flow chart of the first optimal DG siting and sizing approach to reduce system losses.

The approach is implemented using the following steps

Step 1. Run the base case load flow with no DGs using the TCIM of [131].

Step 2. Calculate ${S_P}^{Ploss}$(taking magnitudes of coefficients only) and choose the bus with the highest ${S_P}^{Ploss}$ value as the optimal DG site.

Step 3. Place a DG at the selected bus and run the linearized optimization for the objective function (8-11). Optimization will return the P_{DG-i} and Q_{DG-i}.

Step 4. The optimal DG size and the PF are calculated using (8-15) and (8-14), respectively.

Note: PF is only valid for Type 2 and 3 DGs.

Step 5. For the consequent DG integration, run the load flow with the initially selected optimally sized and sited DG units.

Step 6. Calculate ${S_P}^{Ploss}$again (taking the magnitude only) and choose the bus with highest ${S_P}^{Ploss}$ value as the optimal site of the next DG.

Step 7. Connect another DG at the new optimal location.

Step 8. Solve the objective function (8-11) to evaluate the optimal sizes of all the DG units as expressed in (8-15).

Step 9. Repeat Steps 4-8 until maximum number of DGs or ratings are reached. Ensure voltage thresholds are maintained.

8.4.5 Classical Siting Approach with the Proposed LSF-Based Sizing Method

In order to evaluate the effectiveness of the proposed LSF siting approach, its performance will be compared (in Chapter 8.6) with the classical approach for siting (CA) which is commonly used for siting of DG [144]. This is done by modifying CA to accommodate multiple DG siting using the following steps:

Step 1. Solve the objective function (8-11) and find the optimal size of DG at each bus and the corresponding system losses.

Step 2. Select the optimal DG site and size at which losses are minimal.

For the consequent DGs,

Step 3. Update DG site data with the DG location data obtained previously.

Step 4. Place a new DG at each remaining bus and solve the objective function to find the new optimal sizes and corresponding power system losses.

Step 5. Objective function evaluates the optimal sizes of the previously allocated DGs and the new DG.

Step 6. Select next optimal DG site and optimal DG sizes at which losses are minimal.

Step 7. Repeat Steps 3-7 until maximum number of DGs or ratings are reached. Ensure voltage thresholds are maintained.

8.5 Numerical Validation of Proposed LSF-Based Optimal Sizing of DGs

This section provides a numerical validation for the LSF-based DG sizing technique adopted for loss reduction. Total loss of a power system against the bus power is a parabolic function. Thus, derivative of total loss with respect to the bus injection power becomes zero at minimum losses. The analytical derivation of this is extremely challenging or impossible without unrealistic pre-established assumptions or approximations especially for meshed power systems.

For the sake of brevity, only the validation for bus 18 is shown in Fig. 8-3. To do this, a Type 1 DG was added at bus 18 and P_{DG-18} was varied from 0.0kW to 930kW in small steps of 0.5kW. Then, P_{loss} and its sensitivity at DG bus were evaluated by

solving the load flow problem at each increment (Fig. 8-3). From Fig. 8-3, as the DG injection increases, the total power loss begin to reduce, consequently the real value of the sensitivity changes from negative to positive or its magnitude starts to drop. At a certain DG capacity, sensitivity reaches zero and losses are minimized. When the DG size is increased beyond this capacity, sensitivity and losses rise again. This capacity of DG is the optimal size of DG required at bus 18. Therefore, if DGs are not sized correctly power loss may increase instead of reducing the system losses.

Note that:

- The numerical optimal DG size 852.50kW matches very closely with the resultant optimal size of 852.62kW from the proposed DG sizing technique of Chapter 8.4.

- In addition, the theoretical approach in [88] and the technique in [144] returned nearly the same results for bus 18, proving the accuracy of the approach. Paper in [88] defines an analytical approach for Type 1 single DG sizing based on current injections for radial systems. Method in [144] uses an approximated analytical expression to determine the optimal site and a numerical approach for sizing.

- For further validations, the result from the linearized IP method was supplied to the PS to ensure the solution reaches a global minimum. No improvement in the solution was noticed. This further confirms the accuracy of the solution from the linearized IP method as the loss function is a parabolic function with a single minimum.

- Conditioning through linearization of the loss function is needed to ensure computational speed and derivative of F_{loss} reaches zero. The first order optimality measure was less than 1x10e-9. Without the linearization, there is no guarantee that derivative of F_{loss} will reach its minimum. The DG size found without the linearization deviated from the optimal size by about 5% while the simulation run time was reduced by about 75% (considering the average results from 20 runs).

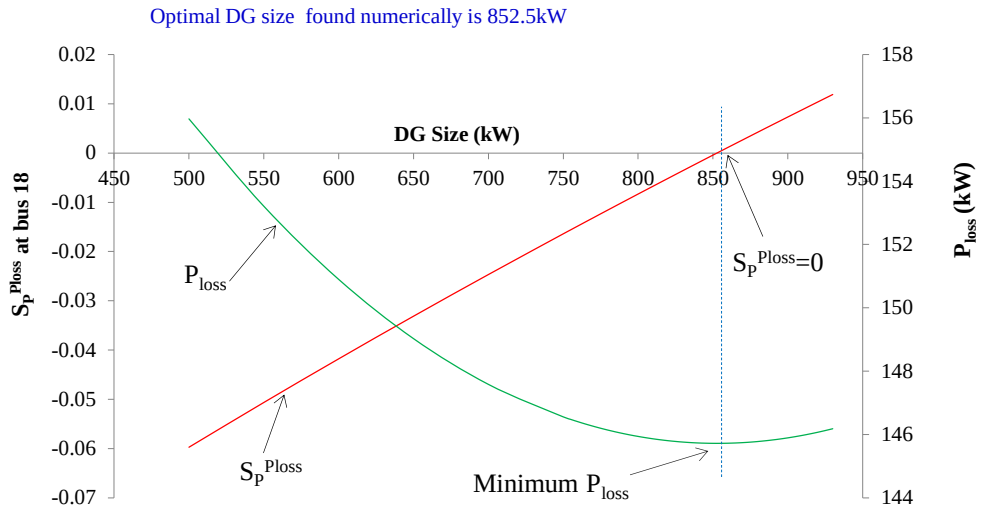

Fig. 8-3. Total active power loss and its sensitivity with respect to incremental increases in DG size connected to bus 18 of Fig. 8-1.

8.6 Simulation Results for LSF-Based Approach

The proposed LSF based optimal DG planning strategy of Chapter 8.4 was tested on the 33 bus test system of Fig. 8-1. The maximum number of DG units and the permissible voltage limits were set to 4 units and 1±0.06p.u., respectively.

Generally the capital cost of DG (determined by its rated value) dominates the total systems costs than its operating costs. Thus, the main objective is to integrate DG/s with minimum rating/s that would improve the system performance.

A performance index (PI) technique is adopted to evaluate the efficiency of LSF and CA siting approaches. PI measures the amount of DG required to achieve total loss reduction:

$$PI = \frac{Total\ DG\ size}{(P_{loss}{}^{no\ DG} - P_{loss}{}^{with\ DG})} \tag{8-17}$$

Where, $P_{loss}{}^{no\ DG}$ and $P_{loss}{}^{with\ DG}$ are total system losses with and without DG respectively.

PI can be used to compare the cost effectiveness of the LSF-based and CA siting approaches. Higher PI values indicate poor performance efficiencies, requiring higher DG capacities to reduce the same amount of losses.

In the following subsections, results of the proposed LSF-based siting approach are compared against that of CA. The optimal sizing obtained using the proposed sizing technique with CA offer similar or further reduced losses than the improved analytical (IA) method presented in [90]. IA method uses the classical siting approach similar to the CA using an expression for approximating losses. Sizing in IA is derived numerically and simulation results are carefully compared.

8.6.1 Case 1 – with Constant Power Load

8.6.1.1 Type 1 DG with Only P Injection

Table 8-1 illustrates the results of placing Type 1 DG by the proposed LSF method, CA and IA method. It can be seen that DG planning by CA matches very closely with IA while for some cases it offers more loss reductions.

For both single and multiple DG placements, CA offers more loss reduction than the LSF method. However, total size of the DG units required is relatively higher with high PI results. Although the loss reductions by LSF are slightly lower, the efficiencies of the DG units are much higher resulting in low PIs. The total DG size for three DGs by LSF is still lower than the total DG size required by CA single or multiple DG installations. Furthermore, the computational time required by LSF method is approximately 50% less when compared to CA for placement of DG units. Therefore, based on low PI values, LSF is more cost effective for Type 1 single, two or four DG installations while CA is suitable for planning of three DG units. However, the difference in the PI for three DGs by LSF and CA are very minimal.

Resultant voltage profiles by LSF and CA are plotted in Fig. 8-4 and Fig. 8-5, respectively. The voltage profile improves with the amount of DG units. Voltage distributions with three or four DG units by both methods match very closely.

TABLE 8-1: SUMMARY OF RESULTS FOR TYPE 1 DGS - CASE 1.

Case	**DG Size in kW-(Bus Number)**					**Total DG Size (kW)**	**P_{loss} (kW)**	**PI (8-17)**
No DG						0	211.00	
1 DG	LSF	852.62 (18)				852.62	145.72	13.06
	CA	2590.13 (6)				2590.13	111.03	25.91
	IA	2601 (6)				2601	111.10	26.04
2 DGs	LSF	667.45 (18)	1003.02 (33)			1670.47	100.06	15.06
	CA	1902.54 (6)	646.70 (14)			2549.24	91.31	21.30
	IA	1800 (6)	720 (14)			2520	91.63	21.11
3 DGs	LSF	634.91 (18)	932.23 (33)	940.79 (25)		2507.94	84.01	19.75
	CA	1189.11 (6)	646.82 (14)	686.34 (31)		2522.28	78.45	19.03
	IA	900 (6)	900 (12)	720 (31)		2520	81.05	19.39
4 DGs	LSF	341.24 (18)	785.75 (33)	869.46 (25)	766.71 (9)	2763.16	73.10	20.04
	CA	926.33 (6)	646.74 (14)	686.36 (31)	967.22 (24)	3226.65	67.63	22.51
	IA	N/A						

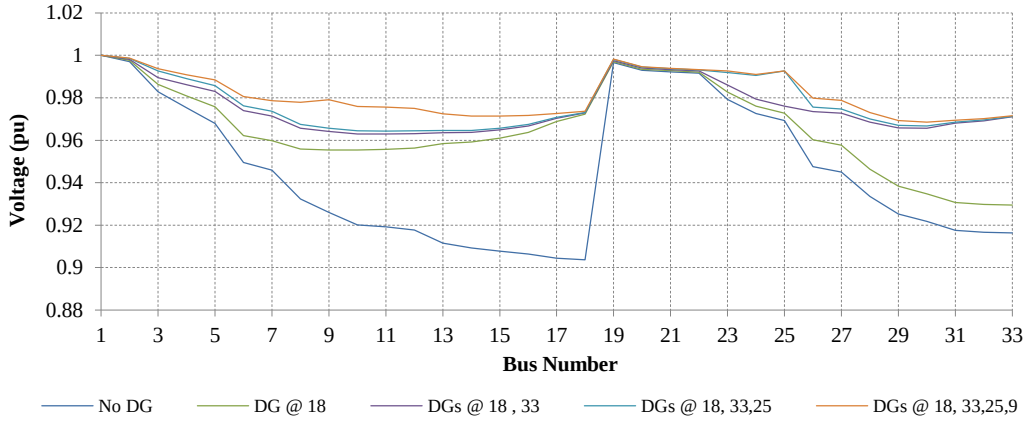

Fig. 8-4. Voltage distributions with optimal Type 1 DG units using LSF siting.

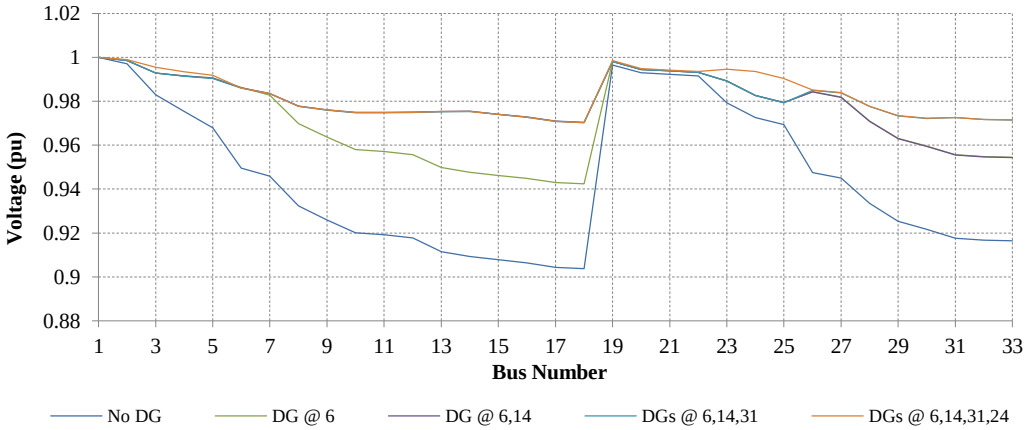

Fig. 8-5. Voltage distributions with optimal Type 1 DG units using CA.

8.6.1.2 Types 2 or 3 DGs with P and Q Injections

Table 8-2 summarizes the optimal allocations and sizing for Types 2-3 DG using LSF, CA and IA. Results also indicate the total optimal PF and the apparent power of DG. Clearly loss reductions by CA are comparable to that of by IA. In contrast to the IA, the proposed approach has the ability to determine the optimal PF of DGs. Hence, the method shows improved loss reductions.

TABLE 8-2: SUMMARY OF RESULTS FOR TYPE 2-3 DGS- CASE 1.

Case	**DG Size in kVA(Bus Number)**					**Total DG Size (kVA)**	**P_{loss} (kW)**	**PI (8-17)**
No DG						0	211.00	
1 DG	LSF	1028.07 (18)				1028.07	123.57	11.76
		PF=0.862				PF=0.862		
	CA	3106.19 (6)				3106.19	67.87	21.70
		PF=0.824				PF=0.824		
	IA	3107 (6)				3107	67.90	21.72
		PF=0.82				PF=0.82		
2 DGs	LSF	753.21 (18)	1340.53 (33)			2078.57	47.57	12.72
		PF=0.893	PF=0.753			PF=0.809		
	CA	1927.15 (6)	1174.34 (30)			3041.09	42.05	18.00
		PF=0.901	PF=0.655			PF=0.824		
	IA	2195 (6)	1098 (30)			3293	44.39	19.77
		PF=0.82	PF=0.82			PF=0.82		
3 DGs	LSF	713.96 (18)	1257.50 (33)	1035.70 (25)		2981.35	28.51	16.34
		PF=0.893	PF=0.743	PF=0.892		PF=0.837		
	CA	1158.18 (6)	1174.55 (30)	712.16 (14)		2983.18	19.95	15.61
		PF=0.902	PF=0.655	PF=0.906		PF=0.824		
	IA	1098 (6)	1098 (30)	768 (14)		2963	22.29	15.71
		PF=0.82	PF=0.82	PF=0.82		PF=0.82		
4 DGs	LSF	376.45 (18)	1089.03 (33)	958.04 (25)	854.15 (9)	3245.96	16.13	16.66

		PF=0.914	PF=0.721	PF=0.893	PF=0.872	PF=0.841		
	CA	861.36 (6)	1174.13 (30)	712.10 (14)	1062.04 (24)	3741.04	7.13	18.35
		PF=0.903	PF=0.655	PF=0.906	PF=0.900	PF=0.841		
	IA	N/A						

Results for DG placement by LSF and CA techniques show significant loss reductions with reactive power control. Even though CA offer more reductions in losses than LSF based siting, DG sizes by CA is significantly high with a high PI in comparison to LSF method. The total DG size for three DGs by LSF is still lower than the total DG size required by CA single or multiple DG installations.

In general, overall DG sizing requirements by LSF are considerably lower than that of by CA with significant loss reductions. DG sizing required with reactive power support by both siting approaches are higher than Type 1 DGs. Similar to Type 1 DGs, based on PI, LSF-based siting offer more value. The PI for three DGs by LSF and CA matches very closely.

Combined PFs by both approaches for all cases matches closely with each other and with the total system demand PF of 0.85. DG size at first optimal site by LSF and CA drops significantly with the addition of a DG regardless of its type.

Corresponding bus voltages by LSF and CA are shown in Fig. 8-6 and Fig. 8-7 respectively. Both LSF and CA achieve enhanced voltage regulation with reactive power capability of DG enabled. It can be seen that, the reactive power compensations from DG sources have caused a slight increase in the voltage at the interconnection point. However, this is within acceptable limits.

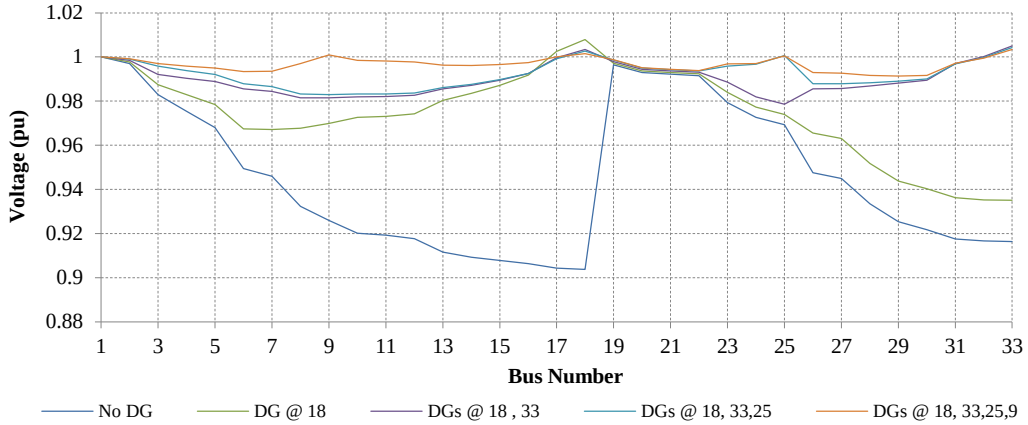

Fig. 8-6 Voltage distributions with optimal Types 2-3 DG using LSF.

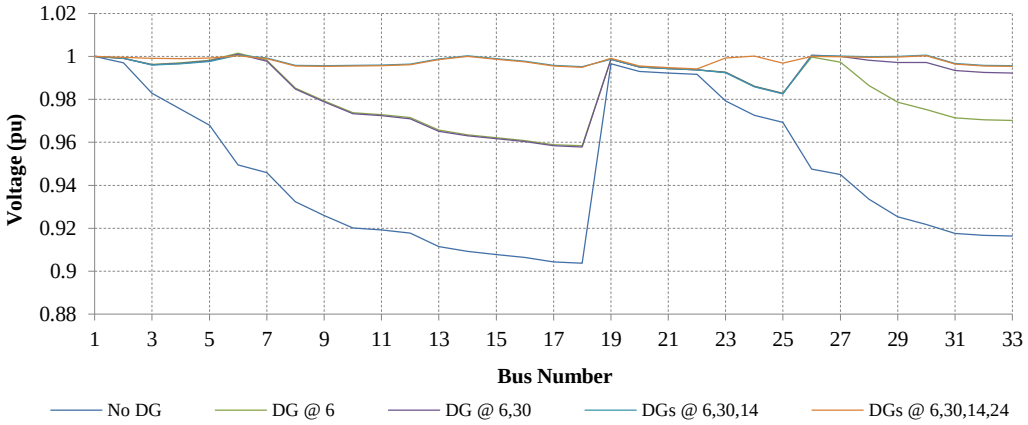

Fig. 8-7. Voltage distributions with optimal Types 2-3 DG using CA.

8.6.2 Case 2 -with Mixed Load

In this section, the proposed approach is tested considering generalized loads. Table 8-3 and Table 8-4 present the summary of results for type 1 and type 2/3 DG placement for a mixed load model defined in Chapter 8.3.5. The optimal sites by the approaches still match with the Case 1 results.

From Table 8-4, the optimal PFs of DGs for the non-constant power load model are comparable to results of the constant power load model. The percentage reductions in the losses are lower than in Case 1. Compared to the constant power load model, a similar trend in the DG rating with LSF-based siting and CA siting can be observed with the assumed load composition.

For all types of DGs, the possible optimal sizes of DGs are now reduced relative to

the constant power load model. Hence the load model can have a significant impact on the DG integration planning. DG sizing derived assuming constant power load models can be uneconomic and ineffective especially if consumers fed by the distribution system have a variable power demand.

TABLE 8-3: SUMMARY OF RESULTS FOR TYPE 1 DGS - CASE 2.

Case	**DG Size in kW-(Bus Number)**					**Total DG Size (kW)**	**P_{loss} (kW)**	**PI (8-17)**
No DG						0	185.61	
1 DG	LSF	792.58 (18)				792.58	132.99	15.06
	CA	2421.38 (6)				2421.38	103.58	29.52
2 DGs	LSF	633.35 (18)	941.65 (33)			1575.00	94.68	17.32
	CA	1794.89 (6)	621.56 (14)			2416.45	86.15	24.30
3 DGs	LSF	603.33 (18)	875.67 (33)	920.96 (25)		2399.96	79.61	22.64
	CA	1146.23 (6)	621.59 (14)	645.06 (31)		2412.89	75.11	21.84
4 DGs	LSF	327.76 (18)	739.39 (33)	854.57 (25)	735.66 (9)	2657.38	69.72	22.93
	CA	892.18 (6)	621.64 (14)	645.24 (31)	953.91 (24)	3112.97	64.77	25.76

TABLE 8-4: SUMMARY OF RESULTS FOR TYPE 2-3 DGS - CASE 2.

Case	**DG Size in kVA(Bus Number)**					**Total DG Size (kVA)**	**P_{loss} (kW)**	**PI (8-17)**
No DG						0	185.61	
1 DG	LSF	972.27 (18)				972.27	114.06	13.59
		PF=0.865				PF=0.865		
	CA	2982.02 (6)				2982.02	64.77	24.68
		PF=0.824				PF=0.824		
2 DGs	LSF	736.53 (18)	1316.20 (33)			2037.49	46.28	14.62
		PF=0.894	PF=0.752			PF=0.809		
	CA	1862.84 (6)	1171.02 (30)			2973.56	40.21	20.45
		PF=0.902	PF=0.654			PF=0.822		
3 DGs	LSF	700.07 (18)	1237.93 (33)	1029.66 (25)		2941.96	27.94	18.66
		PF=0.894	PF=0.742	PF=0.892		PF=0.837		
	CA	1148.01 (6)	1170.94 (30)	708.49 (14)		2965.82	19.53	17.86
		PF=0.902	PF=0.654	PF=0.906		PF=0.824		
4 DGs	LSF	374.85 (18)	1077.45 (33)	954.91 (25)	847.39 (9)	3223.13	15.96	19.00
		PF=0.914	PF=0.721	PF=0.893	PF=0.872	PF=0.841		
	CA	858.58 (6)	1170.61 (30)	708.32 (14)	1059.32 (24)	3728.18	7.08	20.88
		PF=0.903	PF=0.654	PF=0.906	PF=0.900	PF=0.841		

8.7 VCZ-Based Optimal VSDG Placement and Sizing to Improve Voltage Regulation

Integration of voltage support DG (VSDG) can enhance the system voltage profile; especially in rural areas where low voltages are significant. However, optimal sizing and siting of VSDGs is essential for ensuring required levels of voltage support are realized [145]-[146]. A sequential optimization approach based on a set of algebraic equations is developed in [91] for uniformly distributed loads in radial feeders to determine the optimal size and location of a single DG. The method in [91] achieves requisite levels of voltage support by installing DG so that the weakest bus voltage can be improved to a reference voltage.

The main aim of the proposed second analytical approach is to optimally place and size DGs such that the feeder voltages are regulated within desired levels. This method considers a reference voltage for DG buses. The approach is simple, accurate and requires the load flow to be run twice; firstly for siting and secondly for sizing. Thus, it is computationally less demanding and efficient. Optimal DG locations are determined by identifying voltage control zones (VCZs) while optimal DG capacities are calculated using a modified load flow approach.

8.7.1 Zones of Influence for DG Placement

VCZs are identified for effective DG integrations depending on the voltage sensitivity of buses to variations in active power (dV/dP). The mismatch sensitivities are calculated by taking inverse of the Jacobian:

$$\begin{bmatrix} \frac{d\delta}{dP} & \frac{d\delta}{dQ} \\ \frac{dV}{dP} & \frac{dV}{dQ} \end{bmatrix} = \begin{bmatrix} \frac{dP}{d\delta} & \frac{dP}{dV} \\ \frac{dQ}{d\delta} & \frac{dQ}{dV} \end{bmatrix}^{-1} = J^{-1}; \quad \rightarrow VSF = \begin{bmatrix} \frac{dV}{dP} \end{bmatrix} \tag{7-1}$$

Where, the dV/dP entry of J^{-1} is defined as VSF which is a $(n-1)X(n-1)$ matrix. The diagonal and off diagonal elements of VSF indicate the impact on a particular bus voltage due to its own power variations and the power variations of the rest of the buses, respectively.

Using (7-1), optimal DG site selections are performed using the following four steps.

Step 1. Obtain the dV_i/dP_j matrix from (7-1).

Step 2. Identify bus j that returns the maximum dV_i/dP_j value for each bus i or for each row of VSF matrix.

Step 3. Identify VCZs and optimal DG sites as follows:

a. Cluster the buses that returned the same j.

b. Ensure that $j = i$ is not the only element in a cluster or the size of the cluster is greater than one; otherwise, eliminate the clusters of size one.

c. The remaining j buses are the optimal DG sites.

d. The remaining clusters are defined as the VCZs.

e. The eliminated buses in Step 3(b) can be clustered into a remaining VCZ that will return the highest dV_i/dP_j for the eliminated bus, where j is one of the optimal sites.

Step 4. The maximum number of DG units required is equal to the number of identified zones.

For a selected VCZ the highest dV_i/dP_j of the zone occurs when $i = j$. Therefore, the identified optimal sites can be ranked in a descending order based on $\left|dV_j/dP_j\right|$. This ranking is then used to determine the highest priority sites which assist the determination of optimal sites in events where other constraints such as budget or geography don't allow the installations of maximum number of DG found in Step 4.

8.7.2 Optimal Sizing of DG

Optimal sizes of DG are derived using the proposed ALF approach of Chapter 7.3.1 assuming that either the PF of DG or Q_{DG-i} is known. Load flow needs to be run once with DG units placed at the optimal sites. To achieve the preferred voltage regulation, DG buses are set to "QV" type. The bus voltage and the reactive power (or the PF) at a QV bus are considered as independent variables. QV bus voltage can be set to a desired reference voltage (e.g., the slack bus voltage to minimize voltage drop errors).

The solution algorithm for optimal DG sizing is summarized below.

Step 1. Initialize iteration counter ($iteration = 0$), voltage magnitudes and phase angles. Identify optimal DG nodes (Chapter 8.7.1).

Step 2. Construct the Y matrix ((Eqs. (7-11)-(7-12)) and determine current injections (for QV buses Eqs. (7-5)-(7-6)) and for PV and PQ buses as defined in [131]).

Step 3. Calculate subsequent power mismatches.

$$\Delta P_i = P_i^{sp} - P_i^{calc} \tag{7-15}$$

$$\Delta Q_i = Q_i^{sp} - Q_i^{calc} \tag{7-16}$$

Step 4. If $max(\Delta P, \Delta Q) \leq tolerance$, then go to Step 5; otherwise, determine bus voltage and power corrections using (7-13), update bus voltages and go back to Step 2.

Step 5.

- For *PQ* buses, update voltages using (7-17) and (7-18):

$$V_i = V_i^h + \Delta V_i = V_i^h + \left(\frac{V_{r_i}}{V_i}\Delta V_{r_i} + \frac{V_{m_i}}{V_i}\Delta V_{m_i}\right) \tag{7-17}$$

$$\theta_i = \theta_i^h + \Delta\theta_i = \theta_i^h + \left(\frac{V_{r_i}}{V_i^2}\Delta V_{m_i} - \frac{V_{m_i}}{V_i^2}\Delta V_{r_i}\right) \tag{7-18}$$

- For QV buses, voltage angles are updated using (7-18) while P_i^{calc} is calculated with updated voltages.

Step 6. Therefore, DG sizes can be calculated from,

$$P_{DG-i} = P_i^{calc} + P_{L-i} \tag{8-18}$$

For DG of known PF, Q_{DG-i} can be written as:

$$Q_{DG-i} = P_{DG-i}.tan(\theta_{PF_i}) \quad (8\text{-}19)$$

8.7.3 Flow Chart of Optimal Siting/Sizing of DGs

Fig. 8-8 shows the flow chart of the proposed approach for multiple DG placement and sizing for voltage regulation.

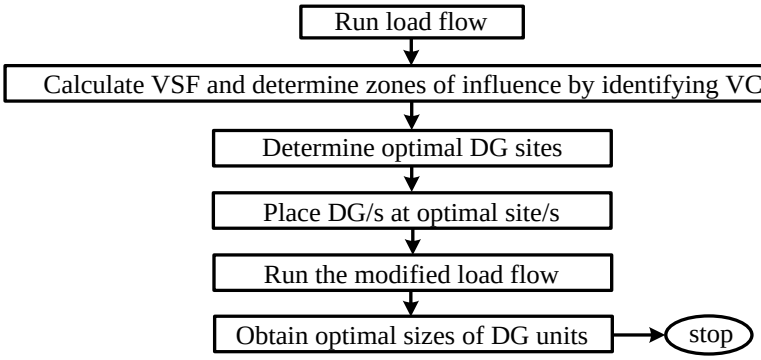

Fig. 8-8. Flow chart of proposed optimal DG siting & sizing (Eqs. (8-18)-(8-19)) approach to improve voltage regulation.

8.8 Simulation Results for VCZ-Based Voltage Regulation Approach

The proposed VCZ based analytical method of Section VII for optimal DG siting and sizing was tested on the 33 bus system of Fig. 8-1. The maximum number of DG units and the permissible voltage limits were set to 4 units and 1±0.06p.u., respectively.

8.8.1 Optimal Siting

Testing of voltage regulation approach (VRA) was carried out under varying number of zones of influence and varying reference voltages for optimal DG buses with the slack bus voltage set to 1.0p.u. Four voltage control zones of influence were identified as depicted in Fig. 8-9. Optimal sites and the zones are buses 18 (zone 1), 33 (zone 2), 25 (zone 3) and 22 (zone 4), in a descending order from highest to lowest priorities. Simulations for Case 1 and Case 2 returned the same results for siting.

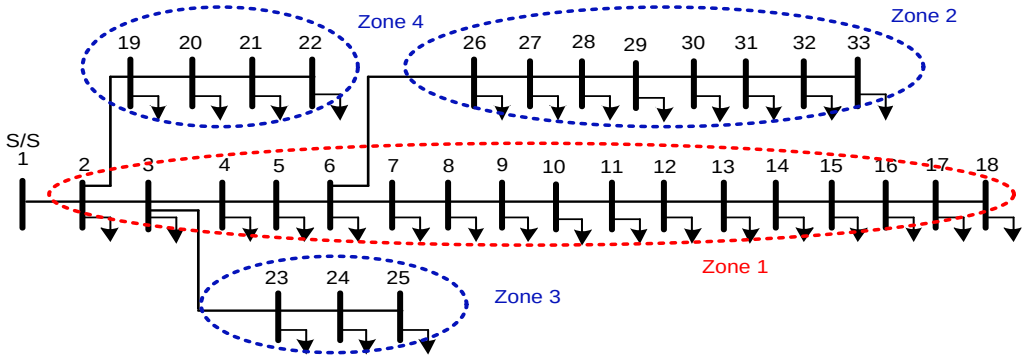

Fig. 8-9. Voltage control zones that define zones of DG influence.

8.8.2 Case 1- with Constant Power Load

8.8.2.1 Type 1 DG with Reference Voltage of 1.0pu

Type 1 DGs may be preferred in distribution systems with high R/X ratios. These highly resistive networks characteristically will require high amounts of active power compensation by DGs for supporting the system voltages. Hence, reactive power injections will not have a significant impact on the voltage performances. From the cost perspective, maximum cost benefits will be realized when the DG operates at unity PF as the cost of real power is generally much higher.

Table 8-5 represents the resultant DG sizes and corresponding losses with varying number of zones of influence for type 1 DG. The voltages at DG buses were set to a reference voltage of 1.0p.u. Fig. 8-10 provides a graphical comparison of the voltage profiles under various cases.

For Type 1 DGs, VRA offers enhanced voltages with considerable reductions in the system losses. Improvements in the voltage profile and reduction in the system losses increase with the increased number of zones as expected. However, consideration of 4 zones for Type 1 DGs with a reference voltage of 1.0p.u. may not be desirable for the 33 bus system as the total DG size exceed the total demand with four DGs. Two or three Type 1 DGs with the reference voltage of 1.0p.u. is adequate as the difference in the voltage profiles with four DGs is not significant with respect to the total DG size.

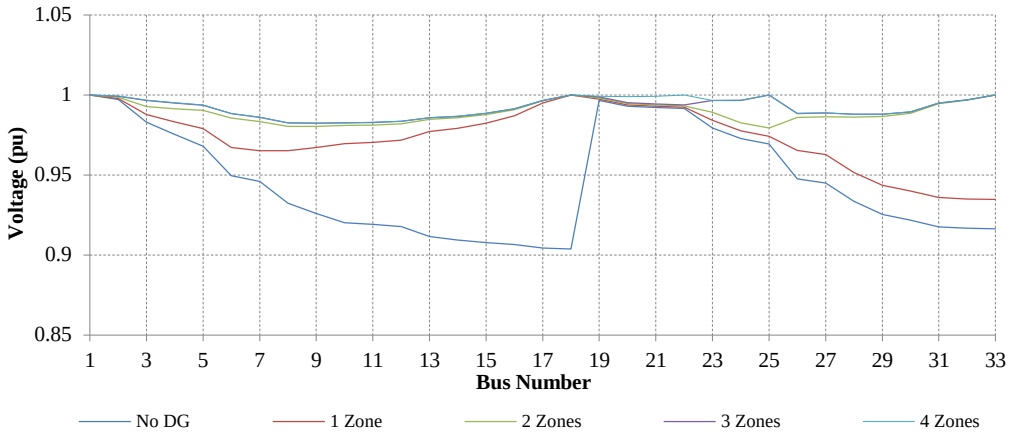

Fig. 8-10. Voltage profiles with optimal Type 1 DG using VRA.

TABLE 8-5: SUMMARY OF RESULTS WITH 1P.U. REFERENCE VOLTAGE.

Case	**DG Size (kW)**				**Total DG Size (kW)**	**P_{loss} (kW)**
No DG						211.00
1 Zone	Bus 18					
	1247.23				1247.23	157.25
2 Zones	Bus 18	Bus 33				
	929.02	1643.31			2572.32	126.47
3 Zones	Bus 18	Bus 25	Bus 33			
	883.80	1189.81	1544.03		3617.64	110.80
4 Zones	Bus 18	Bus 22	Bus 25	Bus 33		
	882.11	348.34	1179.29	1540.34	3950.08	109.76

8.8.2.2 Types 2 and 3 DGs with Reference Voltages of 1.0p.u.

A similar analysis as for Type 1 DG was conducted for Types 2-3 DGs (Table 8-6). The PF of the DGs were set to the total load PF of 0.85. The test system under study is a highly resistive feeder with R/X ratios that varies between ~2 and 3. Thus, a PF of the aggregated load is a suitable assumption. For highly inductive systems, line impedance may need to be taken into account when deriving the PFs.

TABLE 8-6: SUMMARY OF RESULTS WITH 1P.U. REFERENCE VOLTAGE FOR TYPE 2-3 DGS.

Case	**DG Size (kVA)**				**Total S_{DG} (kVA)**	**P_{loss} (kW)**
No DG						211.00
1 Zone	Bus 18					
	939.29				939.29	124.16
2 Zones	Bus 18	Bus 33				
	715.12	1266.59			1981.69	49.85
3 Zones	Bus 18	Bus 33	Bus 25			
	682.74	1195.59	1006.39		2884.72	30.81
4 Zones	Bus 18	Bus 33	Bus 25	Bus 22		
	681.68	1193.25	999.31	255.52	3129.77	29.45

The required reference voltage was assumed to be 1.0p.u. From the Fig. 8-11, no significant changes in the voltage profiles are evident. However, as shown in the Table 8-6 the required DG sizes show a substantial drop with more loss reductions. Active power injections required by DG are now lower. Enabling reactive power support compensates the line and load reactive power components to a degree thus improve the voltage quality. The resultant losses match closely with those obtained using the loss reduction approach with PQ control.

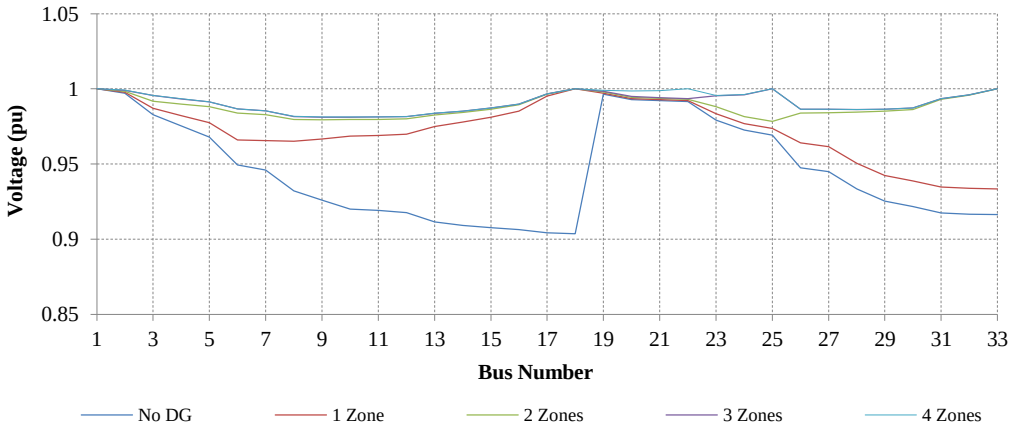

Fig. 8-11. Voltage profiles with optimal Types 2-3 DG using VRA.

8.8.2.3 Type 1 DG with Varying Reference Voltages and 4 Zones

In this section, the reference voltage at the DG buses was incrementally dropped by 0.01p.u. steps to 0.95p.u. As the reference voltage was reduced, no DG was placed if the selected DG bus voltage exceeded the new reference. If this action was not taken, the DG will absorb power to drop the voltage at the interconnection point. This is shown in the last row of the Table 8-7 for 0.97p.u. The negative signs indicate import of power at buses 22 and 25 as their original voltages without DG were above reference voltage 0.97p.u. In other words, if the reference voltage is higher, number of zones that require voltage support rise.

TABLE 8-7: SUMMARY OF RESULTS WITH VARYING REFERENCE VOLTAGES.

Ref. Volt. (p.u.)	**DG Size (kW)**				**Total DG Size (kW)**	**P_{loss} (kW)**
No DG						211.00
	Bus 18	Bus 33	Bus 25	Bus 22		
1	882.21	1540.31	1179.28	348.34	3950.13	109.76
0.99	799.86	1359.59	661.74	0.00	2821.18	95.14
0.98	719.62	1183.33	157.02	0.00	2059.97	96.22
0.97	579.45	875.61	0.00	0.00	1455.06	86.65
0.96	483.80	665.67	0.00	0.00	1149.47	92.21
0.95	390.72	461.41	0.00	0.00	852.13	104.17
0.97*	649.07	1028.38	-286.83	-1190.41	200.21	152.00

(*) Negative signs indicate import of power.

With low reference voltages, the level of compensation or DG injections requirement is low. Therefore, the sizes of the DGs decrease with the threshold voltage as shown in Table 8-7.

Even though all the tested reference voltages reduce system losses significantly, reference voltage of 0.97p.u. offers the lowest losses. This can be explained from the fact that more DG injections are needed to maintain a higher voltage at the PCC

while voltage support by lower reference voltages is not sufficient.

Fig. 8-12 illustrates the voltage profiles with varying reference voltages. Depending on the system requirements and availability of resources, each zone may hold dissimilar reference voltages. Same sizing approach can be employed for such cases.

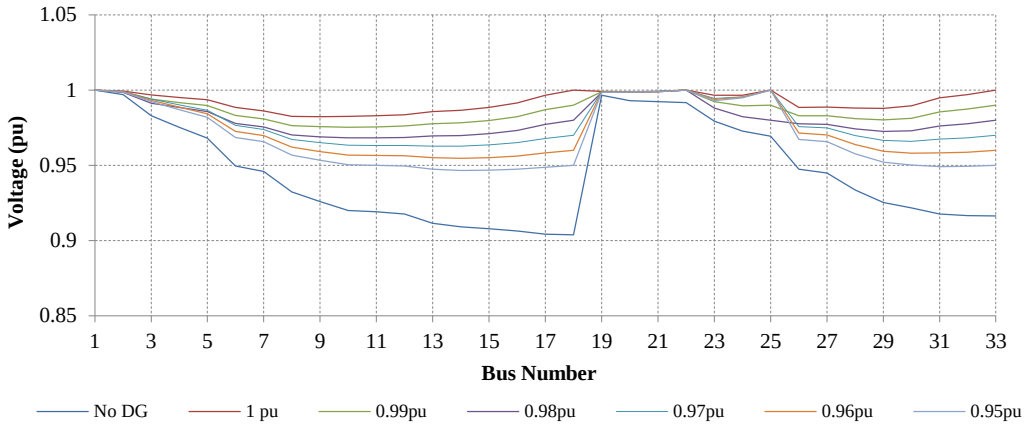

Fig. 8-12. Voltage profiles with optimal Type 1 DG using VRA with varying reference voltages.

8.8.3 Case 2- with Mixed Load

Practical distribution system loads are not explicitly constant power, constant current or constant impedance models. In this section, a study is carried out considering a mix of voltage dependent loads to study the effect of mix load models and to test the robustness of the proposed approach. A similar sizing/siting approach is applied for DGs with and without reactive power support for the non-constant power load case. Summary of results for DGs with active power control and DGs with both active and reactive power capabilities are presented in Table 8-8 and Table 8-9, respectively. In Table 8-9, the PF of the DG systems are set to the combined load PF of 0.851.

Based on the investigations, the optimal locations for DGs did not vary from that found with constant power load. However, this observation is dependent on the configuration of the system and the load composition of the feeder. In Case 2, the assumption was made that each load follows the same voltage dependency.

However, as indicated in Table 8-8 and Table 8-9 the sizing of DGs with the non-constant power load model are different from that found with constant power load.

Thus, DG planning considering the nature of the distribution system loads is more economic and ensures that DG units are fully utilized.

TABLE 8-8: SUMMARY OF RESULTS WITH 1P.U. REFERENCE VOLTAGE FOR TYPE 1 DG.

Case	**DG Size (kW)**				**Total DG Size (kW)**	**P_{loss} (kW)**
No DG						185.61
1 Zone	Bus 18					
	1213.21				1213.21	145.44
2 Zones	Bus 18	Bus 33				
	918.41	1627.73			2546.14	123.48
3 Zones	Bus 18	Bus 25	Bus 33			
	874.94	1186.45	1531.71		3593.10	108.80
4 Zones	Bus 18	Bus 22	Bus 25	Bus 33		
	873.30	347.90	1176.04	1528.10	3925.34	107.78

TABLE 8-9: SUMMARY OF RESULTS WITH 1P.U. REFERENCE VOLTAGE FOR TYPE 2-3 DGS.

Case	**DG Size (kVA)**				**Total S_{DG} (kVA)**	**P_{loss} (kW)**
No DG						185.61
1 Zone	Bus 18					
	914.14				914.14	114.33
2 Zones	Bus 18	Bus 33				
	706.72	1253.67			1960.39	48.42
3 Zones	Bus 18	Bus 25	Bus 33			
	675.64	1003.00	1185.14		2863.78	30.14
4 Zones	Bus 18	Bus 22	Bus 25	Bus 33		
	674.61	255.24	996.00	1182.86	3108.70	28.80

8.9 Conclusions

Two analytical approaches for optimal placement and sizing of multiple DG units are proposed, formulated and implemented in this chapter. The primary aim of the LSF-based approach is to minimize total system losses while the main objective of the VCZ-based approach is to improve voltage profiles. Detailed simulations are presented and analysed for optimal siting and sizing of Types 1, 2 and 3 DGs in a 33 node distribution system. Investigations were first carried out considering a constant power load model and secondly with a generalized load model. The main conclusions are:

- Based on the PI, the LSF-based approach shows superior performance in terms of simplicity, accuracy and loss reduction when compared to CA solutions.

- The DG ratings produced by the LSF approach are considerably lower than the CA ratings with significant reductions in losses (Table 8-1-Table 8-4) and improved voltage profiles (Fig. 8-4-Fig. 8-7).

- In general, DG sizes with reactive power support (Types 2-3 DGs) are substantially higher than Type 1 DGs. However, further loss reductions and improved voltage profiles are apparent with Types 2-3 DGs (Table 8-1-Table 8-4).

- The VCZ-based voltage regulation approach shows superior performance in terms of simplicity, accuracy and voltage regulation.

- The improvement in the voltage profile and the reduction in losses increase with the increased number of zones. For Types 2-3 DGs with voltage references set to 1.0p.u. offer no significant changes in voltage profiles (Fig. 8-11); however, the required DG sizes and network losses are lower (Table 8-6).

- The required DG size decreases with lower reference voltages for DG buses (Table 8-7). For Type 1 DG, lowest losses were obtained when the reference

voltage was 0.99p.u. Depending on the system requirements and availability of resources, each zone may have dissimilar reference voltages.

- The proposed LSF-based and VCZ based approaches can effectively conduct DG planning studies for practical systems with non-constant power loads. Based on the results obtained for mixed load model, it is clear that consideration of voltage dependency affects the optimal DG parameter selection.

Chapter 9. Conclusions

9.1 Summary and Contributions

This doctoral research project is motivated by the need to transform the electricity grid into a smart grid that will have the ability to host high penetrations of DG (particularly renewable resources) and loads while supporting electricity generation market de-carbonization. In order to enable the transformation, integration of BESSs is proposed in this dissertation. The novel approaches developed in this thesis explicitly deal with the issues that combine optimal dispatch control, siting and sizing of BESSs for efficient integration to the grid. They can be used to maximize techno-economic benefits and value of battery storage systems; thereby allowing seamless integration of variable DG into the electricity grid.

Different sectors could benefit from the work presented in this thesis. Three key beneficiaries would be DNOs, consumers and the society. The investigations offer DNOs a better understanding of the capabilities and the role of BESSs in the capacity mix. Furthermore, the research shows that the optimal BESS integration and dispatch management will improve system performance and supply voltage quality enabling efficient utilization of power system assets. The transition towards a decentralized electricity network will affect the energy market operations. Over the years to come, consumers will experience the adoption of DER and their impacts at varying levels, altering the traditional demand curves and tariff structures. Therefore, all three parties will benefit from improved supply quality, efficiency, reductions in greenhouse gas emissions and flexibility in terms of electricity prices and choices of generation sources. The proposed techniques will also serve as a reference to academics, who have concerns on how to effectively connect storage to the grid.

The core contributions of this research are summarized below:

- **Modelling of battery energy profile within an optimization problem:** Optimization of the holistic problem of optimal siting, sizing and dispatch management of BESS requires repeated evaluation of a solution vector of

battery energy. This vector needs to be subject to three key constraints; an energy balance constraint, constraint for periodicity and a constraint to limit the differences between any two adjacent charge states. Therefore, in Chapter 3, periodic battery energy is represented using a vector of Fourier coefficients. Fourier series presentation inherently encapsulates the above constraints. The compact representation, therefore, reduces the dimensionality of the optimization problem and improves the computational efficiency while effectively maintaining the periodicity and continuity of the battery energy function. Method allows problem specific constraints to be applied effectively. This battery model is used in the cost based battery optimization problems in Chapters 4, 5 and 6. Furthermore, battery cost components, mathematical formulations for grid connection and formulations for BESS optimization problem considering a single system are presented in Chapter 3.

- **Adaptive management of community scale BESS for peak shaving:** The first stage storage integrations in the evolution of the electricity grid are likely to emerge at the distribution side mostly co-located with distribution transformers or at the grid scale. Therefore, in Chapter 4, the problem of optimizing the size and diurnal operation of large scale grid tied storage BESS for peak shaving is addressed. A cost based predictive optimization approach and a simple rule-based predictive approach, are proposed. Then an exponential smoothing method is applied to recursively update the battery energy profile as new information become available, to adapt for changing future predictions in loads and DG productions. Numerical results reveal the ability of the proposed models to reduce the peak while achieving a smoothed demand curve. A case study also highlights that the conventional grid can become a secondary supply in the presence of intelligently managed BESS in the next generation grid.

- **Optimizing the distribution network load and generation hosting capacity:** In Chapter 5, a cost function that incorporates costs incurred due to peak support, distribution system losses, poor voltage levels and battery

cycling is developed for the optimization of grid scale BESS dispatch and sizing. This method is able to take into consideration various network topologies, load patterns and DG penetration levels as well as network fundamental capacity, voltage and battery constraints. Optimal installation sites are chosen as the buses at which the cost function is at minimum. This chapter also provides a review on usage of storage for the exclusive and simultaneous control of voltage regulation, peak demand and loss reduction. A quantitative analysis on the impact of installation site on the services provided, dispatch management scheme and size of BESS is also carried out. Detailed results show that the amount of tradeoffs highly depends on the installation site, the network topology and the load/generation distribution. Furthermore, the importance of addressing the problem with the aim of improving system voltages to enhance the DG absorption is highlighted. Maximum tradeoffs are achieved when installing battery considering its ability to simultaneously provide multiple services.

- **Optimal management of residential BESS in unbalanced distribution networks:** Real and reactive power flow coordination using residential level BESSs in three phase four wire distribution system with high penetrations of rooftop PVs is investigated in Chapter 6. Optimization method in Chapter 5 is improved with the inclusion of a voltage unbalance factor cost component to minimize effects of imbalances. Results show the capability of the proposed algorithm to reduce distribution losses, reduce the peak demand and improve the feeder voltage profile with respect to voltage magnitude and phase balance. Chapter 6 also makes a major contribution in highlighting the influence of the battery location on the daily charge profile and grid performance.

- **Analytical approach for optimal placement, sizing and management of battery storage:** Chapter 7 proposes an effective analytical approach for optimal placement, sizing and charge/discharge management of single or multiple BESSs. The method is developed with the key objective of regulating the system voltages while improving the DG absorption ability of

the grid. A strategic analytical approach that identifies zones of BESS influence for voltage control is established for optimal placement. Optimal sizing and dispatch control are achieved analytically through a combine real-time and offline smart management technique. Results demonstrate the ability of the approach to manage the BESS bus voltage and to improve system performance levels in terms of reduced losses, peak shaving and smart coordination of available generation. In comparison to single BESS installation, integration and management of multiple BESSs show further enhanced performance levels with more flexibility to manage feeder voltage profile and absorb mass quantities of DG. The proposed method avoids the need for exhaustive optimization algorithms, therefore, improves the accuracy and speed.

- **Optimal DG siting and sizing:** Integration of grid scale DG units is becoming increasingly popular due to the rising demand requirements, grid stability and system security issues, as well as environmental and economic concerns. However, inappropriate siting and sizing of DG units may cause negative impacts on the operation and performance of the system. Therefore, Chapter 8 proposes two analytical approaches for optimal placement and sizing of DG units in radial and/or mesh systems. These approaches are simple and effective compared to most available methods that rely on iterative numerical solutions. Both approaches are able to model generalized loads as well as improve system performance in terms of total loss reductions and overall voltage profiles. However, the primary objective of the first approach which is based on the loss sensitivity factors is to minimize system losses while the main aim of the second approach is to minimize node voltage deviations through identification of voltage control zones.

9.2 Recommendations for Future Work

Through testing of the proposed methods, techno-economic capabilities of BESS in grid applications have been confirmed. However, methods can be improved to gain further insights into the issue of improving distribution system capacity, performance

and efficiency through integration of battery storage while improving the cost competitiveness of BESSs.

As an extension of the work presented in this thesis, the following suggestions for future work can further strengthen the proposed methods:

- **Expand the models to include various DER technologies:** The battery integration methods presented in this thesis are generalized approaches with high flexibility. The studies, however, have been carried out mostly considering PV type non-dispatchable DGs that are interfaced to the grid through inverters. Therefore, further modellings by adding various DER technologies such as dispatchable fuel based DG can be used to study effects of their characteristics and compare competing technologies.

- **Develop a DER management strategy for distribution systems with high penetrations of DG and plug-in electric vehicles:** Community scale storages can be used to shift the peak generation to peak vehicle charging periods and vehicle batteries can be managed to provide vehicle-to-grid discharging. This may considerably promote the uptake of both DG and plug-in electric vehicles.

- **Improve input data:** A larger data base that contain various real network topologies, operational constraints, load and generation information would facilitate the opportunity for a more comprehensive analysis. Furthermore, it will more effectively capture variety of network features and load/generation characteristics as well as provides the opportunity thoroughly explore applications of storage for the service of grid.

- **Establishment of rules and regulations for grid integration:** Work presented in this thesis shows the BESSs ability to change the way we generate, use and manage electricity. However, at present, no general standards or policies are in place for BESS integrations beyond the normal network access rules for generation. Standards, rules and regulations can be established by understanding the capabilities of BESSs using the proposed

approaches, which in turn will strongly influence the growth of the storage market for decentralized electricity networks. The proposed methods can also be extended to determine sensible pricing schemes or market opportunities based on technical benefits to the grid and deferral of network investment projects to further encourage BESSs interconnections. Moreover, benefits of BESSs can even be passed on to consumers in a form of an incentive scheme or rebate.

References

Every reasonable effort has been made to acknowledge the owners of copyright material. I would be pleased to hear from any copyright owner who has been omitted or incorrectly acknowledged.

[1] H. Farhangi, "The path of the smart grid," *IEEE Power and Energy Magazine*, vol.8, no.1, pp. 18-28, Feb. 2010.

[2] E. M. Lightner and S. E. Widergren, "An orderly transition to a transformed electricity system," *IEEE Trans. on Smart Grid*, vol. 1, no. 1, pp. 3-10, Jun. 2010.

[3] (2014). "World energy investment outlook: Special Report", International Energy Agency, France. [Online] Available: http://www.worldenergyoutlook.org/

[4] K. Auret, "State of the energy market 2013: National electricity market", Australian Energy Regulator, Dec 2013. [online] Available: http://www.aer.gov.au/node/23147

[5] (2014). 2014 Australian energy update, Bureau of Resources and Energy Economics, Canberra. [online] Available: www. bree.gov.au

[6] (Oct. 2012), "Grid integration of large-capacity renewable energy sources and use of large-capacity electrical energy storage", International Electrotechnical Commission. [online] Available: http://www.iec.ch/whitepaper/gridintegration/

[7] F. Li, W. Qiao, H. Sun, H. Wan, J. Wang, Y. Xia, Z. Xu and P. Zhang, "Smart transmission grid: Vision and framework," *IEEE Trans. on Smart Grid*, vol. 1, no. 2, pp. 168-177, Sep. 2010.

[8] D. Costello, "Intelligent grid research cluster Project 5: Intelligent grid social impacts", iGrid an Australian Research Collaboration.

[9] (Jul. 2011). "Network management plan", Western Power, Western Australia. [online] Available: http://www.westernpower.com.au/

[10] (2013). "National transmission network development plan: For the national electricity market", Australian Energy Market Operator. [online] Available: http://www.aemo.com.au/

[11] R. J. Hyndman and S. Fan, "Density forecasting for long-term peak electricity demand," *IEEE Trans. on Power Syst.*, vol. 25, no. 2, pp. 1142-1153, May 2010.

[12] P. Toner, "Electricity privatisation in Australia: A briefing note", University of Sydney- Department of Political Economy, Oct. 2012. [online] Available: www.asu.asn.au/

[13] S. McGushin and A. Seeto, "Australia: NSW electricity privatisation - the renewable assets", Corrs Chambers Westgarth, Sep. 2013. [online] Available: http://www.corrs.com.au/publications/corrs-in-brief/nsw-electricity-privatisation-the-renewable-assets/

[14] D. Green, "Centralized to de-centralized energy: What does it mean for Australia? - Draft Discussion Paper", Clean Energy Council, Mar. 2014.

[15] G. T. Heydt, R. Ayyanar, W. K. Hedman and V. Vittal, "Electric power and energy engineering: The first century," *IEEE Proceedings,* vol. 100, pp. 1315-1328, May 2012.

[16] S. Jebaraj and S. Iniyan. "A review of energy models", *Journal of Renewable and Sustainable Energy Reviews,* vol. 10, no.4, pp.281-311, 2006.

[17] P. Harsha and M. Dahleh, "Optimal management and sizing of energy storage under dynamic pricing for the efficient integration of renewable energy," *IEEE Trans. on Power Syst.*, IEEE Early Access Article.

[18] C. A. Hill, M. C. Such, D. Chen, J. Gonzalez and W. M. Grady, "Battery energy storage for enabling integration of distributed solar power generation," *IEEE Trans. on Smart Grid*, vol. 3, no. 2, pp. 850-857, Jun. 2012.

[19] R. S. Rao, K. Ravindra, K. Satish, and S. V. L. Narasimham, "Power loss minimization in distribution system using network reconfiguration in the presence of distributed generation," *IEEE Trans. Power Syst.*, vol. 28, no. 1, pp. 317–325, Feb. 2013.

[20] D. Singh and K. S. Verma, "Multiobjective optimization for DG planning with load models," *IEEE Trans. Power Syst.*, vol. 24, no. 1, pp. 427–436, Feb. 2009.

[21] Z. Ghofrani-Jahromi, Z. Mahmoodzadeh and M. Ehsan, "Distribution loss allocation for radial systems including DGs," *IEEE Trans. on Power Delivery*, vol. 29, no. 1, pp. 72-80, Feb. 2014.

[22] Z. Wang, C. Gu, F. Li, P. Bale and H. Sun, "Active demand response using shared energy storage for household energy management," *IEEE Trans. on Smart Grid*, vol. 4, no.1, pp. 1888-1897. Dec. 2013.

[23] Y. Riffonneau, S. Bacha, F. Barruel and S. Ploix, "Optimal power flow management for grid connected PV systems with batteries," *IEEE Trans. on Sustainable Energy*, vol.2, no. 3, pp. 309-320. Jul. 2011.

[24] B. Shen, G. Ghatikar, Z. Lei,, Jinkai Li, G. Wikler and P. Martin, "The role of regulatory reforms, market changes, and technology development to make demand response a viable resource in meeting energy challenges," *Journal of Applied Energy*, vol. 130, pp. 814-823, Oct. 2014.

[25] D. Setlhaolo, X. Xia and J. Zhang, "Optimal scheduling of household appliances for demand response", *Journal of Electrical Power Systems Research*, vol. 116, pp.24-28, Nov. 2014.

[26] N. O'Connell, P. Pinson, H. Madsen and M. O'Malley, "Benefits and challenges of electrical demand response: A critical review", *Journal of Renewable and Sustainable Energy Reviews*, vol. 39, pp. 686-699, Nov. 2014.

[27] N. Leeprechano, A. David, S. S. Moorthy and F. Liu, "Transition to an electricity market: A model for developing countries," *IEEE Trans. Power Syst.*, vol. 17, no. 3, pp. 885-894, Aug. 2002.

[28] (2013). "World energy outlook: Renewable energy outlook", International Energy Agency, France. [Online] Available: http://www.worldenergyoutlook.org/

[29] G. Masson, S. Orlandi, and M. Rekinger, "Global Market Outlook: For Photovoltaics 2014-2018", European Photovoltaic Industry Association.2013. [online] Available:

http://www.epia.org/fileadmin/user_upload/Publications/EPIA_Global_Market_Outlook_for_Photovoltaics_2014-2018_-_Medium_Res.pdf

[30] (2012). "Rooftop PV information paper: National electricity forecasting," Australian Energy Market Operator. [online] Available: http://www.aemo.com.au/

[31] I. Das, K. Bhattacharya, C. Cañizares and W. Muneer, "Sensitivity-indices-based risk assessment of large-scale solar PV investment projects," *IEEE Trans. on Sustainable Energy*, vol. 4, no. 2, pp. 370-378, Apr. 2013.

[32] (2013). "Australian energy resource assessment – Chapter 10: Solar energy", Australian Renewable Energy Agency, [online] Available: http://arena.gov.au/about-renewable-energy/solar-energy/

[33] (2014). Edge of grid, Western Power. [online] Available: http://www.westernpower.com.au/network-projects-your-community-edge-of-grid.html

[34] (2013). Smart modelling of optimal integration of high penetration of PV-Smooth PV: Final report, Energynautics GmbH. [online] Available: http://www.smooth-pv.info/

[35] G. Masson, M. Latour, M. Rekinger, I. Theologitis and M. Papoutsi, "Global market outlook: For Photovoltaics 2013-2017", European Photovoltaic Industry Association, 2014. [online] Available: http://www.epia.org/fileadmin/user_upload/Publications/GMO_2013_-_Final_PDF.pdf

[36] P. Denholm, R. Margolis, T. Mai, G. Brinkman, E. Drury, M. Hand, and M. Mowers, "Bright future: solar power as a major contributor to the U.S. grid," *IEEE Power and Energy Magazine*, vol. 11, no. 2, pp. 22-32, Apr. 2013.

[37] E. Wesoff, (Mar. 2014). Jinko first to take solar module costs below 50c/watt", Renew Economy. [online] Available: http://reneweconomy.com.au/2014/jinko-first-to-take-solar-module-costs-below-50cwatt-36076

[38] G. Parkinson, "How far away is grid parity for residential battery storage?," Renewable Economy, Aug. 2014. [online] Available:

http://reneweconomy.com.au/2014/how-far-away-is-grid-parity-for-residential-battery-storage-62637

[39] Y. T. Tan and D. S. Kirschen, "Impact on the power system of a large penetration of photovoltaic generation," in *Proc. IEEE Power Eng. Soc. Gen. Meet.*, pp. 1–8. Jun. 24–28, 2007.

[40] W. A. Omran, M. Kazerani and M. M. A. Salama, "Investigation of methods for reduction of power fluctuations generated from large grid-connected photovoltaic systems," *IEEE Trans. on Energy Conversion*, vol. 26, no. 1, pp. 318-327, Mar. 2011.

[41] C. Parrotte, "Challenges facing the electricity network, *Australasian Universities Power Engineering Conference,* 2014. [online] Available: http://aupec2014.com.au/wp-content/uploads/2014/10/Cameron-_-WE_n12338949_Presentation_-_AUPEC_2014_-_Cameron_Parotte_-_30_September_2014.pdf

[42] S. Eftekharnejad, V. Vittal, G. T. Heydt, B. Keel, and J. Loehr, "Impact of increased penetration of photovoltaic generation on power systems," *IEEE Trans. on Power Syst.*, vol. 28, no. 2, pp. 893-901, May 2013.

[43] C. A. Silva-Monroy and J. Watson, "Integrating energy storage devices into market management systems," *Proceedings of the IEEE*, vol. 102, no. 7, pp. 1084-1093, Jul. 2014.

[44] G. James and J. Hayward, "AEMO 100% Renewable Energy Study: Energy Storage", Commonwealth Scientific and Industrial Research Organisation (CSIRO), Sep. 2012.

[45] M. T. Lawder, B. Suthar, P. W. C. Northrop, S. De, C. M. Hoff, O. Leitermann, M. L. Crow, S. Santhanagopalan, and V. R. Subramanian, "Battery energy storage system (BESS) and battery management system (BMS) for grid-scale applications," *Proceedings of the IEEE*, vol. 102, no. 6, pp. 1014-1030, Jun. 2014.

[46] DOE Global Energy Storage Database, Sandia Corporation. [online] Available: http://www.energystorageexchange.org/

[47] A. Akhil, G. Huff, A. B. Currier, B. C. Kaun, D. M. Rastler, S. B. Chen, A. L. Cotter, D. T. Bradshaw, and W. D. Gauntlett, "DOE/EPRI 2013 Electricity

Storage Handbook in Collaboration with NRECA," Sandia National Laboratories, Jul. 2013.

[48] "Overview brochure: Energy storage keeping smart grids in balance", ABB. 2014. [online] Available: http://www05.abb.com/global/scot/scot221.nsf/veritydisplay/59a2be960fdb777a48257a680045c04a/$file/ABB%20Energy%20Storage_Nov2012.pdf

[49] "Energy white paper: Strengthening the foundations for Australia's energy future," Department of Resources, Energy and Tourism, 2012.

[50] J. Pyper and ClimateWire, (Sep. 2014). "Elon Musk's Tesla picks Nevada to host battery Gigafactory", Scientific American. [online] Available: http://www.scientificamerican.com/article/elon-musk-s-tesla-picks-nevada-to-host-battery-gigafactory/

[51] V. Muenzel, I. Mareels, J. Hoog, A. Vishwanath and S. Kalyanaraman, (Jul. 2014). "Affordable batteries for green energy are closer than we think", The Conversation. [online] Available: http://theconversation.com/affordable-batteries-for-green-energy-are-closer-than-we-think-28772

[52] W. Flanagan, (Sep. 2014). "Battery storage with solar PV: The next logical step", Renewable Energy World.Com. [online] Available: http://www.renewableenergyworld.com/rea/news/article/2014/09/battery-storage-with-solar-pv-the-next-logical-step

[53] P. D. F. Ferreira, P. M. S. Carvalho, L. A. F. M. Ferreira and M. D. Ilic, "Distributed energy resources integration challenges in low-voltage networks: voltage control limitations and risk of cascading," *IEEE Trans. on Sustainable Energy*, vol. 4, no. 1, pp.82-88, Jan. 2013.

[54] I. Song, W. Jung, J. Kim, S. Yun, J. Choi and S. Ahn, "Operation schemes of smart distribution networks with distributed energy resources for loss reduction and service restoration," *IEEE Trans. on Smart Grid*, vol. 4, vo. 1, pp. 367-374, Mar. 2013.

[55] P. Mallet, P. Granström, P. Hallberg, G. Lorenz, and P. Mandatova, "Power to the people: European perspectives on the future of electric distribution," *IEEE Power and Energy Magazine*, vol.2, no.2, pp. 51-64, Apr. 2014.

[56] K. S. Reddy, M. Kumar, T. K. Mallick, H. Sharon and S. Lokeswaran, "A review of integration, control, communication and metering (iccm) of renewable energy based smart grid", *Journal of Renewable and Sustainable Energy Reviews*, vol. 38, pp. 182-192, Jun. 2014.

[57] S. Salinas, M. Li, P. Li and Y. Fu, "Dynamic energy management for the smart grid with distributed energy resources," *IEEE Trans. on Smart Grid*, vol. 4, no. 4, pp. 2139-2151, Dec. 2013.

[58] J. Driesen, F. Katiraei, "Design for distributed energy resources," *IEEE Power and Energy Magazine*, vol.6, no. 3, Jun. 2008.

[59] A. Vargas and M. E. Samper, "Real-time monitoring and economic dispatch of smart distribution grids: high performance algorithms for DMS applications," *IEEE Trans. on Smart Grid*, vol. 3, no. 2, pp. 866-877, Jun. 2012.

[60] M. A. Abdullah, A. P. Agalgaonkar, K. M. Muttaqi, "Probabilistic load flow incorporating correlation between time-varying electricity demand and renewable power generation," *Journal of Renewable Energy*, vol. 55, pp. 532-543, Jul. 2013.

[61] (Aug. 2013), "Energy Analysis: Distributed Generation Renewable Energy Estimate of Costs", National Renewable Energy Laboratory, US. [online] Available: http://www.nrel.gov/analysis/tech_lcoe_re_cost_est.html

[62] R. F. Arritt, and Roger C. Dugan, "Distribution system analysis and the future smart grid," *IEEE Trans. on Ind. Applications*, vol. 47, no. 6, pp. 2343-2350, Dec. 2011.

[63] S. Henry, P. Panciatici, and A. Parisot, "Going green: Transmission grids as enablers of the transition to a low-carbon European economy," *IEEE Power & Energy Magazine*, vol. 12, no. 2, pp. 26-35, 2014.

[64] M. Yilmaz and P. T. Krein, "Review of the impact of vehicle-to-grid technologies on distribution systems and utility interfaces," *IEEE Trans. on Power Electron*., vol. 28, no. 12, pp. 5673-5689. Dec. 2013.

[65] A. Y. Saber and G. K. Venayagamoorthy, "Plug-in vehicles and renewable energy sources for cost and emission reductions," *IEEE Trans. on Ind. Electron*., vol. 58, no. 4, pp. 1229-1238, Apr. 2011.

[66] Z. Tan, P. Yang and A. Nehorai, "An optimal and distributed demand response strategy with electric vehicles in the smart grid," *IEEE Trans. on Smart Grid*, vol. 5, no. 2, pp. 861-869, Mar. 2014.

[67] X. Fang, S. Misra, G. Xue, and D. Yang, "Smart grid – The new and improved power grid: A survey," *IEEE Com. Surveys & Tutorials,* vol. 14, no. 4, pp. 944-980, Fourth quarter 2012.

[68] Z. Ding, Y. Guo, D. Wu and Y. Fang "A market based scheme to integrate distributed wind energy," *IEEE Trans. on Smart Grid*, vol. 4, no. 2, pp.976-984, Jun. 2013.

[69] B. Hamilton and M. Summy, "Benefits of the smart grid: part of a long term economic strategy", *IEEE Power and energy Magazine,* vol. 9, no.1 pp.100-103, Feb. 2011.

[70] J. Bhatt, V. Shah and O. Jani, "An instrumentation engineer's review on smart grid: Critical applications and parameters," *Journal of Renewable and Sustainable Energy Reviews,* vol. 40, pp. 1217-1239, 2014.

[71] J. O. Dada, "Towards understanding the benefits and challenges of Smart/Micro-Grid for electricity supply system in Nigeria", *Journal of Renewable and Sustainable Energy Reviews*, vol. 38, pp. 1003-1014, Jul. 2014.

[72] F. Bouhafs, M. Mackay and M. Merabti, "Links to the future: Communication requirements and challenges in the smart grid", *IEEE Power and Energy Magazine*, vol.10 no.1, pp. 24-32, 2012.

[73] V. C. Güngör, D. Sahin, T. Kocak, S. Ergüt, C. Buccella, C. Cecati, and G. P. Hancke, "Smart grid technologies: Communication technologies and standards", *IEEE Trans. on Ind. Informatics*, vol. 7, no. 4, pp. 529-539, Nov. 2011.

[74] Y. Yan, Y. Qian, H. Sharif, and D. Tipper, "A Survey on smart grid communication infrastructures: motivations, requirements and challenges," *IEEE Com. Surveys & Tutorials*, vol. 15, no. 1, pp. 5-20, First quarter 2013.

[75] C. W. Gellings, "Power to the people: New distribution technologies on the horizon", *IEEE Power and Energy Magazine*, vol.9 no.5, pp. 52-63, 2011.

[76] S. Kahrobaee, R. A. Rajabzadeh, L. Soh, and S. Asgarpoor, "A multiagent modelling and investigation of smart homes with power generation, storage, and trading features," *IEEE Trans. on Smart Grid*, vol. 4, pp. 659-668, no. 2, Jun. 2013.

[77] D. Manz, R.Walling, N. Miller, B. LaRose, R. D'Aquila, and B. Daryanian, "The grid of the future: Ten trends that will shape the grid over the next decade," *IEEE Power and Energy Magazine*, vol.12, no. 3, pp.26-36, Apr. 2014.

[78] (2014). Technologies: Solid state batteries, Energy Storage Association. [online] Available: http://energystorage.org/energy-storage/storage-technology-comparisons/solid-state-batteries

[79] B. M. Grainger, G. F. Reed, A. R. Sparacino and P. T. Lewis, "Power electronics for grid-scale energy storage," *Proceedings of the IEEE*, vol. 102, no. 6, pp. 1000-1013, 2014.

[80] A. Poullikkas, "A comparative overview of large-scale battery systems for electricity storage," *Journal of Renewable and Sustainable Energy Reviews*, vol. 27, pp. 778-788, Jul. 2013.

[81] B. B. McKeon, J. Furukawa, and S. Fenstermacher, "Advanced lead–acid batteries and the development of grid-scale energy storage systems," *Proceedings of the IEEE*, vol. 102, no. 6, pp. 951-963, Jun. 2014.

[82] P. Wolfs, "An economic assessment of "second use" lithium-ion batteries for grid support," *Australasian Universities Power Engineering Conference (AUPEC)*, 2010.

[83] (2014). "Nanophosphate basics: An overview of the structure, properties and benefits of A123 Systems' proprietary lithium ion battery technology", NEC Energy Solutions Inc. [online] Available: http://www.neces.com/lithium-iron-phosphate-battery.htm

[84] A123 Systems ALM 12V& User's Guide, A123 Energy Solutions, 2013. [Online]. Available: http://www.a123energy.com

[85] H. Kirkham, D. Nightingale, and T. Koerner. "Energy management system design with dispersed storage and generation," *IEEE Trans. on Power Apparatus and Syst.*, vol. 100, no. 7, Jul. 1981.

[86] H. L. Willis, "Analytical methods and rules of thumb for modelling DG-distribution interaction," in *Proc. IEEE Power Eng. Soc. Summer Meeting*, pp. 1643–1644, Jul. 2000.

[87] C. Wang and M. H. Nehrir, "Analytical approaches for optimal placement of distributed generation sources in power systems," *IEEE Trans. Power Syst.*, vol. 19, no. 4, pp. 2068–2076, Nov. 2004.

[88] T. Gözel and M. H. Hocaoglu, "An analytical method for the sizing and siting of distributed generators in radial systems," *Elect. Power Syst. Res.*, vol. 79, no. 6, pp. 912–918, Jun. 2009.

[89] D. Q. Hung, N. Mithulananthan, and R. C. Bansal, "Analytical expressions for DG allocation in primary distribution networks," *IEEE Trans. Energy Convers.*, vol. 25, no. 3, pp. 814–820, Sep. 2010.

[90] D. Q. Hung and N. Mithulananthan, "Multiple distributed generators placement in primary distribution networks for loss reduction," *IEEE Trans. Ind. Electron.*, vol. 60, no. 4, pp. 1700–1708, Apr. 2013.

[91] K. M. Muttaqi, A. T. Le, M. Negnevitsky and G. Ledwich, "An algebraic approach for determination of DG parameters to support voltage profile in radial distribution networks," *IEEE Trans. Smart Grid*, vol. 5, no. 3, pp. 1-10, May 2014.

[92] P. S. Georgilakis and N. D. Hatziargyriou, "Optimal distributed generation placement in power distribution networks: Models, methods, and future research," *IEEE Trans. Power Syst*., vol. 28, no. 3, pp. 3420–3428, Aug. 2013.

[93] Z. Wang, B. Chen, J. Wang, J. Kim, and M. M. Begovic, "Robust optimization based optimal DG placement in Microgrids," *IEEE Trans. on Smart Grid*, vol. 5, no. 5, Sep. 2014.

[94] D. Singh, R. K. Misra, and D. Singh, "Effect of load models in distributed generation planning," *IEEE Trans. on Power Syst*., vol. 22, no. 4, pp. 2204-2212, Nov. 2007.

[95] H. Khan and M. A. Choudhry, "Implementation of distributed generation (IDG) algorithm for performance enhancement of distribution feeder under

extreme load growth," *Int. Journal of Electrical Power & Energy Syst*., vol. 32, no. 9, pp. 985–997, Nov. 2010.

[96] Y. M. Atwa and E. F. El-Saadany, "Optimal allocation of ESS in distribution systems with a high penetration of wind energy," *IEEE Trans. on Power Syst.*, vol. 25, no. 4, Nov. 2010.

[97] M. Nick, R. Cherkaoui and M. Paolone, "Optimal allocation of dispersed energy storage systems in active distribution networks for energy balance and grid support", *IEEE Trans. on Power Syst*., vol. 29, no. 5, Sep. 2014.

[98] S. X. Chen, H. B. Gooi, and M. Q. Wang, "Sizing of energy storage for Microgrids," *IEEE Trans. on Smart Grid*, vol. 3, no. 1, Mar. 2012.

[99] F. S. Abu-Mouti and M. E. El-Hawar, "Optimal distributed generation allocation and sizing in distribution systems via artificial bee colony algorithm," *IEEE Trans. on Power Delivery*, vol. 26, no. 4, pp. 2090-2101, Oct. 2011.

[100] M. F. Shaaban, Y. M. Atwa and E. F. El-Saadany, "DG allocation for benefit maximization in distribution networks," *IEEE Trans. on Power Syst*., vol. 28, no. 2, pp. 639-649, May 2013.

[101] Y. Luo, L. Shi and G. Tu, "Optimal sizing and control strategy of isolated grid with wind power and energy storage system", *Energy Conversion and Management*, vol. 80, pp. 407–415, Oct. 2013.

[102] G. Celli, S. Mocci, F. Pilo, and M. Loddo, "Optimal integration of energy storage in distribution networks," *IEEE Power Tech*, pp. 1–7, 2009.

[103] C. Chen, S. Duan, T. Cai, B. Liu, and G. Hu, "Optimal allocation and economic analysis of energy storage system in Microgrids," *IEEE Trans. Power Electron.*, vol. 26, no. 10, pp. 2662–2773, Oct. 2011.

[104] S. Chakraborty, T. Senjyu, H. Toyama, A. Y. Saber, and T. Funabashi, "Determination methodology for optimising the energy storage size for power system," *IET Generation, Transmission & Distribution*, vol. 3, no. 11, pp. 987–999, 2009.

[105] Y. Zheng, Z. Y. Dong, F. J. Luo, K. Meng, J. Qiu, and K. P. Wong, "Optimal allocation of energy storage system for risk mitigation of DISCOs with high

renewable penetrations," *IEEE Trans. on Power Syst*., vol. 29, no. 1, Jan. 2014.

[106] G. Carpinelli, F. Mottola, D. Proto, and A. Russo, "Optimal allocation of dispersed generators, capacitors and distributed energy storage systems in distribution networks," *Modern Electr. Power Syst*., pp. 1–6, 2010.

[107] S. Teleke, M. E. Baran, S. Bhattacharya and A. Q. Huang, "Rule-based control of battery energy storage for dispatching intermittent renewable sources," *IEEE Trans. on Sustainable Energy*, vol.1 no. 3, pp. 117-124. Oct. 2010.

[108] M. J. E. Alam, K. M. Muttaqi and D. Sutanto, "Mitigation of rooftop solar PV impacts and evening peak support by managing available capacity of distributed energy storage systems," *IEEE Trans. on Power Syst*., vol. 28 no. 4, pp. 3874-3884. Nov. 2013.

[109] H. Sugihara, K. Yokoyama, O. Saeki, K. Tsuji, and T. Funaki, "Economic and efficient voltage management using customer-owned energy storage systems in a distribution network with high penetration of photovoltaic systems, *IEEE Trans. on Power Syst*., vol. 28, no. 1, Feb. 2013.

[110] E. I. Vrettos and S. A. Papathanassiou, "Operating policy and optimal sizing of a high penetration RES-BESS system for small isolated grids," *IEEE Trans. on Energy Conversion*, vol. 26, no. 3, Sep. 2011.

[111] A. Damiano, G. Gatto, I. Marongiu, M. Porru, and A. Serpi, "Real-time control strategy of energy storage systems for renewable energy sources exploitation," *IEEE Trans. on Sustainable Energy*, vol. 5, no. 2, Apr. 2014.

[112] I. Atzeni, L. G. Ordóñez, G. Scutari, D. P. Palomar, and J. R. Fonollosa, "Demand-side management via distributed energy generation and storage optimization," *IEEE Trans. on Smart Grid*, vol. 4, no. 2, Jun. 2013.

[113] A. D. Lamont, "Assessing the economic value and optimal structure of large-scale electricity storage," *IEEE Trans. on Power Syst*., vol. 28, no. 2, May 2013.

[114] H. Rahimi-Eichi, U. Ojha, F. Baronti and M. Chow, "Battery management system: An overview of its application in the smart grid and electric vehicles," *IEEE Ind. Electron. Magazine*, vol. 7 no. 2, pp. 4-16, Jun. 2013.

[115] "Battery and Energy Technologies, Battery life", Electropaedia, Woodbank Communications Ltd, 2005.

[116] R. G. Wandhare and V. Agarwal, "Reactive power capacity enhancement of a PV-grid system to increase PV penetration level in smart grid scenario," *IEEE Trans. on Smart Grid*, vol. 5, no. 4, pp. 1845-1854, Jul. 2014.

[117] P. Wolfs, C. Gunathilake, P. Martino, I. Khanna, "Distributed renewables and battery storage for the support of the edge of the rural grid", *Australasian Universities Power Engineering Conference*, 2011.

[118] R. Charni and M. Maier, "Impact study of collaborative implementation models on total cost of ownership of integrated fiber wireless smart grid communications infrastructures", *IEEE Smart Grid Com.*, 2013.

[119] Z. Jiazhan, R. Q. Hu and Q. Yi, "Scalable distributed communication architectures to support advanced metering infrastructure in smart grid," *IEEE Trans. on Parallel and Distribution Syst*.", vol. 23 no. 9, pp. 1632-1642, 2012.

[120] X. Lu, W. Wang and J. Ma, "An empirical study of communication infrastructures towards the smart grid: Design, implementation and evaluation", *IEEE Trans. on Smart Grid*, vol. 4 no.1, pp. 170-183, Mar. 2013.

[121] N. Jayasekara and P. Wolfs, "A hybrid approach based on GA and direct search for periodic optimization of finely distributed storage," *IEEE Innovative Smart Grid Technologies Asia (ISGT)*, 2011.

[122] P. K. Dash, A. K. Pradhan and G. Panda, "Application of minimal radial basis function neural network to distance protection", *IEEE Trans. on Power Delivery*, vol. 16 no.1, pp. 68–74, 2001.

[123] W. Lin, C. Hong and C. Chen, " Neural-network-based MPPT control of a stand-alone hybrid power generation system", *IEEE Trans. on Power Electron.*, vol. 26 no. 12, pp. 3571-3581, 2011.

[124] H. Razmi, M. Teshnehlab and H.A. Shayanfar, "Neural network based on a genetic algorithm for power system loading margin estimation", *IET Generation, Transmission and Distribution*, vol. 6 no. 11, pp. 1153-1163, 2012.

[125] S. Karsoliya, "Approximating number of hidden layer neurons in multiple hidden layer BPNN architecture", *Int. Journal of Engineering Trends and Technology*, vol.3 no. 6, pp. 714-717, 2012.

[126] A. Alfaris, "Multidisciplinary System Design Optimization: Multiobjective Optimization," Massachusetts Institute of Technology, 2010. [online] Available: http://ocw.mit.edu/courses/engineering-systems-division/esd-77-multidisciplinary-system-design-optimization-spring-2010/lecture-notes/MITESD_77S10_lec14.pdf

[127] AEMC, "Possible future retail electricity price movements: 1 July 2012 to 30 June 2015," Electricity Price Trends Report, Mar. 2013.

[128] Design Guide: Managing Peak Demand in Live Performance Venues [Online].Available: http://liveperformance.com.au/sites/liveperformance.com.au/files/resources/design_guide_-_managing_peak_energy_demand_in_venues.pdf

[129] J. V. Annette, B. B. Banerjee, "Assessment of voltage unbalance," *IEEE Trans. on Power Delivery*, vol. 16 no. 4, pp. 782-790, Oct 2001.

[130] A. Domahidi, A. U. Zgraggen, M. N. Zeilinger, M. Morari and C. N. Jones, "Efficient interior point methods for multistage problems arising in receding horizon control", *Conference on Decision and Control (CDC)*, Maui, HI, USA, pp. 668–674, Dec. 2012.

[131] V. M Costa, N. Martins and J. L. R. Pereira, "Developments in the Newton Raphson power flow formulation based on current injections," *IEEE Trans. Power Syst.*, vol. 14, no. 4, pp. 1320-1326, Nov. 1999.

[132] P. A. N. Garcia, J. L. R. Pereira, S. Carneiro, V. M. da Costa and N. Martins, "Three-phase power flow calculations using the current injection method," *IEEE Trans. on Power Syst*., vol.15 no.2, pp. 508-514, May 2000.

[133] B. Venkatesh, R. Ranjan, and H. B. Gooi, "Optimal reconfiguration of radial distribution systems to maximize loadability," *IEEE Trans. on Power Syst*., vol. 19, no. 1, pp. 260–266, Feb. 2004.

[134] Y. M. Atwa, E. F. El-Saadany, M. M. A. Salama, R. Seethapathy, M. Assam, and S. Conti, "Adequacy Evaluation of Distribution System Including

Wind/Solar DG During Different Modes of Operation," *IEEE Trans. Power Syst*., vol. 26, no. 4, pp. 1945–1952, Nov. 2011.

[135] D. Q. Hung and N. Mithulananthan, "Alternative Analytical Approaches for Renewable DG Allocation for Energy Loss Minimization," *IEEE Power and Energy General Meeting*, 2012.

[136] (2014). "Smart power tariff", Synergy, [online] Available: http://www.synergy.net.au/at_home/smartpower_sm1_tariff.xhtml

[137] A. Ellis, R. Nelson, E. V. Engeln, R. Walling, J. McDowell, L. Casey, E. Seymour, W. Peter, C. Barker and B. Kirby, "Reactive power interconnection requirements for PV and wind plants- Recommendations to NERC," SANDIA Report, Feb. 2012.

[138] A. Piccolo and P. Siano "Evaluating the impact of network investment deferral on distributed generation expansion," *IEEE Trans. on Power Syst*., vol. 24, no. 3, pp. 1559-1567, Aug. 2009.

[139] G. P. Harrison, A. Piccolo, P. Siano, and A. R. Wallace, "Exploring the tradeoffs between incentives for distributed generation developers and DNOs," *IEEE Trans. on Power Syst*., vol. 22, no. 2, pp. 821-828, May 2007.

[140] Supply Forecasting, "Capacity Expansion Modelling", Australian Energy Market Operator, Feb 2013.

[141] 2013, "Wind Power capacity factor", Boston, MA. [Online] Available: http://www.umass.edu/windenergy/publications/published/communityWindFactSheets/RERL_Fact_Sheet_2a_Capacity_Factor.pdf

[142] Y. M. Atwa, E. F. El-Saadany, M. M. A. Salama, and R. Seethapathy, "Optimal renewable resources mix for distribution system energy loss minimization," *IEEE Trans. on Power. Syst*., vol. 25, no. 1, pp. 360-370, Feb. 2010.

[143] W. Ouyang, H. Cheng and X. Zhang1 F. Li, "Evaluation of distributed generation connecting to distribution network based on long-run incremental cost", *IET Generation, Transmission and Distribution*, Aug. 2010.

[144] N. Acharya, P. Mahat, and N. Mithulananthan, "An analytical approach for DG allocation in primary distribution network," *Int. Journal of Electrical Power & Energy Syst*, vol. 28, no. 10, pp. 669–678, Dec. 2006.

[145] K. Zou, A. P. Agalgaonkar, K. M. Muttaqi, and S. Perera, "Voltage support by distributed generation units and shunt capacitors in distribution systems," *IEEE Power Eng. Soc. General Meeting*, 2009.

[146] M. A. Kashem and G. Ledwich, "Multiple distributed generators for distribution feeder voltage support," *IEEE Trans. on Energy Conversion*, vol. 20, no. 3, pp. 676-684, Sep. 2005.

Appendix A. IEEE 33-bus System Data

The Table A - 1 shows the original IEEE 33 bus system data used in this thesis [133].

TABLE A - 1: IEEE 33 BUS SYSTEM DATA [133].

Branch No.	Sending Bus No.	Receiving Bus No.	Resistance (Ω)	Reactance (Ω)	Load at Receiving Bus	
					Real Power (kW)	Reactive Power (kVAr)
1	1	2	0.0922	0.0477	100	60
2	2	3	0.493	0.2511	90	40
3	3	4	0.366	0.1864	120	80
4	4	5	0.3811	0.1941	60	30
5	5	6	0.819	0.707	60	20
6	6	7	0.1872	0.6188	200	100
7	7	8	1.7114	1.2351	200	100
8	8	9	1.03	0.74	60	20
9	9	10	1.04	0.74	60	20
10	10	11	0.1966	0.065	45	30
11	11	12	0.3744	0.1238	60	35
12	12	13	1.468	1.155	60	35
13	13	14	0.5416	0.7129	120	80
14	14	15	0.591	0.526	60	10
15	15	16	0.7463	0.545	60	20
16	16	17	1.289	1.721	60	20
17	17	18	0.732	0.574	90	40
18	2	19	0.164	0.1565	90	40
19	19	20	1.5042	1.3554	90	40
20	20	21	0.4095	0.4784	90	40
21	21	22	0.7089	0.9373	90	40
22	3	23	0.4512	0.3083	90	50
23	23	24	0.898	0.7091	420	200
24	24	25	0.896	0.7011	420	200
25	6	26	0.203	0.1034	60	25
26	26	27	0.2842	0.1447	60	25
27	27	28	1.059	0.9337	60	20
28	28	29	0.8042	0.7006	120	70
29	29	30	0.5075	0.2585	200	600
30	30	31	0.9744	0.963	150	70
31	31	32	0.3105	0.3619	210	100
32	32	33	0.341	0.5302	60	40
Substation Voltage is 12.66 kW and the Base is 10MVA						